UNIVERSITY OF SOUTHAMPTON

FACULTY OF ENGINEERING AND THE ENVIRONMENT

Civil, Maritime and Environmental Engineering & Science

A Numerical Investigation of the Effect of Particle Shape on the Strength of Coarse Granular Materials

by

Matthew J. Potticary

Thesis submitted for the degree of Doctor of Philosophy

December 2018

ABSTRACT

It has long been recognised that the macroscopic mechanical behaviour of a granular material depends on particle shape. However, a systematic investigation into particle shape is lacking. There are three different aspect of shape each considering shape at a different scale, typically these are called form, angularity and roughness.

The form of a particle can be quantified using the Longest (L), Intermediate (I) and Shortest (S) dimension of an equivalent scalene ellipsoid; two independent parameters of particle form are defined, termed platyness and elongation. The angularity of a particle can be quantified by the volumetric deviation between the true particle shape and the idealised equivalent scalene ellipsoid. This volume is then normalised against the the original volume of the particle.

We used DEM simulations with the Potential Particle Method to investigate the effect of particle shape on the friction angle of a granular material at critical state. By studying particle form and angularity in isolation, it is found that deviation of particle form and angularity (from that of a sphere) leads to higher angles of friction at critical state. It is found that the higher critical state strength exhibited by non-spherical particles is due to form suppressing particle rotation and leading to increased interparticle sliding, a mechanism that in comparison requires more energy to be expended.

It is found that for particles combining non-spherical form and angularity that both measures act cooperatively with regards to increasing the angle of friction at critical state. It is also seen that these two effects are not independent of each other as the effectiveness of particle angularity is dependant on the underlying form of the shape. This is possibly due to particle angularity increasing the effectiveness of mechanisms created due to different particle forms.

Contents

List of Figures

List of Tables

Declaration of Authorship

I, Matthew J. Potticary, declare that the thesis entitled *A Numerical Investigation of the Effect of Particle Shape on the Strength of Coarse Granular Materials* and the work presented in the thesis are both my own, and have been generated by me as the result of my own original research. I confirm that:

- this work was done wholly or mainly while in candidature for a research degree at this University;
- Where any part of this thesis has previously been submitted for a degree or any other qualification at this University or any other institution, this has been clearly stated;
- Where I have consulted the published work of others, this is always clearly attributed;
- Where I have quoted from the work of others, the source is always given. With the exception of such quotations, this thesis is entirely my own work;
- I have acknowledged all main sources of help;
- Where the thesis is based on work done by myself jointly with others, I have made clear exactly what was done by others and what I have contributed myself;
- Parts of this work have been published as: (Potticary et al., 2014), (Potticary et al., 2015) and (Potticary et al., 2016)

Signed:.....

Date:.....

Acknowledgements

First, I would like to thank my supervisor Dr Antonis Zervos who has given me advice and guidance over these past years. He helped me improve my numerical and problem solving skills by sharing his knowledge and experience.

I would also like to thank Dr John Harkness for providing technical support and advice on using the discrete element model.

Many thanks to the university staff and colleges in the faculty who helped provide training and support throughout my time at Southampton.

The love and support from my family who continually encouraged me when my motivation failed me.

I am grateful for my close friends Liam and James with our many lunches and trips to the pub helping keep me sane when time were tough.

I would especially like to thank my partner Janna, who now knows far too much about railway ballast than she cares to know. Her love and support took many forms and without which this thesis wouldn't have been possible.

Finally I would like to thank Network rail, EPSRC and the whole of the "Track 21" team for funding and making this PhD possible.

Nomenclature

$A_{particle}$	Angularity for the particle
A	Area
A_i	Angularity for each corner
L_i	Branch vector between two centroids
$d\epsilon$	Change in volumetric strain
Z	Coefficient of curvature
μ	Coefficient of friction
F_2	Correction factors
F_1	Correction factors
Φ	Correction factor for the eccentricity of the contact
D_r	Diameter of the curvature at the corner
D_i	Diameter of the largest inscribed circle
D_c	Diameter of the smallest inscribed circle
x	Distance tip of the corner to the centre of the maximum inscribed circle
σ'	Effective stress
ζ	Elongation
$\mathbf{G}$	Fabric tensor
F_i	Force at contact
I	Intermediate dimension of a particle
u_c	Interparticle Angle of Friction
L	Longest dimension of a particle
L_w	Longest axis measured through the sharpest corner
a	Measured angle between planes
e_{max}	Maximum void ratio
e_{min}	Minimum void ratio

ϕ	Mobilised angle of friction angle
ϕ_{crit}	Mobilised angle of friction angle at critical state
u_s	Mobilised angle of friction
N	Number of particles in the model
n	Number of corners
F_n	Normal force
K_n	Normal spring stiffness
$\mathbf{n}$	Orientation vectors
δ	Overlap
D_n	Particle size at n % of percentage passing
P	Perimeter
α	Platyness
ν	Poison's ratio
D_k	Radius of curvature of the sharpest corner
D_r	Relative dry density
r	Radius of the maximum inscribed circle
R_a	Radius of curvature at the contact point particle a
R_b	Radius of curvature at the contact point particle b
R_c	Radius of curvature of the contact
F_s	Shear Force
τ'	Shear stress
K_s	Shear spring stiffness
G	Shear modulus
S	Shortest dimension of a particle
σ	Total stress
C_u *or* U	Uniformity coefficient
e	Void ratio
V_v	Volume of voids
V_s	Volume of solids
E	Young's modulus

Chapter 1

Introduction

Railways provide transport for both passengers and freight throughout the world. Many countries are starting to ask more from their transport infrastructure. For the railway this means an ever growing demand on the railway infrastructure to increase the amount of weight it can carry and the speed at which it can carry it whilst being cheaper to maintain. This, however is a problem due to ageing railway lines requiring constant maintenance. To help keep up with these demands ever more inventive solutions are needed to increase efficiencies and reduce the cost of infrastructure.

By far the most common type of railway track in the UK is the ballasted track. This design uses a thick layer of railway ballast material upon which the sleepers and rail sit, (Figure 1.1). Other types of railway track include slab track which replaces the ballast with a concrete slab but this is more expensive and is not suited universally.

Figure 1.1: Railway track

Railway ballast is the largest part of the ballasted track system, both in maintenance cost and by mass. Ballast is a granular material made up of crushed igneous rock, generally granite in the UK, (Figure 1.2). It has remained relatively unchanged since its introduction during the Victorian era. The purpose of ballast is to provide drainage, strength and stiffness to the track system.

Figure 1.2: Ballast particle

One problem faced by ballasted track is the continual monitoring and maintenance. This is because tracks that are closed for maintenance have a serious impact on the passengers and on freight companies by either reducing the speed or the number of trains. The ideal would be a track that didn't require maintenance however due to settlement of the ballast track failures regularly occur, leading to issues such as hanging rails. The reason for this settlement is because the repeated loading and unloading of the ballast causes permanent deformation to take place and the ballast become denser. Sections of track are not uniform in stiffness; this is because the ballast and the soil underneath the track vary in strength this typically leads to differential settlement. This differential settlement is a major maintenance issue for railway engineers, leading to the undulations of the track and reducing both the life of the track and passenger comfort.

Current maintenance of the ballast consists of inserting tamping tines which apply vibrations and squeezing the ballast. This has the effect of loosening the compressed ballast and raising the ballast back up to the rail. However, After a section of track has been tamped the ballast structure becomes loose leading to a reduced stiffnesses. To allow the ballast to resettle into a stiffer structure a intensity and speed of the loading is decreased. This is done by reducing speed of track for a short while after maintenance which leads to a reduced the effectiveness of the line.

An ideal track would have a uniform settlement with a uniform stiffness profile. Current research into reducing this settlement after many load cycles of the ballasted track mainly focus on adding extra material to the ballast. Another approach could be to engineer ballast so that is can resist settlement and operate for longer period of time without maintenance.

The current specification for ballast in the UK is taken from the British Standard for ballast, BS EN (2013). This defines the range of particle size distribution and the properties of the parent material. Current standard also limits the shapes of ballast particles that can be used, categorising them based on their flakiness and elongation. However, the reason for these limits are arbitrary and are based on empirical information. In particular the standards states that:

> "Limits should be selected from the specified range until such a time as there is more data available on railway ballast properties related to performance" (BS EN, 2013)

The mechanical properties of a granular material such as ballast are known to be depend on the shape of its particles. So in principle it should be possible to optimise the ballast properties by using an appropriately shaped particle. However there is a lack of understanding as to the effect particle shape has in relation to ballast performance.

To address this problem this study will analyse the impact different shaped particles have on the properties of a granular material, such as its strength and stiffness. The strength of the ballast is derived from the interactions between the particles. These interactions are influenced by the particle shape, as well as the *insitu* conditions of the material, such as the initial particle orientation, void ratio and fabric.

They can be investigated using numerical modelling which allows study of granular materials under triaxial compression loading conditions with a fine control on particle shape.

Under triaxial compression conditions, the stiffness is dependent on the initial conditions within the granular soil, with denser soils having a stiffer response than looser soils. However, once a granular soil has reach critical state the effects of the initial starting conditions will have been removed thus the effect of particle shape will be more evident. Therefore, this study focused on the effect of particle shape on critical state strength.

Critical state strength however is not directly related to ballast performance under typical cyclic train loads. Simple models which predict the strength under cyclic loading rely on the proportion of the strength mobilised during a cycle to decide whether failure will take place and after how many cycles. It can be argued that higher critical state strength is reasonably expected to lead to higher strength under cyclic loading.

The majority of numerical techniques that model granular materials treat them as a continuum, a single solid mass. Whilst this is an efficient approach it ignores the effects of individual particles and does not allow for particle interaction to be studied.

In this study a technique called the Distinct Element Method (DEM) is used, which models individual grains and their interactions. Particle movement is modelled using traditional Newtonian physics independently for each particle. Forces are transmitted between interparticle contacts with other grains. DEM can model complex arrangements of particles that form naturally and offers insights on the corresponding micromechanics. Studying these micromechanical interactions will provide a better understanding of why assemblies consisting of different particle shapes respond differently when subjected to loading conditions.

1.1 Aims and Objectives

The aim of this work is to investigate the relationship between particle shape and performance of railway ballast. The long term goal is to contribute towards identifying optimal ballast shapes that increase track design life.

The specific objectives of the project are to systematically:

- Review of how particle shape can be described and quantified
- Determine the effect that different aspects of a particle's shape have on the critical state strength of ballast
- Investigate the micromechanical origins of shape-related differences in critical state strength

Chapter 2

Literature Review

The properties of a granular material as a whole are fundamentally controlled by the interactions among its individual particles. An individual particle's properties are controlled by the material properties of the parent material and the shape of the particle. Empirical evidence about how particle shape determines the mechanical properties of a soil, so design is based on direct measurements of soil properties. Ideally soils would be tested insitu to determine the mechanical properties however for some cases this is not practical and in others impossible. Apart from insitu tests there are also lab tests of carefully collected samples.

As is it not always possible to perform an insitu test, such as the cone penetration test, an alternative is to simplify the problem and use numerical techniques to model soil behaviour. Doing so allows for complex interactions to be simulated so that the results can infer what would happen in the real world.

In this section there is a review of the literature including:

- an overview of granular materials and their characterisation
- a review of existing measures of characterizing the shape of granular materials
- the effect that different aspects of shape have upon the properties of granular materials
- current research into specification of railway ballast and what makes a good ballast
- an introduction into DEM theory and application.

2.1 Granular Materials

Granular materials consist of distinct particles that are not bound together thus are free to translate or rotate with respect to each other. Their void may contain a liquid, gas or

both making them three phase materials. The ratio of these phases significantly affects the behaviour of the soil.

There are measures that describe different soil properties such as how dense a soil is or the relative distribution of sizes of particles, and on which the soil's mechanical properties also depend.

2.1.1 Void Ratio

An important factor in predicting how a soil will behave is how densely the soil is packed. A measure used to describe this is the void ratio. A granular soils void ratio is defined as equation (2.1). The void ratio relates the volume of the voids (air and water) to the volume of solid material, showing the quantity of voids within the soil. The lower the void ratio the denser the soil.

$$e = \frac{V_v}{V_s} \tag{2.1}$$

V_v = Volume of voids

V_s = Volume of solids

Whilst the void ratio gives some indication of how a soil will behave when loaded it is difficult to compare to between soils because the maximum and minimum attainable void ratios are different for each soil.

For void ratios to be useful as a comparison between soils a relative measure of density is needed, Equation (2.2).

$$D_r = \frac{e_{max} - e}{e_{max} - e_{min}} \times 100\% \tag{2.2}$$

e_{max} is the maximum void ratio that can be achieved

e_{min} is the minimum void ratio that can be achieved

The relative density quantifies how dense or loose a soil is, compared to its densest and loosest states.

2.1.2 Particle Size Distribution

Soils consist of different geological materials, with particles having undergone different types of weathering. As particles undergo weathering they become fractured which leads

them to break/split taking on a different shape and size. Different materials will break up at different rates leading to a mixture of different size particles.

Soils particles have a range of sizes, from fine (silt $\approx 10\mu m$) to coarse (gravel $\approx 30mm$), ISO (2009). For each soil it is possible to plot the particle size distribution (PSD), which is a graph that shows the range of particles sizes within a soil against the cumulative amount of mass for each size. An example PSD plot is seen in Figure 2.1 showing the range of size classification.

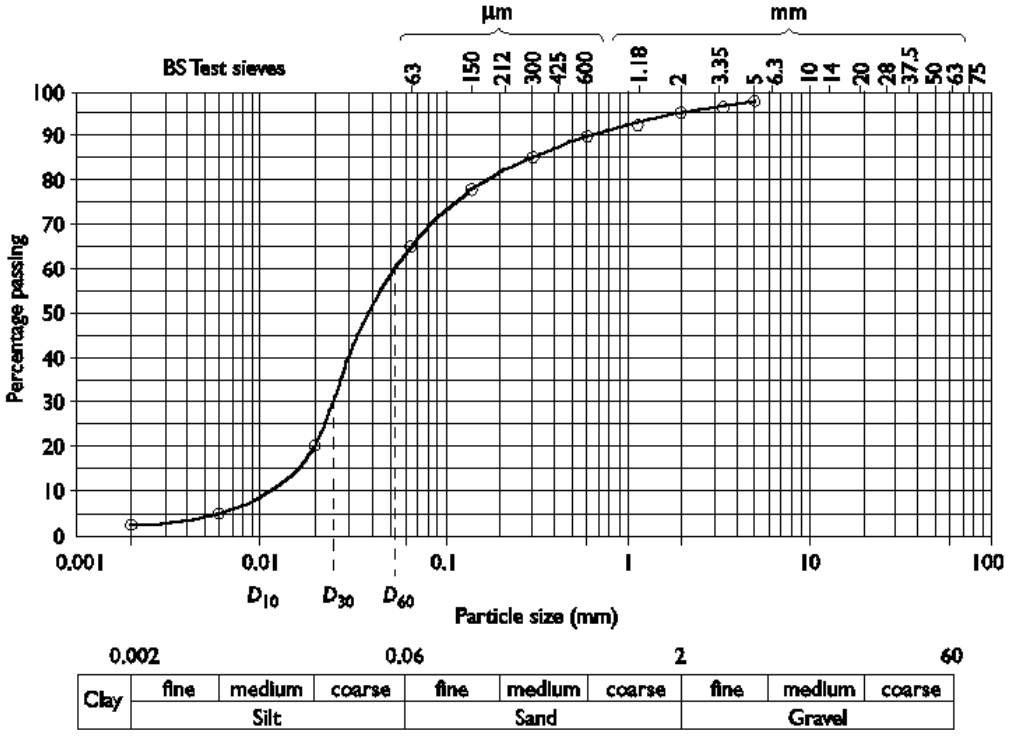

Figure 2.1: Graph showing change in PSD by weight and size classifications example taken from Powrie (2004)

Whilst in theory the PSD plot is a continuous curve, is it impossible to measure this directly and so numerical estimations must be made by passing the soils through a series of progressively finer layered sieves and measuring the mass of soil caught in each layer (BS EN, 2013).

To describe the uniformity of particle size there are two common measures, the uniformity coefficient (U) (Equation (2.3)), sometimes referred to as C_u, and the coefficient of curvature (Z)(Equation (2.4)), (Powrie, 2004). These measures give a representation of how well graded the material is, with low values of U and Z meaning the soil is generally consists of similar particle sizes.

$$U = \frac{D_{60}}{D_{10}} \tag{2.3}$$

$$Z = \frac{D_{30}^2}{D_{60} \times D_{10}} \tag{2.4}$$

D_{60} is the particle size corresponding to 60% of the percentage passing

D_{30} is the particle size corresponding to 30% of the percentage passing

D_{10} is the particle size corresponding to 10% of the percentage passing

2.1.3 Soil Strength and Stiffness

Unlike solid materials which derive their strength from physical bonds and connections, granular materials are unbound and so there are no physical bonds from which to derive strength. Whilst individual particles have an inherent strength from being a solid mass, granular soils obtain their strength and stiffness from how the particles interact.

Soils have different strengths depending on the type of loading that the soil will be subjected to and the internal configuration of the particles. A soil's strength is typically determined through appropriate lab tests, a typical one is trixial compression. Triaxial compression subjects the soil to a confining pressure in the three principal axes and a vertical strain rate applied to the top of the sample which results in a vertical load. Figure 2.2 shows the triaxial loading conditions and figure 2.3 shows the idealised deformed shape.

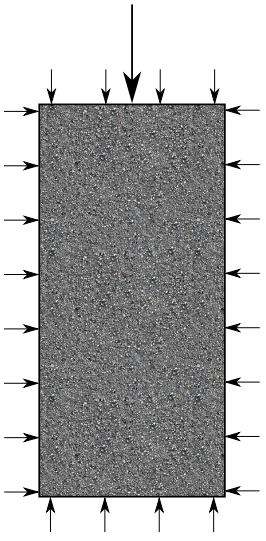

Figure 2.2: Triaxial Loading conditions

The strength mobilised by a soil specimen under triaxial compression conditions is given by the ratio between the stress needed to confine the soil (minor principal stress) and the stress being applied vertically to the soil (major principal stress). Using the Mohr's circle for the sample an angle can be defined by the tangent between the origin and the

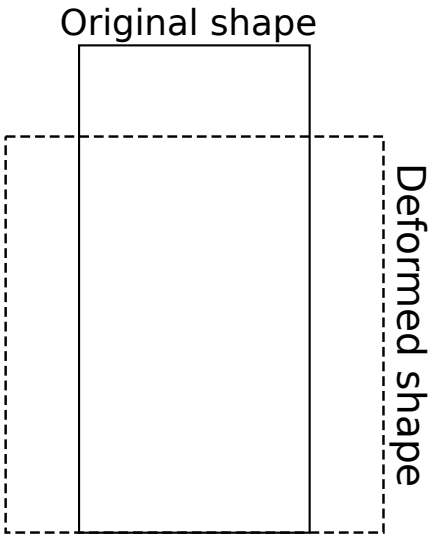

Figure 2.3: Deformed shape

circle, this tangent is referred to as the mobilised angle of friction and is calculated using equation, 2.5.

$$\phi_{mob} = \arcsin\left(\frac{\sigma_{11} - \sigma_{33}}{\sigma_{11} + \sigma_{33}}\right) \tag{2.5}$$

σ_{11} = major principal stress

σ_{33} = minor principal stress

The deviatoric stress will start to level out as the rate of dilatancy Equation (2.6) reduces to zero. At this point the model reaches a critical/steady state where there is constant deviatoric stress. One of the main characteristics of a densely packed material is attainment of a peak stress; the magnitude of peak stress reduces as initial relative density reduces. With a loose material compaction rather than dilation will take place, with a reducing rate until critical state is reached.

Under triaxial compression conditions the initial response will change depending if the soil is dense or loose.

$$\tan(\psi) = \frac{d\epsilon}{d\gamma} \tag{2.6}$$

γ = Shear strain

ϵ = Volumetric strain

When a soil with a high relative density is subjected to triaxial compression conditions it will initially have a stiffer response than the same material at a lower relative density. The stiffer response of a denser material is because its particles are in a dense configuration. When a dense material is loaded the configuration will initially compact,

however the material cannot continue to compress for long and the particles are forced to rearrange, leading to dilation. This continues to a point at which the deviatoric stress starts to decrease; this is known as peak stress.

Figure 2.4.A shows how the mobilised angle of friction changes against the shear strain of the soil, it can be seen for the dense sample there is a peak in strength and then a reduction down to a steady state.

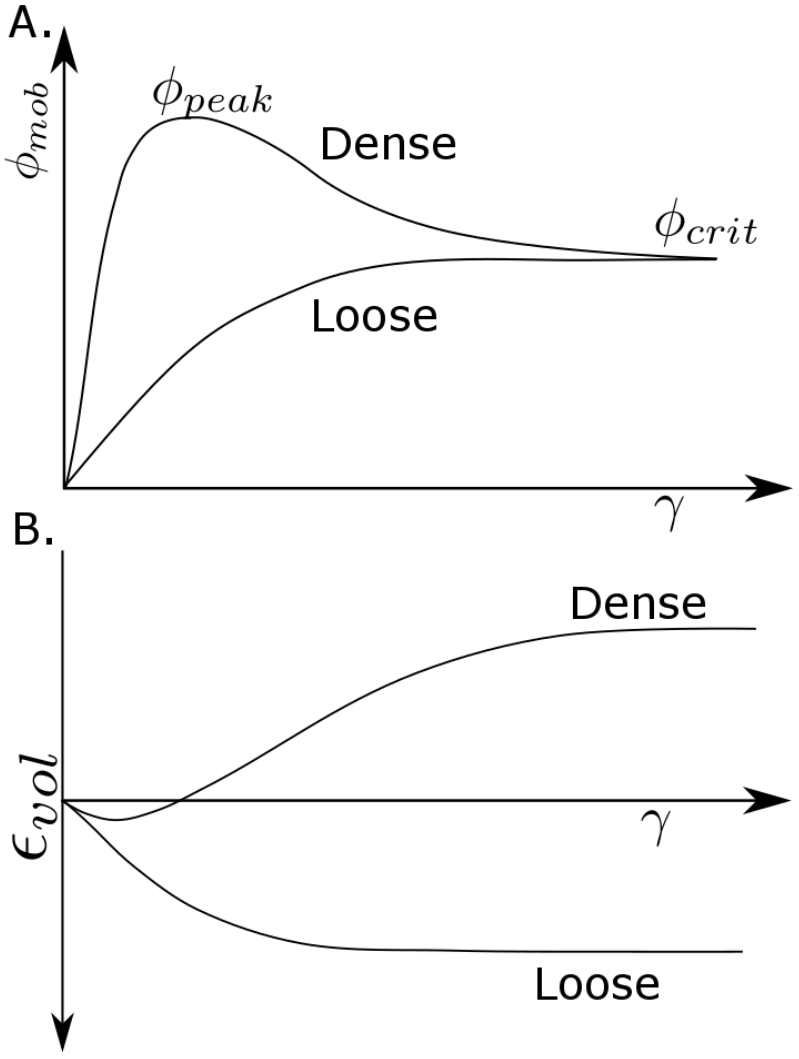

Figure 2.4: A. Figure showing mobilised angle of friction vs shear strain, B. Figure showing volumetric strain vs shear strain

Figure 2.4.B shows the change in volumetric strain against shear strain. When a soil with an initial low relative density (a loose soil) is subjected to triaxial compression conditions, there is no peak mobilised angle of friction. It will however continue to increase until the sample has reached a steady state of dilation after which the friction angle plateaus to the critical state value for the material.

Whilst the critical state mobilised angle of friction between the dense and loose model is the same, is not true for the volumetric strain. Where as the dense sample initially

compacts and eventually loosens, the loose sample continues to compact until it reaches a steady state. At the critical state the void ratio of the sample will be same regardless if it started out as dense or loose. This is due to the void ratio at critical state being a property of the soil and is dependant on the confining pressure.

2.1.3.1 Critical State Theory

Critical state is the point at which the rate of dilatancy remains zero and the effective and shear stresses remain constant despite continuing increase in shear strain. Regardless of the initial configuration of the particles the material will reach the same deviatoric stress ratio for the same effective stress. This is related to the particle material and shape.

The strength of the material is dependent on the ratio of the deviatoric stress and the confining pressure. Material failure takes place when the shear stress within the material reaches the capacity of the material to carry that stress. Figure 2.5 shows the Mohr circle for the material with the line signifying the maximum mobilised angle of friction for the material. The maximum mobilised stress a material can effectively use is the critical state strength.

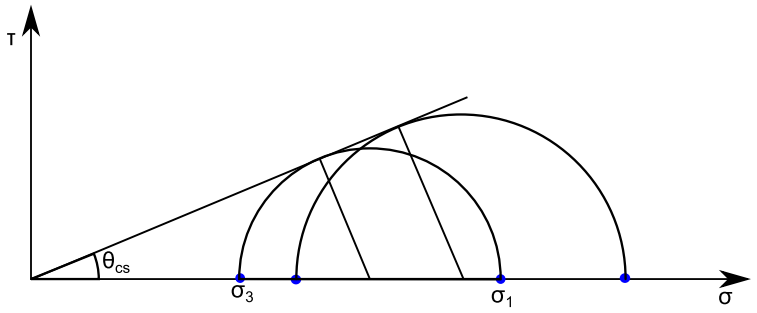

Figure 2.5: Principal stress vs shear stress, Mohr's circle

By rearranging Equation (2.5) the maximum shear stress within a material can be found.

$$\tau = \sigma' \sin(\phi) \tag{2.7}$$

τ = shear stress

σ' = Effective normal stress

2.1.4 Granular Fabric

Relative density is partly dependant on how the particles are arranged within a soil, i.e. granular fabric.

The effect of particle form on granular properties is mediated by the specific granular texture/fabric induced by each particle, Azéma and Radjaï (2010). This is most evident when fabric and texture contribute to the peak strength of the granular material, defining how dense the soil packing is.

Granular fabric, sometimes referred to as texture, describes the relationship between particles within the soil. Properties such as laminations and bedding planes are regularly used in description of soils; these are regions where particles are orientated in a regular pattern. These localized regions will cause differences in how the soil will initially behave in terms of stiffness and strength until the structure has time to deform. Particle orientation influences how anisotropic the soil properties will be, Oda and Kazama (1998); Ken-Ichi (1984); Rothenburg and Bathurst (1989); Iwashita and Oda (1999). If there is a random orientation of particles there will be no preferential direction for the particles to displace and any internal structures that form will be of a random nature.

A method for quantifying the orientation of the fabric is to use the Fabric Tensor, (Oda, 1972), this describe the average orientation of a set of vectors within a given control volume, Equation (2.8). Using Equation (2.8) allows a set of unit vectors to be represented as a [3 X 3] tensor, (Li and Dafalias, 2012).

$$\mathbf{G} = \frac{1}{N} \sum_{k=1}^{N} \mathbf{n}^k \otimes \mathbf{n}^k \tag{2.8}$$

$\mathbf{G}$ is the fabric tensor

N is the number of particles in the model

$\mathbf{n}$ is an n-d dimensional vector which normally represents particle orientation and contact forces

Figure 2.7,2.8, and 2.9 show 2D examples of fabric structures for ellipse particles and their corresponding fabric tensor. The orientation of an ellipse is described using the directions of the L and S vectors, Figure 2.6. However due to the symmetry of an ellipse the fabric tensor can be simplified by only calculating the tensor for the L vectors and the tensor describing the S vectors is the inverse.

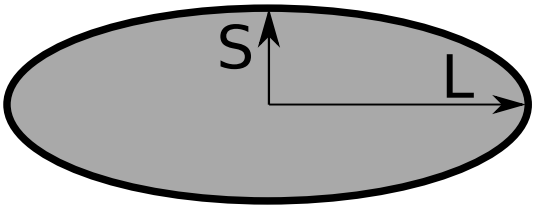

Figure 2.6: Examples of fabric orientation

Figure 2.7 shows an arrangement of particles with the L radius horizontal. This arrangement of particles corresponds to:

$$\mathbf{G} = \begin{pmatrix} 1 & 0 \\ 0 & 0 \end{pmatrix}$$

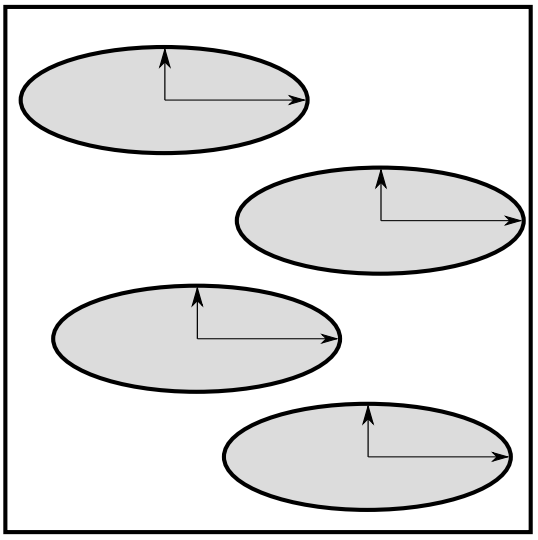

Figure 2.7: Examples of fabric orientation - Horizontal

Figure 2.8 shows an arrangement of particles with the L radius cross aligned. This arrangement of particles corresponds to:

$$\mathbf{G} = \begin{pmatrix} 0.5 & 0 \\ 0 & 0.5 \end{pmatrix}$$

Figure 2.9 shows an arrangement of particles with the L radius aligned to the same diagonal. This arrangement of particles corresponds to:

$$\mathbf{G} = \begin{pmatrix} 0.5 & 0.5 \\ 0.5 & 0.5 \end{pmatrix}$$

2.1.5 Summary

This section discussed some properties of granular materials and how they relate to their macroscopic behaviours. It also discussed the triaxial stress conditions and how soil strength is measured and described as well as the key assumptions related to the

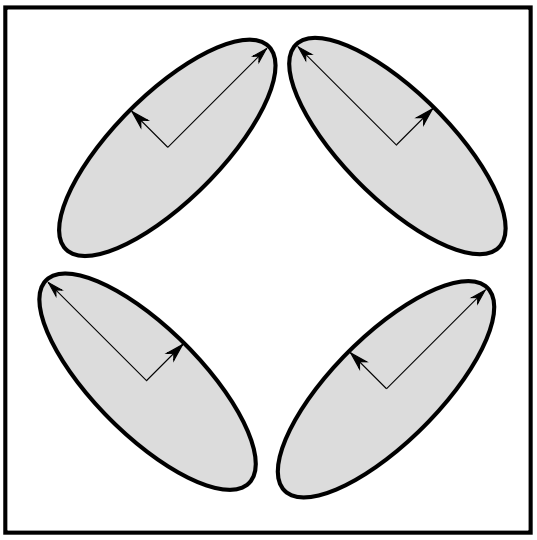

Figure 2.8: Examples of fabric orientation - Cross aligned

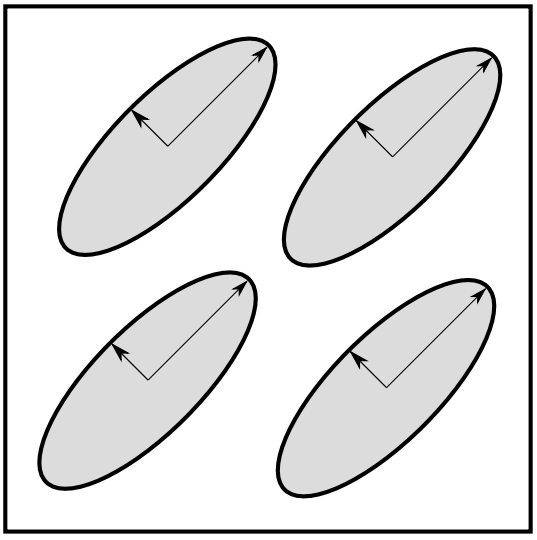

Figure 2.9: Examples of fabric orientation - Diagonal

test. Granular fabric is used to describe how particles are arranged within a soil; it can indicate if particles are aligned, have a cross pattern or a random ordering.

2.2 Characterisation of Particle Shape

Soils are generally described at a macroscopic level using the measures presented in the previous section. But as granular soils consist of individual particles each particle has a shape which can be used to fundamentally describe the particle. This section presents a discussion of previous literature on how particle shape is quantified.

One of the most common ways to describe the shape of a particle is to define it in terms of sphericity and roundness, Figure 2.10. Whilst these two words sounds similar they

represent different aspects of shape in this case; sphercity describes how spherical the overall shape is, where as roundness, more accurately called angularity, describes the relative sharpness of the corners. For example a star would be highly spherical however it would also be highly angular. However the use of this chart, in figure 2.10, is reliant on the engineer performing the description visually so results may not be consistent. Even though the chart is visual representation of Wadell's sphericity and roundness, (Wadell, 1932), a consistent measure is needed to measure dimensions on the particle so that the shape of the particle can be described; this idea was first conceived by Wentworth (1922).

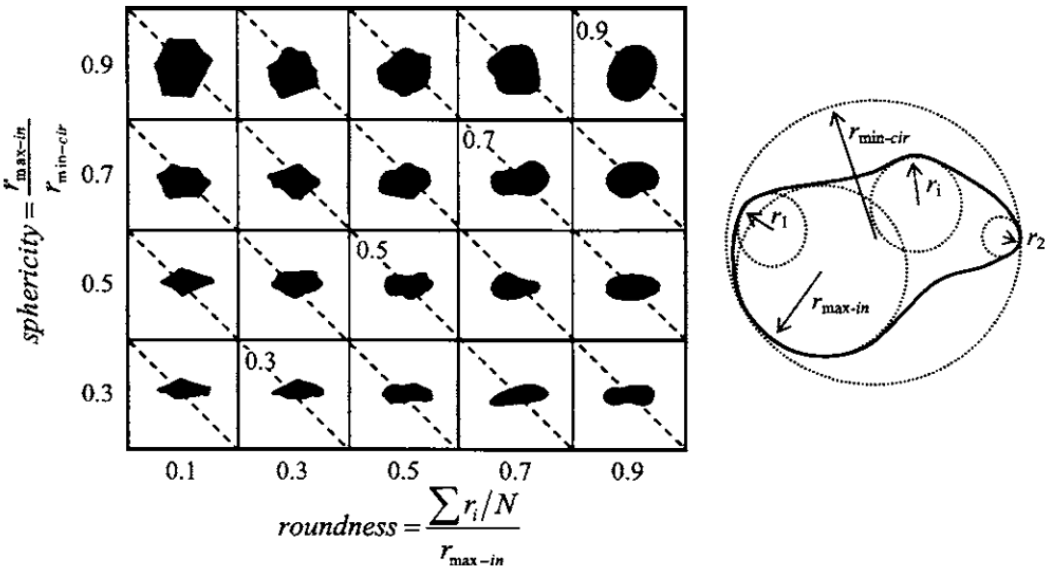

Figure 2.10: Sphericity and roundness chart defined in Krumbein (1941)

The description of shape is a well-developed field of research with multiple approaches having been made to characterize different shapes, (Blott and Pye, 2008). There is, however, a lack of consensus among researchers as to which method to use. It is generally agreed that particle shape has three independent aspects (Barret, 1980):

- Form / Sphericity: The form of a particle describes the general overall shape of the particle at a macroscopic level
- Angularity / Roundness: This describes the degree of sharpness of its corners and angles
- Roughness / Surface Texture: This describes the microscopic variations of a particle's surface and can be considered to control the interparticle angle of friction

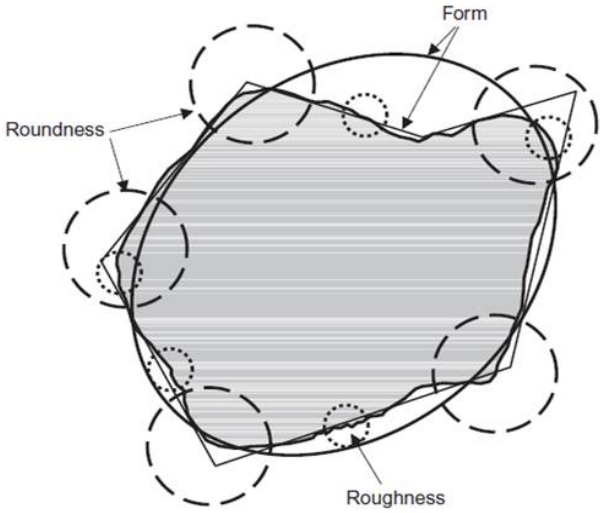

Figure 2.11: Different description of shape from Barret (1980) redrawn in Le Pen (2008)

2.2.1 Form

The first requirement of quantifying form is to define the dimensions used to describe the particle; this is the basis on which form is measured. One approach is to use the Length, Breadth and Depth dimensions, referred to as longest (L), intermediate (I) and shortest (S), (Blott and Pye, 2008). Whilst using L, I and S allows for more complicated forms to be represented, it is only used for describing coarse particles sizes. This is because measuring L, I and S is easily done by hand for coarse particles with the process becoming ever more time consuming the smaller the particle. For finer particles like clays this method becomes unusable as the individual particles are too small to see at individually so a different approach is required, (Clayton et al., 2009).

Despite the widespread use of L, I and S, these terms have never been strictly defined. It is generally agreed that these three distances must be measured orthogonally to each other but their point of intersection may vary. Krumbein (1941) and Blott and Pye (2008) made the case that it is important to have a consistent definition of L, I and S. It can be seen that the way the dimensions L, I and S are measured can vary the resulting form (Figure 2.12).

One of the earliest attempts to quantify form was introduced by Wentworth (1922) where the author introduced a term called flatness ratio (Equation (2.9)). The author's measurement is a significant improvement on the qualitative verbal description of shape previously used. Being only a single measure it has the limitation of being able to describe the flatness ignoring the difference of L and I. For example a particle with $L = 0.5$, $I = 0.5$ is represented by the same value as a particle $L = 0.9$, $I = 0.1$.

$$Wentworth\ Flatness = \frac{L + I}{2S} \tag{2.9}$$

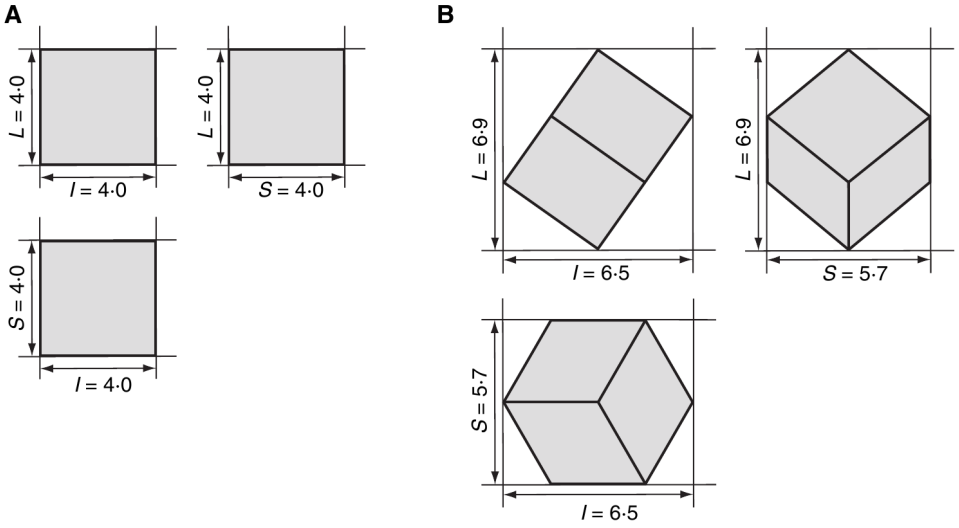

Figure 2.12: L, I and S measurements of a cube Blott and Pye (2008)

One of the most commonly used tools for measuring and verbally describing form is shown in Figure 2.13 (Zingg, 1935). Where measurement of form takes the simple ratios of the dimensions defining two measures, one for elongation and one for flatness (Equations (2.10) and (2.11)). The author differentiates forms into Spherical, Bladed, Elongated and Platy. These groups allow for a verbal description of a particle's form.

$$Elongation\ Ratio = \frac{I}{L} \tag{2.10}$$

$$Flatness\ Ratio = \frac{S}{I} \tag{2.11}$$

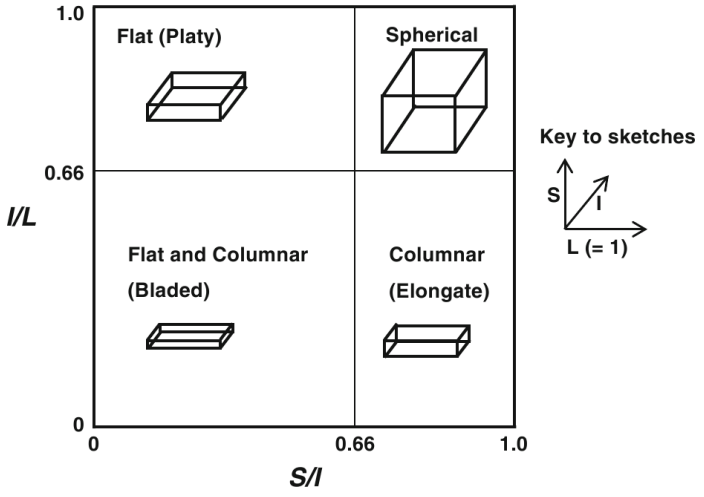

Figure 2.13: Plot showing range of forms available using the measurements in Zingg (1935) redrawn from Le Pen et al. (2013)

In Wadell (1932), the author introduces the idea of describing form in terms of its deviation from a reference particle which in this case was a sphere. The measure of form is termed sphericity and is defined as the deviation of surface area of the real particle compared to the surface area of a sphere with the same volume. This idea is then improved upon in a later publication, (Wadell, 1933), which compares the volume of the particle to the volume of the minimum circumscribed sphere (Equation (2.12)). This improvement was made due to the difficulties in measuring the area of the irregular surfaces of particles. Nevertheless Barret (1980) shows that the rounding of the edges of a cube changed the measured value of Wadell sphericity, demonstrating that this was not a measure of form but of angularity as well.

$$Wadell\ sphericity = \sqrt[3]{\frac{Vol_{original}}{Vol_{mincircumsphere}}} \tag{2.12}$$

Krumbein (1941) follows on from the ideas introduced by Wadell (1932) and Zingg (1935) to create a measure of form using L, I and S also called sphericty. However the major difference in assumptions compared to Wadell sphericity is that it uses an ellipsoid as the reference particle. The measure introduced is called intercept sphericity. This was argued to be conceptually purer measure than Wadell's sphericity as it is a measure of form alone, (Barret, 1980)

$$Intercept\ Sphericity = \sqrt[3]{\frac{I \times S}{L^2}} \tag{2.13}$$

The use of a single measure of form can not fully describe the general shape of a particle. Using a single measure will always lead to particles with different forms categorised by the same value, (Sneed and Folk, 1958). Also as a result of having three lengths, any normalisation needs two parameters to preserve all the information. Methods that use two or more distinct measures of form allow for more detailed description of form, such as in Zingg (1935).

To help distinguish the case of different forms having the same sphericity Aschenbrenner (1956) introduced a second complementary measure called Shape Factor. This ranged from 0 to ∞ and was later modified by Williams (1965) to have a range of -1 to 1.

Aschenbrenner (1956) also introduced a different measure of sphericity based upon a different reference particle shape. The author wanted a plane-sided figure form, finally using a tetrakaidecahedron allowing for a better approximation of real particles (Figure 2.14). The measure uses the ratio of the surface area of the particle to the surface area of the reference particle. Whilst this may have a form closer to real particles, it does not allow a sphere to have a sphericity of 1.

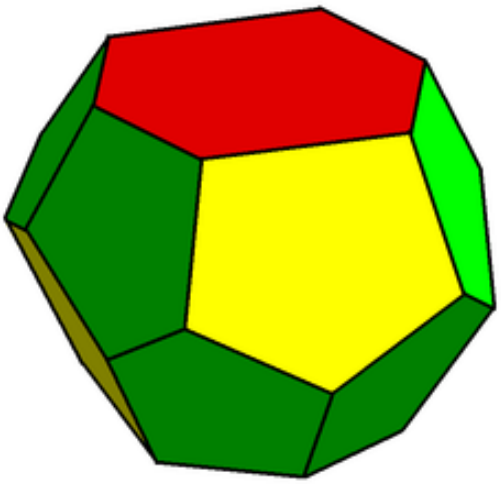

Figure 2.14: Tetrakaidecahedron

Most of these measures are unintuitive and further authors have provided verbal descriptions of particles so that they can be quickly identified and classified in the field.

With many different measures of form being presented it could be inappropriate to choose one measure over the other. Some measures may only be appropriate for different types of particles such as fine and coarse particles Blott and Pye (2008). Table 2.1 shows a variety of different measures of particle form.

2.2.2 Angularity

Whilst form describes the general macroscopic shape of the particle; angularity is generally used to describe the relative sharpness of the corners and edges, however there is no general consensus over that. Some authors treat roundness as the inverse of angularity however this is not universally agreed upon either, e.g. Blott and Pye (2008). Figure 2.15 shows some different measures of angularity.

Wentworth (1919), introduced the first method for characterising particle roundness based upon measuring the minimum radius of curvature for a particles sharpest corner. The measure was normalised against the longest dimension (L) of the projected outline so that the measure is scale invariant, Equation (2.14). However this measure alone does not fully describe the roundness of the whole particle.

$$Wentworth\ roundness = \frac{D_k}{L_w} \tag{2.14}$$

This was later revised in Wentworth (1922) where the measure is normalised against the mean particle diameter, Equation (2.15). This had the benefit over the original measure

Reference	Term	Formula
Wentworth (1922)	Wentworth flatness	$\frac{L+I}{2S}$
Zingg (1935)	Elongation ratio, Flattness ratio	$\frac{I}{L}$, $\frac{S}{I}$
Wadell (1932)	Sphericity	$\sqrt[3]{\frac{Vol_{orig}}{Vol_{mininscsphere}}}$
Krumbein (1941)	Intercept sphercity	$\sqrt[3]{\frac{I \times S}{L^2}}$
Corey (1949)	Corey shape factor	$\frac{S}{\sqrt{L \times I}}$
Folk (1955)	Maximum projection sphericity	$\sqrt[3]{\frac{S^3}{L \times I}}$
Sneed and Folk (1958)	Flatness, Flatness to the long axis	$\frac{S}{L}$, $\frac{L-I}{L-S}$
Aschenbrenner (1956)	Working sphericity	$\frac{12.8 \times \sqrt{P^2 \times Q}}{1+P(1+Q)+6 \times \sqrt{1+P^2(1+Q^2)}}$, $P = \frac{S}{I}$, $Q = \frac{I}{L}$
Aschenbrenner (1956)	Shape factor	$\frac{L \times S}{I^2}$
Williams (1965)	Williams shape factor	$I^2 > L \times S \; 1 - \frac{L \times I}{I^2}$, $I^2 <= L \times S \; \frac{I^2}{L \times S} - 1$
Janke (1966)	Janke form factor	$\frac{S}{\sqrt{\frac{L^2+I^2+S^2}{3}}}$
Dobkins and Folk (1970)	Oblate-prolate index	$\frac{10 \times \left(\frac{L-I}{L-S} - 0.5\right)}{\frac{S}{L}}$

Table 2.1: Table of different measures of particle form

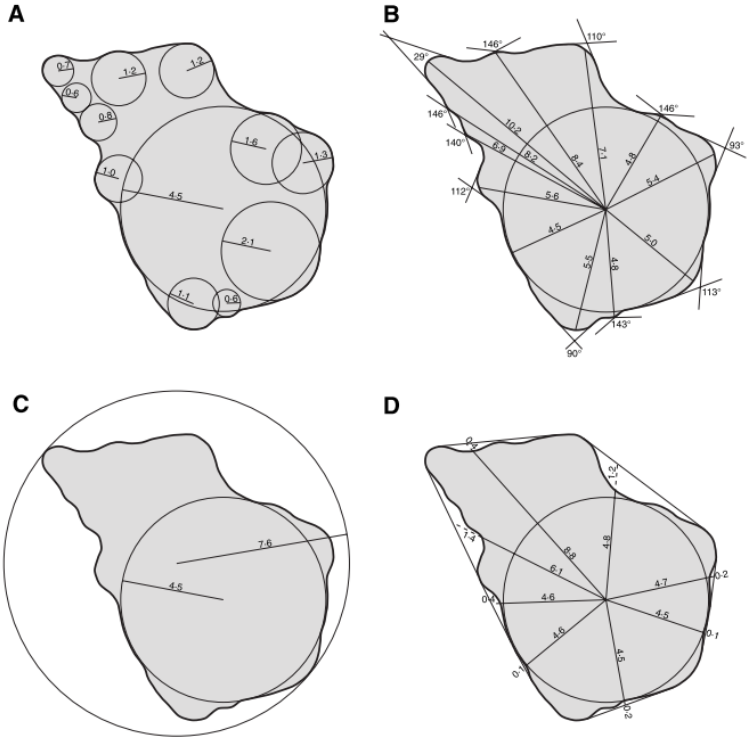

Figure 2.15: Example of common measures of angularity and roundness taken from Blott and Pye (2008). (A) Roundness (Wadell, 1932),(B) Angularity (Lees, 1964), (C) Circularity (Riley, 1941) and (D) Irregularity (Blott and Pye, 2008)

of reducing the effect that elongated forms have on the measure. The advantage that this measure has is it's simplicity and ease to calculate. A disadvantage is that, as the sharpest corner is used, this may not be representative of the whole particle, e.g. the case of slightly fractured particles would not be represented well, (Blott and Pye, 2008).

$$Wentworth\ roundness = \frac{D_k}{\frac{L+I}{2}} \tag{2.15}$$

In Wentworth (1919) the author focused on the sharpest corner. To improve on this idea further Wadell (1933) used the average roundness of all the corners. This introduces another problem , that of the definition of a corner which is:

> "Every such part of the outline of an area which has a radius of curvature equal to or less than the radius of curvature of the maximum inscribed circle of the same area" Wadell (1932)

This allowed for the case of two particles having the same value of roundness despite having different forms, e.g. a sphere and a cylinder topped by two half spheres would have a roundness of zero (Blott and Pye, 2008), Figure 2.16.

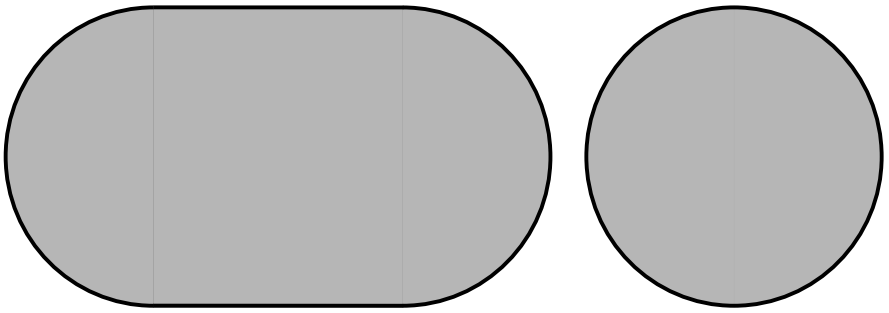

Figure 2.16: Wadell corner definition

There has been some debate about whether angularity is the inverse of roundness, however some authors have argued that they should be considered as independent measures. Lees (1964) proposed a measure called "Degree of Angularity" which sums the angle between bounding planes on a corner. This is normalised by a factor of how far away the corner is as well as the radius of the maximum inscribed sphere (Equation (2.16)). Figure 2.17 shows the values for calculating the angularity of a corner. This uses a 2D image requiring identification of corners so that the bounding planes can be extrapolated, which is time consuming and difficult.

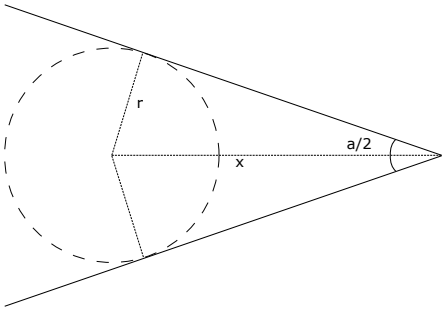

Figure 2.17: Definition of the angularity of a corner from Lees (1964)

$$A_i = (180^\circ - \alpha)\frac{x}{r}, A_{particle} = \sum_{i=1}^{n} A_i \tag{2.16}$$

Sukumaran and Ashmawy (2001) took this idea further by proposing two parameters, a shape and angularity factor. This is done by taking the outline of particles and fitting an approximate form to the outline by drawing 40 successive chords around the perimeter spaced at even angles radiating from the centroid, Figure 2.18.

The shape factor compares the difference in angles between the chords connecting points on the circumference and the chords of inscribed polygon, defining the α angle, Figure 2.19. The Angularity factor is measured as the angle between two chords compared to the internal angle of the inscribed polygon.

A different measure has been proposed called sphericity, which is not to be confused with the measure of form of the same name (for example intercept sphericity). The measure

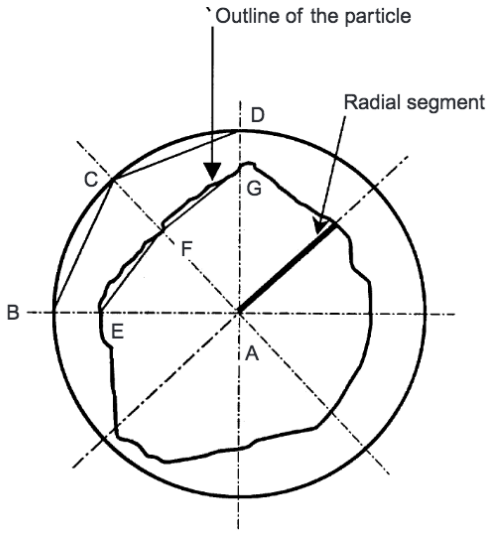

Figure 2.18: Chords around a particle. Taken from Sukumaran and Ashmawy (2001)

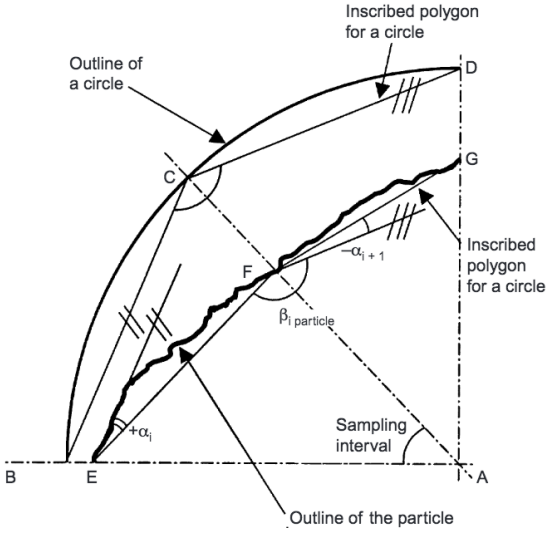

Figure 2.19: Measurements of the internal angles around between chords. Taken from Sukumaran and Ashmawy (2001)

normally compares the surface area or volume of the particle to that of a sphere with the same volume in 3D and perimeter or area of a circle in 2D, Barret (1980); Blott and Pye (2008).

Sphericity has the advantage, compared to other measures of roundness, that a high order polyhedron that has all faces meeting at edges would have a Wentworth Roundness of zero but a high sphericity value. It could also be argued that a sphere has an infinite amount of infinitesimally small faces and thus has no roundness.

Cox (1927) compares the the ratio of the area of the particle to the area of a circle with of the same perimeter length. However the perimeter length is difficult to measure for an irregular particle. Tickell and Hiatt (1938) take a 2D outline of a particle and compare

the ratio of the area of the particle to the area of a circle with the diameter being equal to the smallest circumscribing circle's. Wadell (1933) first method is the square root of the method suggested in Cox (1927).

Other measures of angularity use different variations of the previous measures by using ratios of different particle properties such as area and perimeter:

- Pentland (1927) takes a 2D outline of a particle and compares the ratio of the area of the particle to the area of a circle with diameter equal to the longest dimension of the particle
- Riley (1941) uses the square root of the ratio between the largest and the smallest inscribed circle.
- Janoo (1998) uses the perimeter and the area of the particle.

In Blott and Pye (2008) the authors introduced irregularity as a measure of angularity. For any 2D particle image a convex outline is used around the image as well as finding the inscribed sphere. By taking progressive points around the circle a measurement is made between the centre of the circle and the convex hull; this is summed over the number of points.

All these measures of angularity are calculated using a 2D particle, one way to turn these measures into a 3-dimensional measure is by averaging the angularity on planes following the particles principal axes, (Mollanouri Shamsi and Mirghasemi, 2012). To normalise the results the angularity measured from each projection is weighted by the respective surface area, equation (2.17)

$$Ang_{Particle} = \frac{Ang_{front} \times Area_{front} + Ang_{top} \times Area_{top} + Ang_{side} \times Area_{side}}{Area_{front} + Area_{top} + Area_{side}} \quad (2.17)$$

2.2.3 Summary

The measures presented in this section provide a framework for describing particle shape. This is done by considering three independent aspects of shape; Form, Angularity and Roughness. This is useful for simplifying the problem of describing complex particle shapes and allows for grouping of similar shapes.

There is a lack of a unified descriptor of particle shape that doesn't lead to a significant loss in detail. With particle form there is a general consensus on the concept of L, I and S but not on how the form is measured nor the measures to quantify it. Angularity proves a harder measure to quantify: there is not as much consensus as to what the measure describes and it also uses a 2D projection of the particle, which can lead to a loss of information. It is clear a holistic approach is needed.

Reference	Formula
Wentworth (1919)	$\frac{D_k}{L_w}$
Wentworth (1922)	$\frac{D_k}{(L+I)/2}$
Wadell (1932)	$\frac{\sum \frac{D_r}{D_i}}{n}$
Kuenen (1956)	$\frac{D_k}{I}$
Wentworth (1919)	$\frac{D_k}{D_i}$
Lees (1964)	$A_i = (180° - a)\frac{x}{r}, A_{particle} = \sum_{i=1}^{n} A_i$
Cox (1927)	$\frac{4\pi A}{P^2}$
Pentland (1927)	$\frac{4A}{\pi L^2}$
Tickell and Hiatt (1938)	$\frac{4A}{\pi D_c^2}$
Wadell (1933)	$\sqrt{\frac{4\pi A}{P^2}}$
Wadell (1935)	$\sqrt{\frac{4A}{\pi D_c^2}}$
Riley (1941)	$\sqrt{\frac{D_i}{D_c}}$
Janoo (1998)	$\frac{P^2}{A}$
Blott and Pye (2008)	$I_{2D} = \sum \frac{y-x}{y}$

Table 2.2: Table of different values of particle angularity and roundness

2.3 Effect of Particle Shape

It is generally accepted that soils that consist of different particle shapes will behave differently. For example some particles shapes may be able to form a denser packing or allow for particle interlocking with concavities which is the common explanation as to why angular particles lead to a higher critical state strength. In the previous section the different ways to measure particle shape were discussed, however these measures of shape may not relate to any change in macroscopic granular properties. There have been a mixture of empirical and numerical tests to investigate the effect that particle shape has, however the full extent of the effect of shape has upon granular material properties is unknown. In this section there will be a review of current and past literature on the effect shape has on:

- Void ratio
- Shear Strength
- Particle Size Distribution of a soil

2.3.1 Effect of Shape on Void Ratio

As void ratio describes the relationship between the volume of solids and the volume of voids within a soil, it is no surprise that this is also a function of particle shape. Whilst the theoretical e_{min} and e_{max} of a sample would depend solely on particle shape it may not be possible to reach that for every given soil. Because of this soil, properties such as void ratio in itself is not only effected by particle shape but also by the soil history and fabric.

Particle shape does effect the maximum and minimum void ratio, as stated in an earlier section, and the particles relative density changes the initial behaviour of the soil. The maximum void ratio is a function of both particle shape as well as the particle size distribution, Santamarina and Cho (2004). Some research exists into estimating particle shape effect on packing however this mainly is limited to single and two sized particles, Heitkam et al. (2012); Donev et al. (2004).

2.3.1.1 Particle Form

There does not exist much research of particles form's effect on void ratio but an empirical study from (Cho et al., 2006) which looked at how e_{min} and e_{max} changed with sphericity for a range of sand particles (Equation 2.19 and 2.20). Figure 2.20 shows that spheres are able to have the densest packing but as sphericity increases so does e_{min} and e_{max}. The range of possible void ratios also increases.

$$Sp = \frac{R_{max\ inscribed}}{R_{min\ encribed}} \tag{2.18}$$

$$e_{max} = 1.0 - 0.51Sp \tag{2.19}$$

$$e_{min} = 1.6 - 0.86Sp \tag{2.20}$$

The packing for spherical particles has been studied extensively in the literature as it is something that effects many different fields. The densest packing of mono-sized spheres is a void ratio of 0.35 but this requires a specific arrangement of particles, known as face-centred cubic structure, and is not a realistic estimate of the densest compaction. But as a true dense packing requires an regular ordering of particles a densest random packing can be defined, void ratio of 0.577 (Abbireddy and Clayton, 2010).

Delaney et al. (2011) used elongated ellipsoidal particles to simulate random packing. The random packing was achieved by placing particles in free space and allowing the

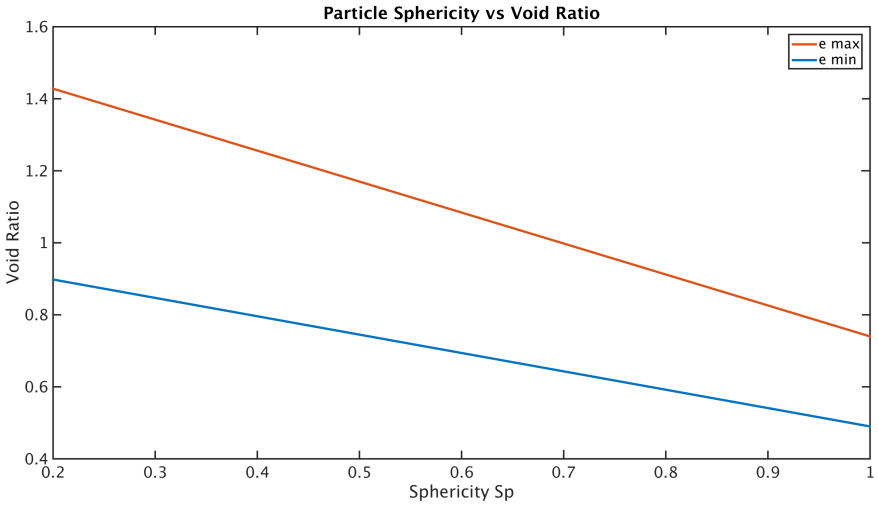

Figure 2.20: Particle sphericity vs empirical void ratio, Cho et al. (2006)

particle to settle, by treating void space as a viscous fluid. The results showed that 2D that spheres have the higher void ratio, initially as a particle becomes elongated the densest void ratio will start to drop. However after a certain point the increased elongation causes the minimum void ratio to rise, this is due to the random orientations of the particles causing large voids to appear.

2.3.1.2 Particle Angularity

Whilst theoretical estimates of e_{min} and e_{max} do exist empirical studies have also shown relationships between roundness and void ratio, Table 2.3.

$$Sp = \frac{\sum r_i/N}{R_{min\ encribed}} \tag{2.21}$$

Reference	e_{min}	e_{max}
Youd (1973)	$0.359 + 0.082R^{-1}$	$0.554 + 0.154R^{-1}$
Rousé et al. (2008)	$0.433 + 0.051R^{-1}$	$0.615 + 0.107R^{-1}$
Cho et al. (2006)	$0.8 - 0.34R$	$1.3 - 0.62R$

Table 2.3: Table of empirical estimates of e_{min} and e_{max} changes with roundness R and Sphericity Sp

Figure 2.21 shows how e_{min} and e_{max} change with roundness. As roundness decreases from 1, e_{min} increases slightly however a greater change is seen in e_{max}. This means as particles become more angular there is a greater range of potential void ratios. All measures consider a uniform particle size distribution with coefficient of uniformity Cu

= 1. As Cu changes the e_{min} will decrease as smaller particles can fill the void spaces between the particles.

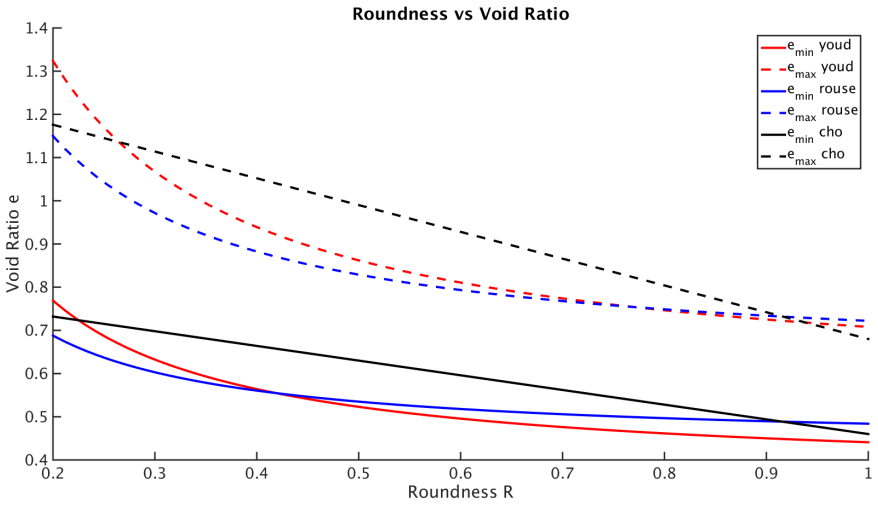

Figure 2.21: Particle roundness vs empirical void ratio, Youd (1973); Rousé et al. (2008); Cho et al. (2006)

Delaney and Cleary (2010) show the effect of different superellipsoidal particles and their random packing. It is found that as the particles become increasingly blockier their void ratio decreases.

2.3.1.3 Particle Roughness

Whilst changing the particle roughness does not significantly impact the theoretical packing of particles, it does practically change that situation. Decreasing the inter-particle friction allows a loose but stable assembly of particles to become unstable and compact. This fact has been used in numerical modelling as a way of allowing the particles to form a denser packing (Abbireddy and Clayton, 2010).

2.3.2 Effect of Shape on Strength

Spherical particles are generally used to model soil particles with DEM. In Radjaï et al. (1999); Radjaï and Azéma (2009); Estrada et al. (2009, 2011); Cambou et al. (2008); Azéma et al. (2013, 2012); Azéma and Radjaï (2010); Nguyen et al. (2015) the authors showed that any deviation in particle form from a sphere leads to an increase in the strength of the granular material. Preliminary results presented in Potticary et al. (2014) showed a similar trend.

Particle Form

To model the effect of form alone, a smooth particle with a constant angularity is needed.

A previous 2D study, Azéma and Radjaï (2010), looked at the effect that elongation has on the critical state strength. The authors used rounded cap rectangles (RCR) shaped particles which join two half spheres on to a rectangular segment (Figure 2.22).

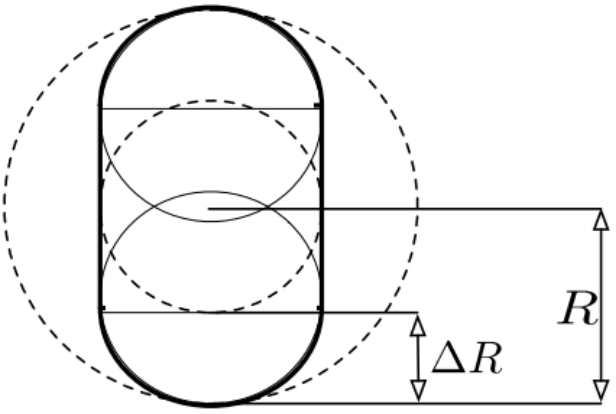

Figure 2.22: Rounded Cap Rectangle from Azéma and Radjaï (2010)

The form of a RCR is defined as the ratio between the radius of the half sphere, ΔR , and the distance from the centroid to the tip, R, Equation (2.22).

$$\eta = \frac{\Delta R}{R} \tag{2.22}$$

η ranges of values between 1 and 0 and the implications for particle form.

The main conclusions form this paper are that; as particle elongation (η) increases there is a linear increase in critical state strength, with particles tending to orientate themselves perpendicular to the major principal stress direction. Contacts can be split into three different categories cap-cap, cap-side and side-side. Cap-side seems to guide the force through the model as elongation increases, cap-side contacts increase as a proportion of contact types.

In Boton et al. (2013) the authors sought to study the effect of platy particles and their change in strength. This was an extension of the work done in Azéma and Radjaï (2010) which used RCR formed particles; in extending this work to 3D the authors used a spheroplate (Figure 2.24). The authors define a term η which describes the flatness of the particle (Equation (2.23)).

η ranges of values between 1 and 0 and the implications for particle form.

$\eta = 0, sphere$

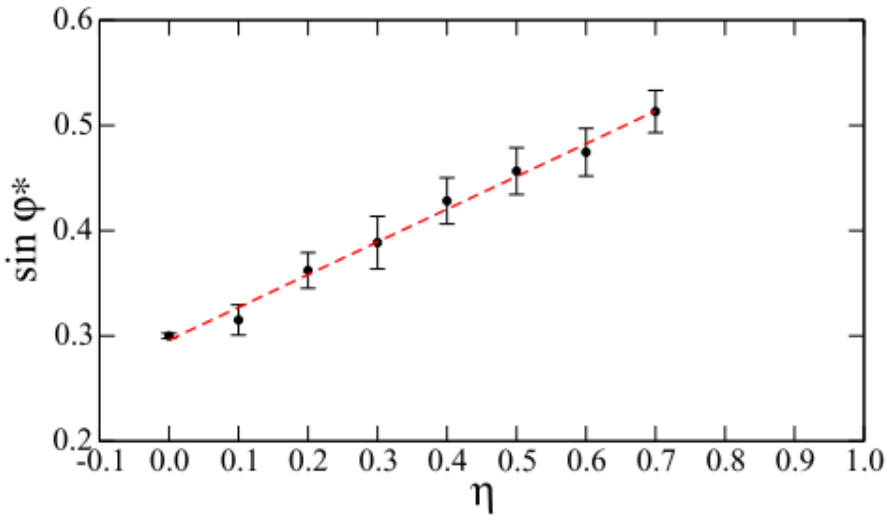

Figure 2.23: Mobilised Angle of Friction against Elongation (η) for RCR, Azéma and Radjaï (2010)

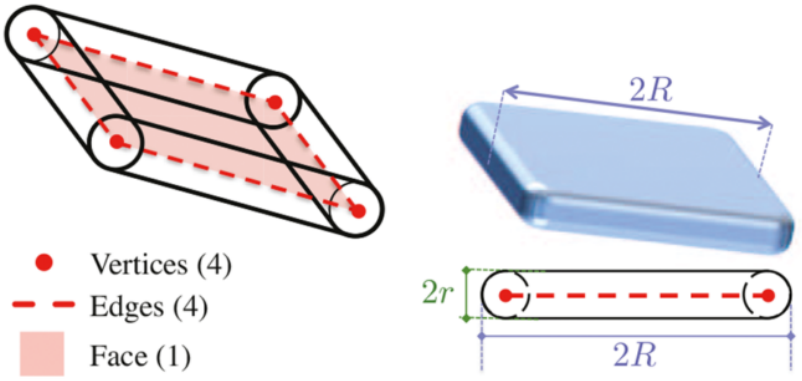

Figure 2.24: Spheroplate from Boton et al. (2013)

$\eta = 1, line$

$$\eta = \frac{R - r}{R} \tag{2.23}$$

In this paper mono-sized particles were used in a DEM model with isotropic stress conditions similar to triaxial stresses, and the model was subjected to straining. At critical state the strength of the model was calculated and this was then compared across different models with different forms (Figure 2.25). This shows that as the particles become flatter there is a linear increase in the soil's strength at critical state.

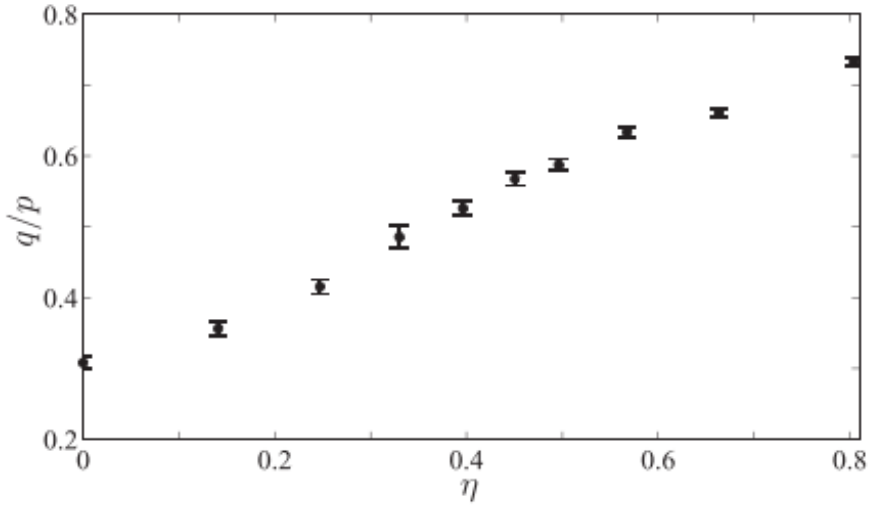

Figure 2.25: Ratio of deviatior stress over average stress for different forms of spheroplates (Boton et al., 2013)

Particle Angularity

In Radjaï et al. (2013), the authors measured the effect of angularity on the critical state strength. The particles were created by randomly adding flats to a spherical particle. Figure 2.26 shows a typical particle. The particle's form was controlled by not allowing the eccentricities to grow in any particular dimension, ensuring that L, I and S remained relatively equal. Whilst the effect of form was not completely removed, it was controlled to the extent so that it's influence should be negligible compared to the different angularities.

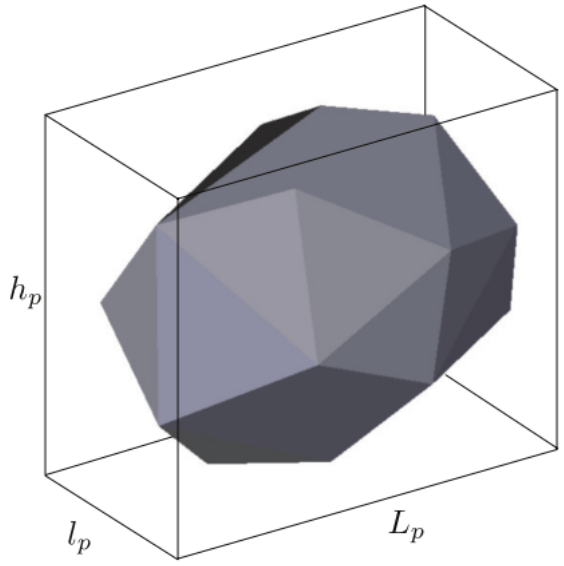

Figure 2.26: Angular particle from Radjaï et al. (2013)

The particle's angularity was measured by using the mean angle between the planes. As the number of planes that represented a particle increase the measured angularity of a particle decreased.

Figure 2.27 shows the critical state stress ratio against different angularity. They showed that by increasing the angularity of the particles there was an increase in the critical state strength.

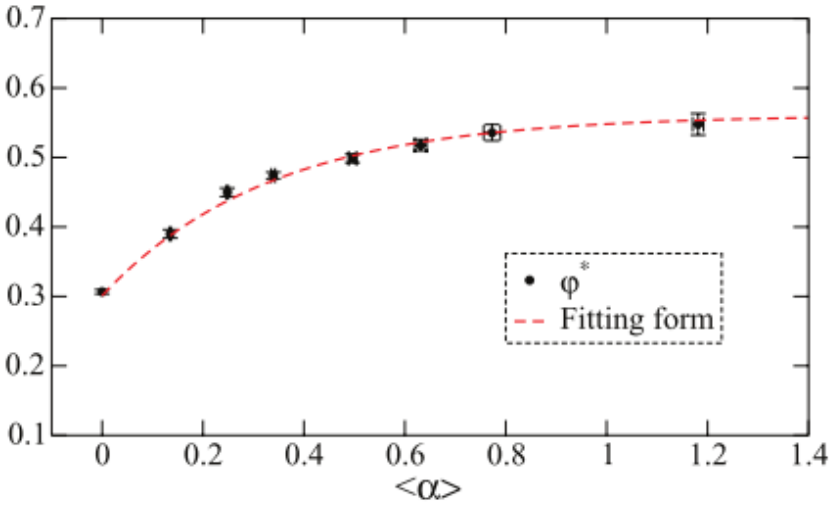

Figure 2.27: Figure showing the change in angularity $< \alpha >$ against critical state strength, Radjaï et al. (2013)

Particle Roughness

Particle roughness can be described as the microscopic variations on the particle's surface. It is related to the interparticle friction angle of the material (Jensen and Bosscher, 1999). This friction angle controls the dry friction of the material. Many authors in the past have studied the effect that varying interparticle friction angle has on the critical state angle of friction (Figure 2.28). It has been found that higher the interparticle friction angles, have a reduced effect on increasing the critical state angle of friction for 2D simulations. At higher interparticle friction angles there is a diminishing increase and past $30° - 40°$ the impact of changing the friction angle is negligible (Cambou et al., 2008; O'Sullivan et al., 2002). An explanation for this is that the friction angle only controls the limit of sliding. As the interparticle friction angle increases the limit of which a contact can slide also increases however there is a maximum amount of shear force that can be generated at a contact.

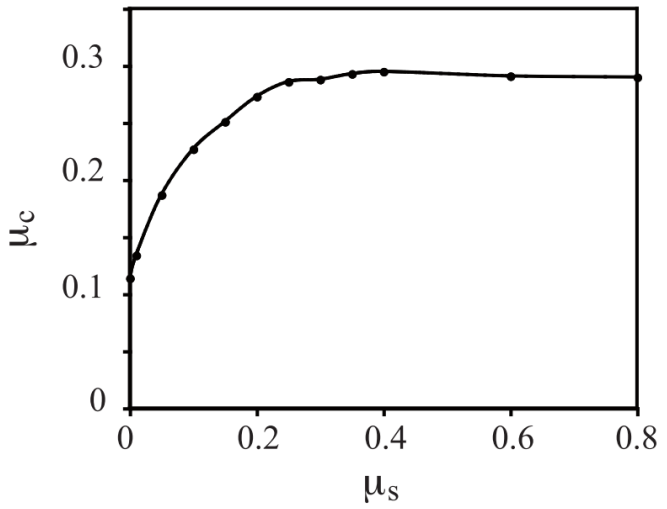

Figure 2.28: Friction angle against critical state angle of friction from Cambou et al. (2008)

2.3.3 Summary

Particle's shape has shown to have a significant effect on the granular properties of a material. It has shown that spherical particles have the lowest strength out different angularity and forms. However for spherical particles the coefficient of friction of the material has a reduced effect the higher the friction. Increasing the coefficient of friction past 30 degrees does not increase the mobilised angular of friction of the soil.

With particle form any deviation from the form of a sphere lead to an increase in strength and with the elongated particles in 2D and 3D tended to orientate themselves perpendicular to the loading.

2.4 Railway Ballast

Whilst most granular soils are created through geological processes, railway ballast is engineered through mechanical processes for a single purpose. As such there are limits placed upon what can be used as ballast. These limits are imposed through the British Standard for Railway ballast however despite being an engineered material there is a lack of understanding as to the micromechanics of ballast and how they relate to it mechanical properties. This sections presents:

- Ballast properties such as PSD, parent material and ballast shape
- Literature related to ballast performance

2.4.1 Ballast properties

Ballast is not a single material but there is a specification for the properties the material has to contain. For example the particle size distribution / Strength of the particles / the limits of proportion of flakiness and platyness of the aggregate.

Surface roughness is fully dependant on the type of material such as the particle shape and if the surface is polished and this will depend on the way the material was prepared.

Whilst the shapes of individual ballast particles are not controlled, there is a limit placed on the amount of different shaped particles, This is controlled by using the flakiness and shape index of a set of ballast particles. The current specification for British standards creates different grades of ballast depending on the flakiness and shape index. Highest specified ballast is one that has a spherical form and is highly angular however no specification on a value / measure of angularity is given.

Ballast Particle Shape

From the specification, there are limits placed on the proportion of flaky and elongated particles that a given amount of ballast can contain, with a preference for particles with a spherical form and high angularity. The shape of ballast is measured using a shape and flakiness index (Equation (2.24) and (2.25)).

$$Flakiness = \frac{Weightofpassingflakyparticles}{remainingweight} \times 100\% \tag{2.24}$$

$$Shape\ index = \frac{1.27^4 \times L^2}{L} \tag{2.25}$$

Once the shapes have been measured the ballast is then placed into categories (Figure 2.29 and 2.30).

A previous study looked at a sample of railway ballast, measuring the particle shape (Le Pen, 2008). Figure 2.31 shows the distribution of the shapes based upon the Zingg measurement of shape. There is a general spread of shapes but it is generally clustered around the spherical forms.

Particle Size Distribution

The particle size distribution for fresh railway ballast specified to be with a range of values given in ISO (2009). Figure 2.32 shows the upper and lower banding for railway ballast in the UK as well as the mean particle size.

Flakiness Index	**Category** FI_{RB}
≤ 15	FI_{RB} 15
≤ 20	FI_{RB} 20
≤ 25	FI_{RB} 25
4 to 25	FI_{RB} 4/25
> 25	FI_{RB} Declared
No requirement	FI_{RB} NR

Figure 2.29: Range of different flakiness values for Network Rail ballast (BS EN, 2013)

Shape Index	**Category** SI_{RB}
≤ 10	SI_{RB} 10
≤ 20	SI_{RB} 20
≤ 30	SI_{RB} 30
5 to 30	SI_{RB} 5/30
> 30	SI_{RB} Declared
No requirement	SI_{RB} NR

Figure 2.30: Range of different shape index values for Network Rail ballast (BS EN, 2013)

In Le Pen et al. (2013), the author looked at the range of shapes of railway ballast and showed a relationship between the size of the catching sieve and the Intermediate axis of the particles (Table 2.4).

Sieve size (mm)	9.5	11.2	13.2	16	22.4	31.5	40	50
Average S (mm)	7.8	9.2	9.5	12.5	19.9	25.9	27.9	30.7
Average I (mm)	11.4	13.1	13.1	18.4	29.4	39.5	47.5	55.3
Average L (mm)	18.9	20.0	19.6	27.5	50.5	71.0	74.9	81.7

Table 2.4: Relationship between passing sieve and the average L, I and S dimensions of the particles

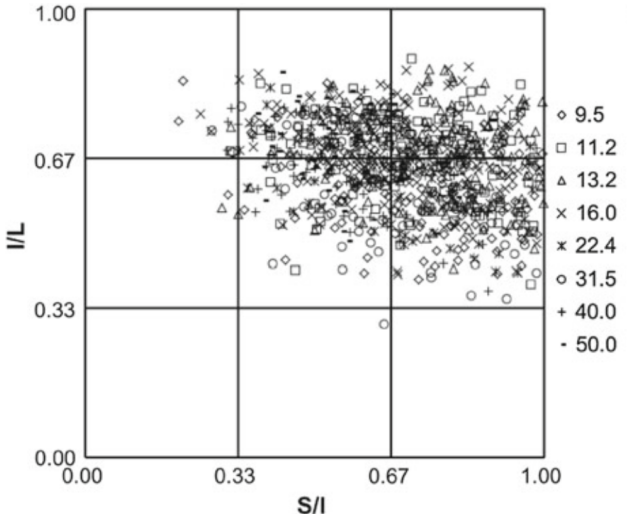

Figure 2.31: Range of particle forms for different ballast sizes

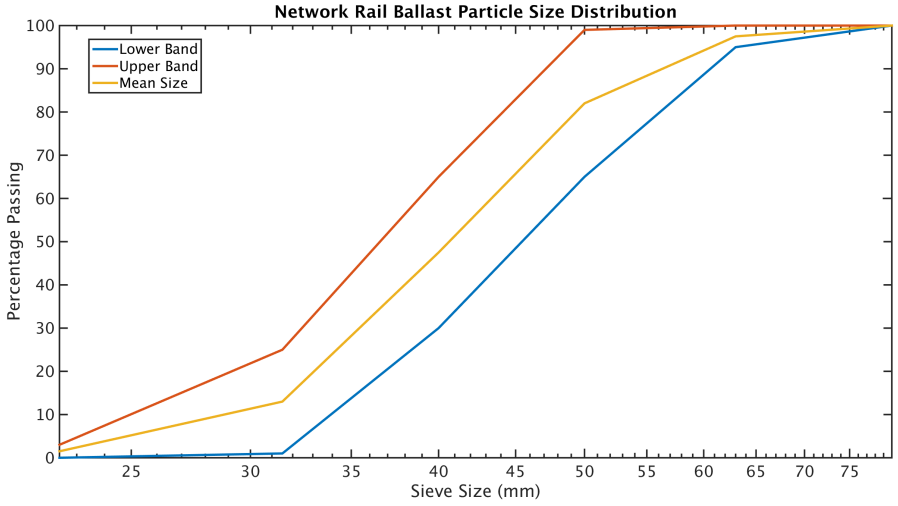

Figure 2.32: The valid range of PSD for railway ballast in the UK

Parent Material

Typically in the UK ballast is made from crushed granite. Table 2.5 shows the range of values of different mechanical properties of granite.

Property	Value
Density ρ	$2650 - 2750 Kg/m^3$
Elastic Modulus	70 GPa
Poisson's Ratio	0.25
Shear Modulus	7 GPa

Table 2.5: Range of properties of granite

2.4.2 Ballast performance

The main purpose of ballast within a track system is to act as a stiff element and to distribute the load down to the subgrade (typically a soft soil in the UK). This reduces the overall settlement of the track by spreading out the load from the highly stiff steel track to the soft subgrade, so as not to overload a single element leading to a catastrophic failure.

The type of loading that the track system is regularly subjected to is that of high frequency cyclic loading. The exact loading is a function of the number of axles present on the train, the speed the train is going and the distributed weight of the train amongst the axles.

These load cycles cause the ballast to compact and cause settlement; this in itself does not cause ballast to fail instead causes differential settlement (The track settling a different rates along it's length). This causes a change in track geometry and increased vertical movement for the train. At a small scale this can be unpleasant for the passengers but at a larger scale this can be dangerous and cause derailments with potentially lethal consequences.

To reduce the risk of this routine maintenance is carried out on the network. This is governed by sending recording instruments along the track, be that on a specialised train or other means.

2.5 Discrete Element Method

In this section a overview of the Distinct element method (DEM) reviewing the differences in contact models and some of the assumptions associated with them. DEM is a modelling technique that models each particle individually. By doing so, organic contact structures develop naturally based upon physical properties of the particles (Cambou et al., 2008). As each particle has to be resolved individually, it can be computationally intensive to solve large problems due to the number of particles involved. As computational speed has increased over the years so have the complexity of the systems tackled.

The following chapter discuss:

- How particles are represented and created
- Contact models
- Boundary Conditions
- Model creation

2.5.1 Particle Representation

The assumptions of how a particle is described within the model sets the limits of what can be modelled;

- A 2D or 3D model of a particle my be used
- Using simple shapes, such as a sphere, ellipsoid or polygons
- Limiting to convex shapes
- Using smooth mathematical functions to describe particle shape

In this study an in house code is used, Harkness (2009), which uses the concept of describing particles using smooth functions ("Potential particles").

2.5.2 Contact Models

Particle motion can be described through Newtonian physics, which does not describe how particles interact. To describe how particles interact a contact model is used (Cambou et al., 2008). A contact model is a set of assumptions and rules that quantify the forces at particle contacts. For modelling coarse particles the contacts are modelled as mechanical ones however to model fine particle such as clay, the electrostatic forces may also be considered (Cambou et al., 2008). For coarse particles, DEM approaches can mainly be split into two types: those considering soft body interactions and those considering hard body interactions (also known as non-smooth dynamics) (Radjaï and Richefeu, 2009).

Soft body interactions allows for some inter-particle penetration (Figure 2.33) and the contact forces arise from a set of spring and dash-pots. The spring dash-pot system consists of two systems, one system to describe the normal force and the other to describe the shear force. With the magnitude of the forces being dependant on the amount of penetration and the spring stiffness. The spring stiffness's can be described by either linear or non-linear equations. The linear spring is the simplest method as it contains a constant spring stiffness. However, this may not describe the type of contact adequately. Non-linear springs derive their spring stiffness for each contact individually. One method of doing this is assuming a Hertzian contact, which depends on the relative curvatures of the particles at the contact, Harkness (2009).

The dash-pot within the model acts to reduce rapid compression of the contact spring and to damp the response (Ahmed et al., 2015). There are two methods for modelling a dash-pot one being viscous damping which is proportional to the velocity of the particles

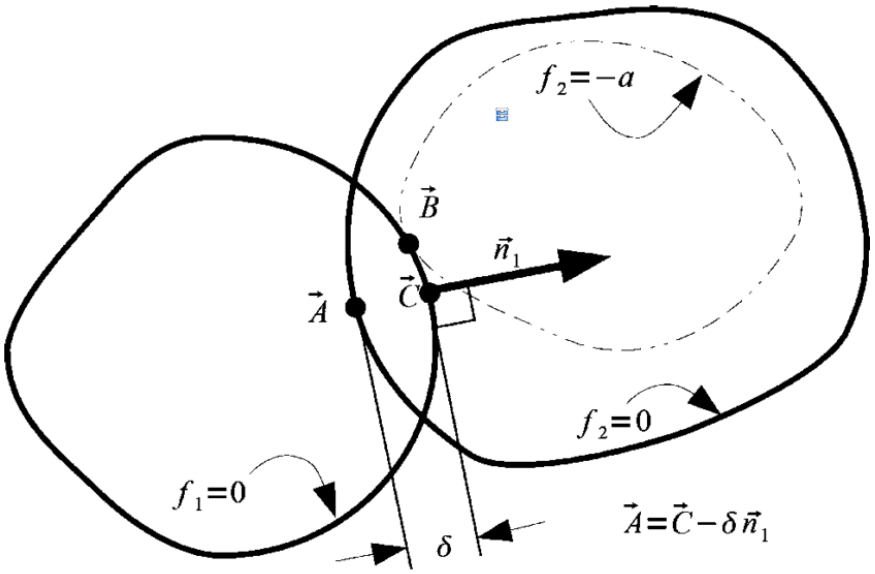

Figure 2.33: Particle overlap Harkness (2009)

and the other being a linear damping which provide a opposite force to the normal spring (Ahmed et al., 2015).

When dry surfaces are in contact there is a limit on the amount of shear force that the contact can develop based on the signorini-coulomb condition (Cambou et al., 2008). This states that the maximum shear force that can be developed is equal to the normal force times by the coefficient of friction (μ) at the contact, Equation (2.26). Once this condition has been met the contact is described as sliding, as the shear force cannot resist the motion of the particle.

$$F_s \leq \mu F_n \tag{2.26}$$

Due to particles being treated as rigid bodies interacting through forces at individual contact points, stress can not be directly measured (Cambou et al., 2008). What can be measured is the average stress tensor (σ_{ij}) corresponding to the contact forces within a reference volume V (Equation 2.27).

$$\sigma_{ij} = \frac{1}{V}\sum_{i=1}^{k} F_i \times L_j \tag{2.27}$$

F is the total force at the contact, L the branch vector between the centroids of two particles in contact and k the number of unique contacts with the volume.

Once the overlap is found a contact model is used to calculate the inter-particle force, based on a Hertzian contact model described in Harkness (2009). The force normal to

the contact plane is calculated directly as a function of the overlap. The tangential force (shear force) is calculated based off the previous timestep and relative movement and rotation.

The normal force is expressed as Equation (2.29)

$$R_c = \sqrt{R_a R_b} \tag{2.28}$$

$$F_n = K_n \delta \tag{2.29}$$

$$K_n = \frac{4}{3} E \left(\frac{R_c \delta}{F_2^3} \right)^{\frac{1}{2}} \tag{2.30}$$

$$F_2 \cong 1 - \left[\left(\frac{R_a}{R_b} \right)^{0.0684} - 1 \right]^{1.531} \tag{2.31}$$

The shear spring is expressed as Equation (2.32)

$$K_s = 8 G F_1 \left(\frac{3 R_c R_a F_n}{4 E R_b} \right)^{\frac{1}{3}} \frac{1}{\Phi} \tag{2.32}$$

$$F_1 \cong 1 - \left[\left(\frac{R_a}{R_b} \right)^{0.0602} - 1 \right]^{1.456} \tag{2.33}$$

$$\Phi = \begin{cases} 1 + (1.4 - 0.8\nu) \log \left[\frac{R_a}{R_b}^{\frac{2}{3}} \right] & R_a < R_b \\ 1 & R_a = R_b \\ 1 + (1.4 + 0.8\nu) \log \left[\frac{R_a}{R_b}^{\frac{2}{3}} \right] & R_a > R_b \end{cases} \tag{2.34}$$

For each particle the resulting forces and moments are summed which give rise to particle accelerations. The accelerations are then integrated using an explicit integration scheme to determine the updated particle positions and velocities at the next time step. Figure 2.34 shows the full algorithm for each time step.

2.5.3 Boundary Conditions

Due to the computational costs involved in modelling large numbers of particles there are limits as to the size of simulations that can be run. There have been many different

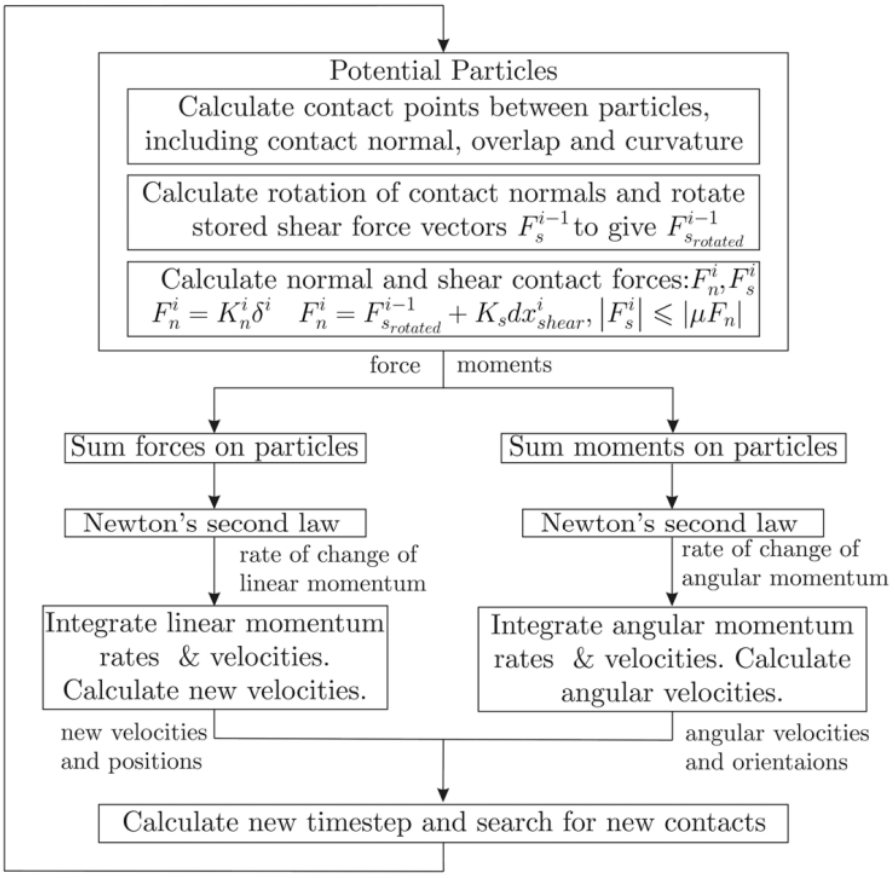

Figure 2.34: DEM simulation cycle Harkness (2009)

attempts to reduce the number of particles involved within the simulation whilst keeping computational cost low. One method is to couple both DEM and FEA models together with DEM controlling local interactions and finite element analysis controlling the far field interactions and boundary conditions. DEM is suited to smaller scale geotechnical simulations where the complexity of the system is relatively low such as triaxial cells or using a representative volume element (RVE). A RVE is used to reduce the size of the model by assuming the volume is larger enough for any microscopic variations within the model to be present within the element so that it is representative of the whole soil.

The types of boundary conditions applied to the model will also affect how the model will behave. A periodic boundary is a technique to increase the number of particles within the model without increasing the size of the model. This is done by mirroring the interactions and contacts of one boundary with the corresponding boundary on the model.

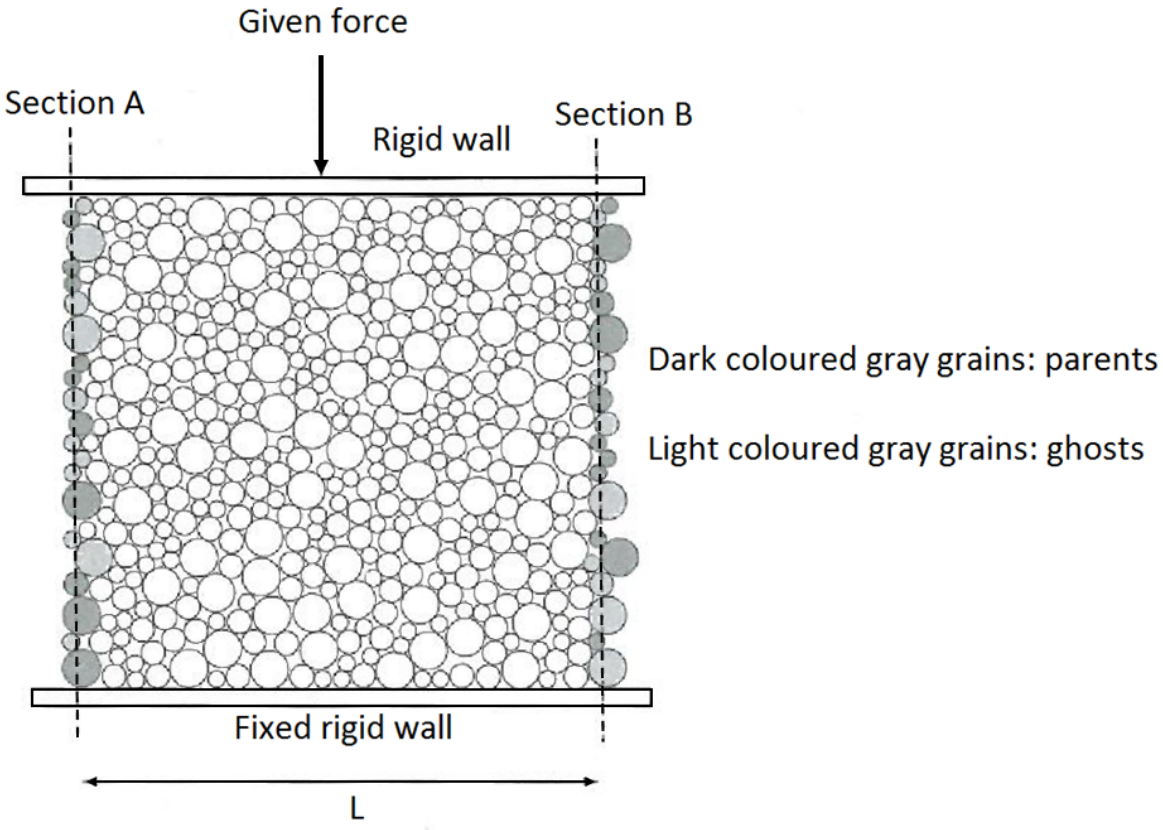

Figure 2.35: Periodic Boundary Condition Cambou et al. (2008)

2.5.4 Model Set Up

Models have been previously set up in different ways. These have different implications on how dense the model will initially be, and different types of model (Periodic cell / simulated membrane) will need different methods.

One method is to allow the objects to fall naturally under gravity and to form a compacted model. This can allow a model to fill a more realistic configuration with a stable structure.

Another method is to distribute the particles randomly and compress them to a desired state. This can allow the structure to reach a relatively dense state however there is not a great deal of control over the final density. If this is done without gravity on there is also a risk of smaller particles being left floating within the void spaces and not contributing towards the skeleton.

2.6 Conclusion

In this chapter has considered relevant literature related to granular materials, the measures and effects of particle form as well as overview of railway ballast and using the discrete element method.

The strength of granular materials is not an easy measure to quantify, as it doesn't follow a consistent measure as the same soil can have different stiffnesses and peak strength depending on how dense the soils was or how the particles are arranged and orientated.

A lot of measures around granular materials are based off the macroscopic properties of the soil with little consideration as to what is happening as a particle scale.

Because of this general macroscopic view little is known about the source of granular soils strengths and the physical mechanisms that control it. Spherical soils appear to have the lowest strength and increasing the angularity of a granular assembly also increase the strength.

Chapter 3

Particle Shape

In the previous chapter many different measures of shape were presented and discussed however there was no single method that considers the shape of a 3D particle with many authors choosing to consider form and angularity separate. In this chapter, a new method for characterising and measuring particles form will be presented. The new measure is based on the concept that form can be represented by an equivilient scalene ellipsoid, first discussed in Clayton et al. (2009). This study uses the traditional three aspects of form, angularity and roughness. Form is measured using the radius of the equivalent scalene ellipsoid and is split into two independent measures, platyness and elongation. Angularity is quantified by the difference between the particle and it's equivalent scalene ellipsoid. Particle roughness is defined based of the interparticle coefficient of friction for the material at the contact.

3.1 Definition of Particle Shape

3.1.1 Form

Over the years many different ways to describe particle form have been presented, with many authors contributing to the debate Aschenbrenner (1956); Folk (1955); Barret (1980); Zingg (1935); Williams (1965); Wentworth (1922); Wadell (1932); Sneed and Folk (1958); Krumbein (1941); Dobkins and Folk (1970). One of the most common methods is to use a simple solid to represent the particle, and assume that the form of the particle can be determined with reference to the geometry of that solid. The simplest such solid that can be defined in 3D is a sphere.

The definition of form that we use in this study is detailed in Potticary et al. (2014). A scalene ellipsoid is used as reference solid; such an ellipsoid is the simplest smooth shape that allows three independent radii, corresponding to a particle's longest (L), intermediate (I) and shortest (S) dimensions, Equation (3.1).

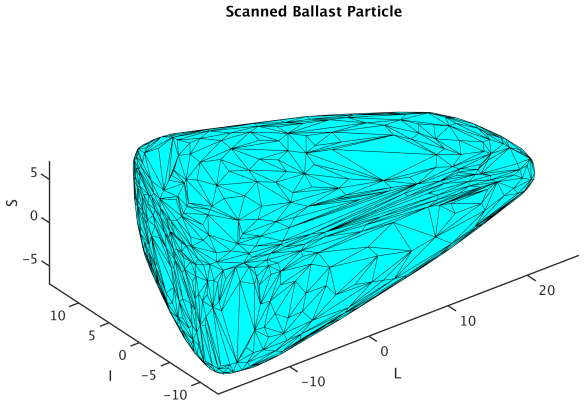

Figure 3.1: Scanned ballast particle

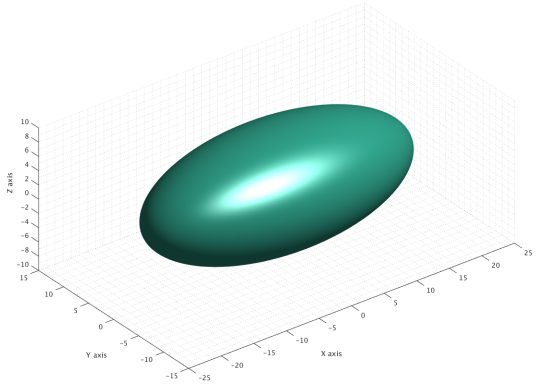

Figure 3.2: Fitted form of ballast particle

$$\left(\frac{x}{R_x}\right)^2 + \left(\frac{y}{R_y}\right)^2 + \left(\frac{z}{R_z}\right)^2 = 1 \tag{3.1}$$

$$R_x = \frac{L}{2} \qquad R_y = \frac{I}{2} \qquad R_z = \frac{S}{2}$$

By considering S , I and L to be coordinates in a three dimensional space, any particle can be represented by a vector $\mathbf{f}$ linking the origin of the axes to point (S, I, L). It can be reasoned that collinear vectors represent particles with the same form but different sizes. Clearly the shape (form) of the particle is represented by the direction of $\mathbf{f}$, whereas the length of $\mathbf{f}$ merely quantifies the size of the particle.

To quantify form, the intersection F of $\mathbf{f}$ with the $S + I + L - 1 = 0$ "deviatoric" plane, which is normal to the spherical axis $S = I = L$ along which all spherical particles plot. The "deviatoric" plane is then limited for the case of a scalene ellipsoid where $L \geq I \geq S$. The form of each particle is then uniquely defined by the two in-plane

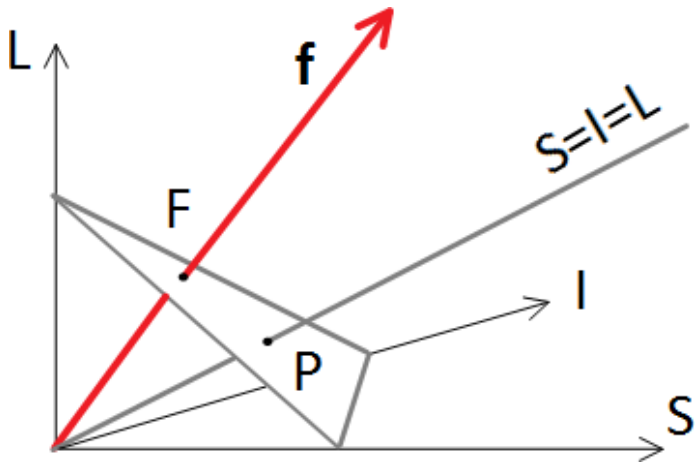

Figure 3.3: LIS space

coordinates of F in a frame of reference centred at the intersection P of the spherical axis. In this way particle form is essentially quantified as the deviation of a particle's shape from that of a sphere. These two independent parameters of form, normalised in the $[0, 1]$ interval for ease of use, are given by Equations 3.2 and are referred to as *platyness* (α) and *elongation* (ζ) respectively.

$$\alpha = \frac{2(I - S)}{L + I + S} \qquad \zeta = \frac{L - I}{L + I + S} \tag{3.2}$$

Ellipsoids that share the same values for both α and ζ are geometrically similar, i.e. they differ only in size but not shape. All possible scalene ellipsoids plot, on the α-ζ plane, within the triangle shown in Figure 3.4. The edges and corners of the triangle correspond to degenerate cases where some of the dimensions are equal and/or zero:

- Sphere $\alpha = \zeta = 0$
- Prolate ellipsoid $\alpha = 0, \zeta > 0$
- Oblate ellipsoid $\alpha > 0, \zeta = 0$
- Flat circular disk $\alpha = 1, \zeta = 0$
- Elliptical disk $\alpha + \zeta = 1$
- Needle $\alpha = 0, \zeta = 1$

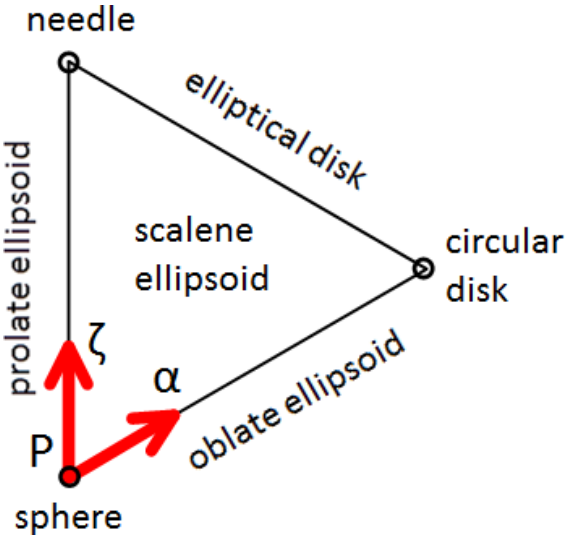

Figure 3.4: Elongation and Platyness space with description of forms

3.1.2 Angularity

In the previous chapter the majority of the measures of angularity required a 2D projection of a particle. This is problematic as it involved a choice of which one to use, this is normally found by allowing the particle to rest on its most stable face. This has some issues in that the angularity can change depending on which projection is used.

For this study a new measure of angularity is used. Angularity is defined here as the similarity between particle shape and particle form (equivalent scalene ellipsoid). A lower value of angularity means that a particle's shape is closer to its form. For example a sphere or an ellipsoid would have zero angularity as the form of the particle exactly fits its shape. As the shape deviates further from its underlying form angularity increases.

Angularity is measured as the volumetric difference between the shape and the form normalised against the particles volume (Equation (3.3)). The limits of this equation are between $[0, 1]$.

$$Angularity = \frac{|\sum Volumetric_{diff}|}{Vol_{particle}} \tag{3.3}$$

Angularity $= 0$, $\sum Volumetric_{diff} = 0$ (The form of the particle exactly matches that of is shape)

Angualrity $= 1$, $\sum Volumetric_{diff} = Vol_{particle}$ (This is an impossible case as the volumetric distance will always be less than the volume of the original particle)

Figure 3.5 shows a 2D analogy for angularity. Both the equilateral triangle and the pentagon have the form of a circle. The outer (blue) area represents the difference in volume between the particle shape and its form. The pentagon has a closer fit to its form, compared to the triangle, therefore it has a lower measure of angularity.

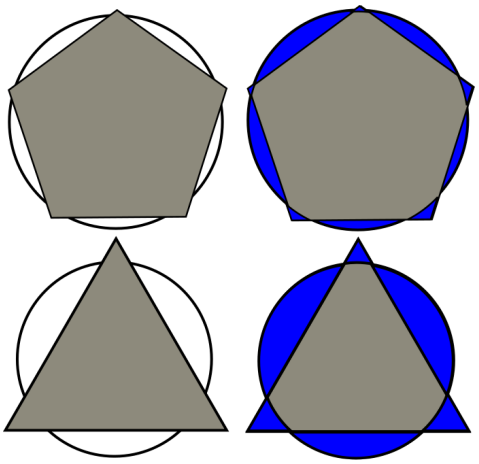

Figure 3.5: Differences in angularity with different perspectives

3.2 Measuring Particle Shape

As it is tedious to measure a particle's shape by hand, it is advantageous to develop an algorithm to automate this. A point cloud was used to describe the particle to the computer. A point cloud is a series of points on the surface or inside the particle given by a series of (x, y, z) coordinates each representing a voxel (3D equivalent of a pixel) or a cube. The number of points representing a shape can vary with a higher resolution the smaller the voxel. Figures 3.6 and 3.7 shows different voxel size and how it relates to the resolution of the particle.

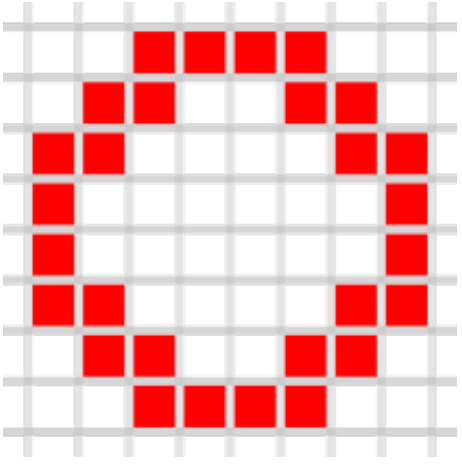

Figure 3.6: Different resolutions of voxels. 8 x 8

There are two types of points clouds that can be used, one consists of points on a regular grid representing voxels of the same, and can be used to describe the whole volume of the particle. This regular grid is normally found from CT-scan data built up using a series of layers. The other consists of individual points, and can be used to describe the surface of a particle. An irregular grid comes from a 3D scanners but this is limited to just the surface data.

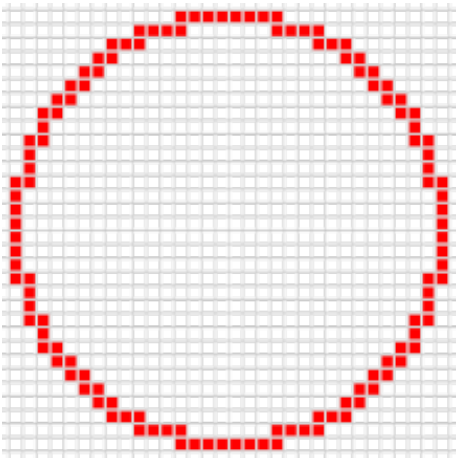

Figure 3.7: Different resolutions of voxels 32 x 32

3.2.1 Form

With particle form being measured using the equivalent scalene ellipsoid which is found by calculating the best fit ellipsoid. To fit an ellipsoid to a set of points there are two main approaches least squares fitting and the geometric fit. The first of the two methods minimises the least squares distance between a point and the surface of the ellipsoid whereas the second minimises the euclidean distance. The first approach is considerably simpler to calculate compared the geometric distance as it is a non trivial problem to find the minimum distance between a point and a surface.

To fit an ellipsoid to a particle, the particle is first turned into a point cloud. The surface of the point cloud is triangulated using Delaunay Triangulation. This produces a set of triangles representing the surface of the point cloud. For each of these triangles, the centroid and surface area is calculated. Using these surface points an initial least squares fit is found with the centre of the ellipsoid fixed at the centroid for the particle. The least squares fit ellipsoid as a starting point the fitted ellipsoid is further refined by minimising the geometric metric distances between the points on the surface of the particle and the surface of the ellipsoid. To avoid the problem of surface points clustering together and pulling the fitted ellipsoid each geometric distance was normalised against the proportion of surface area associated with that point compared to the point cloud as a whole. This allowed for a single point which represent a large surface area to have equal significance as many points densely packed and representing a smaller area.

3.2.2 Angularity

The angularity measure used in this study requires the difference in volumes between the shape and the form. This volume is practically impossible to calculate exactly for a real particle, however it is possible to approximate using a point cloud representation of the

particle (similar to the trapezoidal rule for calculating the area underneath a curve). This is done by assuming that the difference in volume can be discretised into smaller volumes. To calculate the discrete volume a surface area and the distance between the point and the ellipsoid is needed. The surface area is discretised by using Voronoi tessellation allowing for each point on the point cloud to represent a relative surface area. The distance is then found by calculating the minimum geometric distance between the point and the ellipsoid. The volume is measured by extruding the associated area along the distance between the point and the ellipsoid. By summing all of these discrete volumes an estimate of the difference in volumes is calculated This transforms equation (3.3) to (3.4).

$$Angularity = \frac{\sum_{i=1}^{n} d_i \times A_i}{Vol_{particle}} \tag{3.4}$$

d_i = geometric distance between the point i on the surface of the particle and the form.

A_i = the surface area assciated with the point i.

n = number of points on the surface of the point cloud.

Figure 3.8 shows an example of the distance between a point cloud (a square) and its corresponding form (a circle). The blue lines connecting the surface of the square and the circle represent the geometric distances between the point cloud and the corresponding form. Figure 3.9 shows a 2D example of the estimated volumetric distances between the shape and the form.

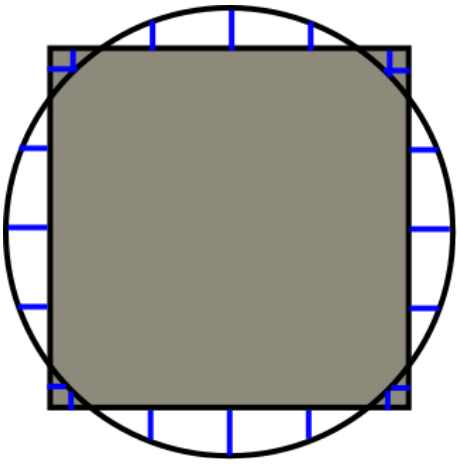

Figure 3.8: 2D example of a point cloud for a square and the best fit ellipse

3.3 Comparison of shape

This section compares the measures of shape presented in this chapter and the measures presented in the previous chapter. Table 3.1 shows the values of different measures of

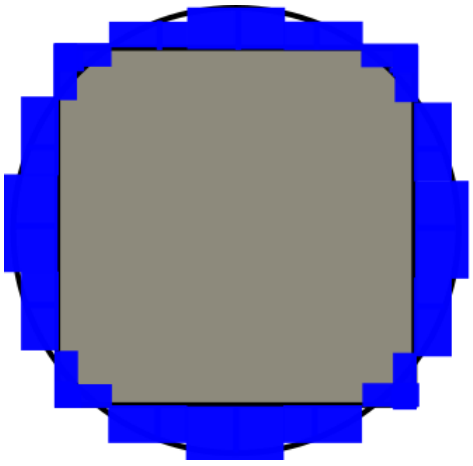

Figure 3.9: 2D example of the area (Volumetric in 3D) difference between a point cloud and the best fit form

particle form for a range L, I and S values. To uniquely describe a particle's form there needs to be a minimum of two independent values. The two most popular measures of particle form are the; "elongation" and "flatness" presented in Zingg (1935), and the "flatness" and "flatness to the longest axis" measures presented in Sneed and Folk (1958). The first measure, commonly referred to as a "Zingg plot" uses simple ratios to describe particle form, Equation (3.5) and (3.6). The particle's form is then classified using a square plot however it is argued that this distorts the distribution of particle form, Benn and Ballantyne (1993).

$$\frac{I}{L} \tag{3.5}$$

$$\frac{S}{I} \tag{3.6}$$

The second measure uses a slightly more complicated formula to describe a particles form, Equations (3.7) and (3.8). This measure was developed specifically to use a ternary instead of a square plot, to distribute particle forms better. However, these measures suffer from the problem of not being valid for all particle shapes with a particle's flatness becoming undefined when L and S are equal.

$$\frac{S}{L} \tag{3.7}$$

$$\frac{L-I}{L-S} \tag{3.8}$$

The method of classifying particle form presented in this chapter is designed to use a ternary plot thus allowing for a greater distribution of particle forms. Unlike the

measure presented in Sneed and Folk (1958), it is valid for all particle forms because of the equations for platyness and elongation being derived mathematically.

Whilst there is consensus amongst authors on the concept of particle form there is no such agreement with regards to particle angularity. Angularity is typically described using either the sharpness of corners or the relative roundness when compared to that of a circle. However, both of these approaches only apply for 2D particles and thus information is lost when trying to apply these measures to 3D particles. The reason for this is because it is trivial to define and measure corners for a 2D particle. There have been attempts to extend these angularity measures into 3D by considering 2D projects of a particle but this solution does not consider the whole shape of the particle. The measure presented here address these issues by considering the whole particle instead of using 2D projections and does not attempt to measure the curvature.

3.4 Real Ballast Particles

Figure 2.31 shows the measured forms of different ballast particles plotted on a Zingg plot. Using the L, I and S data from this plot the forms of the ballast particles can be recalculated using the method of form proposed in this chapter. Figure 3.10 shows the distribution of forms for Network Rail ballast particles. The forms of ballast particles fit within the area of $0 \leq \alpha \leq 0.5$ and $0 \leq \zeta \leq 0.4$.

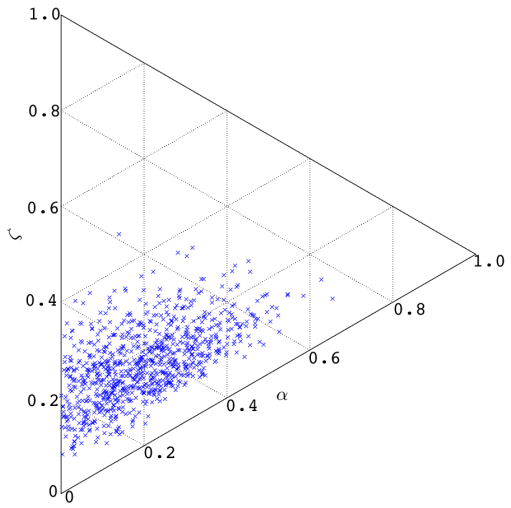

Figure 3.10: Distribution of ballast forms taken from L, I and S data in Le Pen (2008)

			Potticary		Zingg		Sneed and Folk		Wentworth	Wadell
L	I	S	Elongation	Platyness	Elongation	Flattness	Flatness to the longest axis	Flattness	Flattness6	Sphericity
1	1	1	0.000	0.000	1.000	1.000	1.000	Undefined	1.000	1.000
1	1	0.73	0.000	0.198	1.000	0.730	0.730	0.000	1.370	0.900
1	1	0.5	0.000	0.400	1.000	0.500	0.500	0.000	2.000	0.794
1	1	0.3	0.000	0.609	1.000	0.300	0.300	0.000	3.333	0.669
1.35	1	1	0.104	0.000	0.741	1.000	0.741	1.000	1.175	0.819
1.35	1	0.7	0.115	0.197	0.741	0.700	0.519	0.538	1.679	0.727
1.26	1	0.45	0.096	0.406	0.794	0.450	0.357	0.321	2.511	0.657
1.75	1	1	0.200	0.000	0.571	1.000	0.571	1.000	1.375	0.689
1.7	1	0.66	0.208	0.202	0.588	0.660	0.388	0.673	2.045	0.611
1.6	1	0.39	0.201	0.408	0.625	0.390	0.244	0.496	3.333	0.534
2.3	1	1	0.302	0.000	0.435	1.000	0.435	1.000	1.650	0.574
2.15	1	0.62	0.305	0.202	0.465	0.620	0.288	0.752	2.540	0.512
2	1	0.33	0.300	0.402	0.500	0.330	0.165	0.599	4.545	0.435
3	1	1	0.400	0.000	0.333	1.000	0.333	1.000	2.000	0.481
2.7	1	0.56	0.399	0.207	0.370	0.560	0.207	0.794	3.304	0.425
2.55	1	0.25	0.408	0.395	0.392	0.250	0.098	0.674	7.100	0.338

Table 3.1: Table comparing different measures of form

3.5 Conclusions

In this chapter a new method of quantifying particle form and angularity was proposed, using a point cloud representation of a particle (taken from either surface scans or CT-scans).

The new measure of form uses the concept that a particle can be represented by an equivalent scalene ellipsoid. This ellipsoid is then further distilled by using the three radii (L, I and S) to describe the form in terms of particle elongation and platyness.

The new measure for angularity is defined as the similarity between a particle's shape and its form. Angularity is found by measuring the volumetric difference between the shape and form.

These new measures of form and angularity will provide a comprehensive view of shape, any particle represented by a point cloud can be categorised. Applying these measures to different sets of particles allows for the effect of each aspect of shape to be studied, separately and combined.

Chapter 4

Methods and Materials

In the previous chapters a new method for characterising particle shape was presented which uses a 3D scan of a particle to quantify its shape. The shape of the particle has an impact on the granular property of the soil. To measure this impact a range of different shaped particles were systematically chosen and tested, with any differences in mechanical properties being attributed to the change in shape.

Because of the difficulty of finely controlling the shape of physical particles DEM was used. Using the concept of potential particles allows for exact control of the shape being modelled. However, it is limited to convex particles that can be represented by a series of smooth functions.

The individual aspects of particle shape (form, angularity, and roughness) can be separated and modelled numerically.

- Form, using ellipsoids
- Angularity, using superellipsoids and platonic solids
- Combined form and angularity, using scanned ballast particles

To create the particle samples a single shape is selected and fitted to a particle size distribution of network rail ballast. Once the sample is created they are subjected to triaxial compression stress conditions.

4.1 Shapes Tested

To study the effect of shape the different aspects (form and angularity) were initially considered separately. For example when form was studied only shapes with zero angularity were used (ellipsoids). For angularity only shapes with zero form were used (form

of a sphere). After considering form and angularity separately, the combined effect was then investigated.

Each model consisted of a single shape, thus any changes in the over mechanical properties could be attributed to that shape alone.

4.1.1 Form

The measure of form, discussed in the previous chapter, is represented by an equivalent scalene ellipsoid. Using ellipsoidal particles ensures angularity is kept at zero whilst being able to vary the form. The form of a particle is varied by changing the ratio of its three independent radii the L, I and S of the particle.

Equations (3.2) transform the particle's L, I and S into two variables, elongation and platyness. These variables map to points on the form diagram (Figure 4.1).

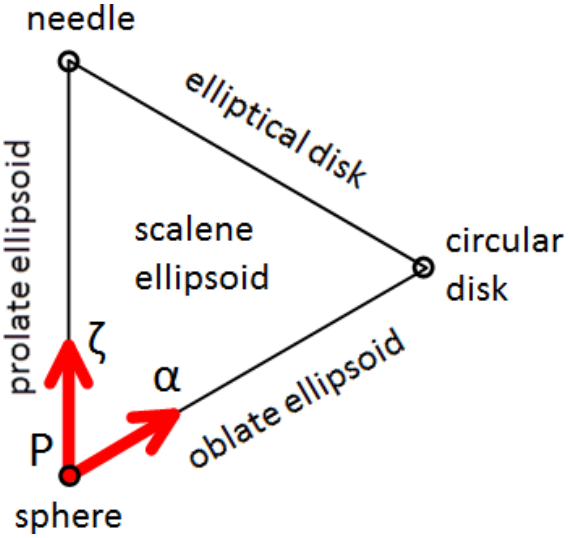

Figure 4.1: Form Diagram

To limit the amount of forms tested, a range was set for elongation and platyness based on the measurements of ballast particles (Figure 3.10).

From the area of real ballast particles a range of forms was selected as shown in figure 4.2. The corresponding ratio of L, I and S for each form modelled is shown in table 4.1.

4.1.2 Angularity

To study the effect of angularity any residual effects from particle form should be removed. This was done by keeping the form at zero (i.e. elongation and platyness are equal to zero or the form of a sphere). The sets of shapes that meet this requirement were superellipsoids and platonic solids.

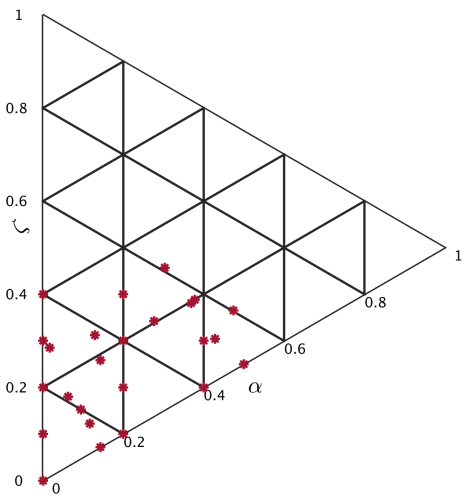

Figure 4.2: Graph showing the distribution of forms tested

L	I	S	Platyness (α)	Elongation (ζ)
1	1	1	0	0
1	1	0.8	0.143	0
1	1	0.73	0.2	0
1	1	0.5	0.4	0
1	1	0.4	0.5	0
1.26	1	0.45	0.4	0.1
1.35	1	1	0	0.1
1.35	1	0.7	0.2	0.1
1.6	1	0.39	0.4	0.2
1.7	1	0.66	0.2	0.2
1.75	1	1	0	0.2
2	1	0.33	0.4	0.3
2.15	1	0.62	0.2	0.3
2.3	1	1	0	0.3
2.55	1	0.25	0.4	0.4
2.7	1	0.56	0.2	0.4
3	1	1	0	0.4

Table 4.1: Table displaying the form of the various ellipsoids being modelled

$$(|\frac{x}{r_x}|^n + |\frac{y}{r_y}|^n)^{\frac{e}{n}} + |\frac{z}{r_z}|^n = 1 \tag{4.1}$$

Superellipsoids are defined by the equation (4.1) with the *nande* parameter controlling the curvature. A range of superellipsoids are shown in figure 4.3. Due to limitations of the potential particles method only convex shapes can be represented, thus limiting *nande* to be less than 1. By varying the *nande* parameter different curvatures can be created along two axes. To limit the effect of different curvatures altering the form a constant curvature was used, $n = e$ (Equation 4.2).

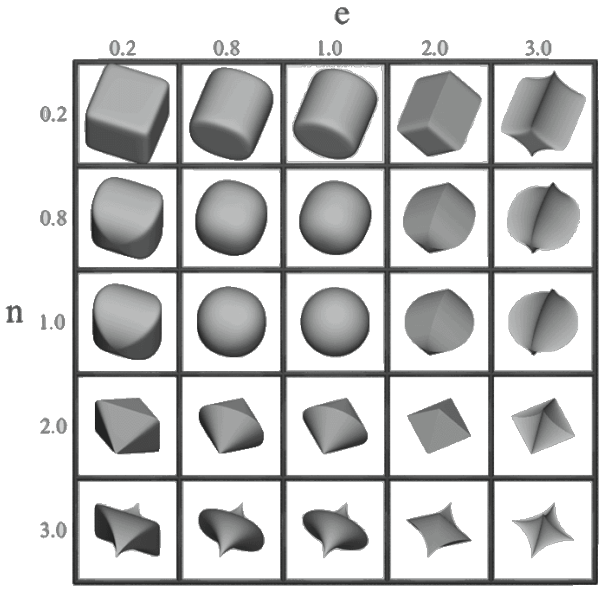

Figure 4.3: Different superellipsoids

$$|\frac{x}{r_x}|^{\frac{2}{n}} + |\frac{y}{r_y}|^{\frac{2}{n}} + |\frac{z}{r_z}|^{\frac{2}{n}} = 1 \tag{4.2}$$

Form was controlled by keeping the independent radii L, I and S equal. By varying the values of n between the range of 1 (sphere) and 0 (cube), shapes with an increasing angularity were modelled. Points were chosen within this range and table 4.2 shows the exponent value and the corresponding angularity measure.

The platonic solids are tetrahedron, cube, octahedron, icosahedron, and dodecahedron. These shapes have sharp edges between their faces which cannot be represented using the potential particles method. Therefore faces and edges are represented with a slight curvature. Figures 4.4, 4.5, 4.6, 4.7, and 4.8 show the respective platonic shapes as modelled with potential particles. Table 4.3 shows the platonic solids and their measured angularity.

Exponent (n)	Angularity
1	0
0.9	0.0325
0.7	0.1019
0.5	0.1799

Table 4.2: Table showing the different superellipsoid exponent and the corresponding measure of angularity

Figure 4.4: Tetrahedron

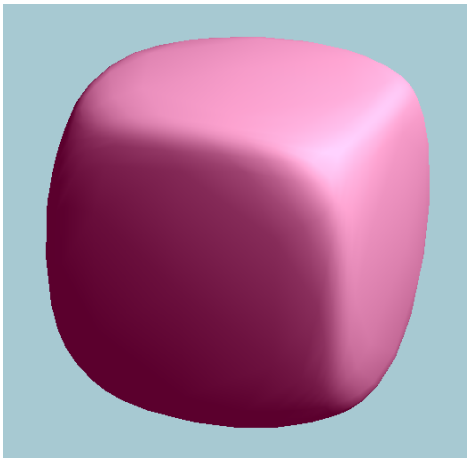

Figure 4.5: Cube

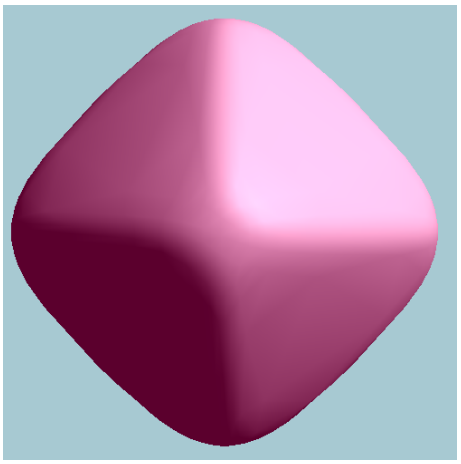

Figure 4.6: Octahedron

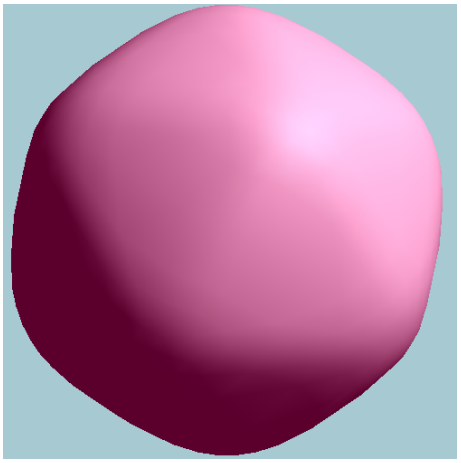

Figure 4.7: Icosahedron

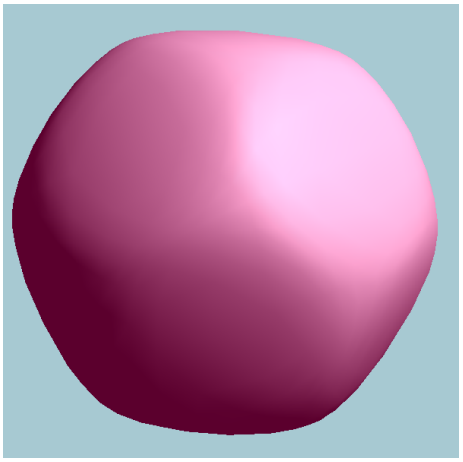

Figure 4.8: Dodecahedron

Shape	Angularity
Tetrahedron	0.4808
Cube	0.2087
Octahedron	0.1844
dodecahedron	0.0496
icosahedron	0.0429

Table 4.3: Table containing the exponents for different platonic solids and their measured angularity

4.1.3 Shape

To study the combined effect of angularity and form a particle must contain both. As in the previous section this is done using superellipsoids, however in this section the form is not kept at a constant and with angularity being varied.

The forms of the models consisted of a platy form, an angular form and a scalene form.

With the form kept at a constant the exponent is varied between 1 (Ellipsoid) and 0 (Rectangle).

To extend the range of angularity measured a modelled ballast particle from a previous study was used (Ahmed et al., 2015) (Figure 4.9). This introduces flat faces to model angularity as was previously done for the platonic solids.

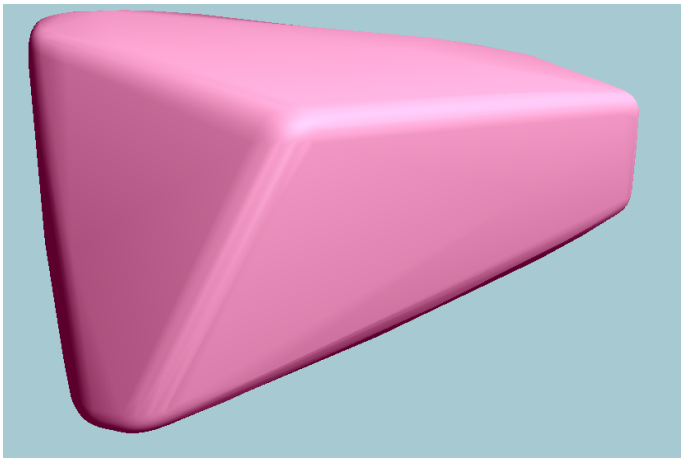

Figure 4.9: Modelled ballast particle

The form of this ballast particle was measured using the method presented in the previous chapter and an equivalent scalene ellipsoid created. The range of shapes tested is shown in table 4.4.

Name	Platyness (α)	Elongation (ζ)	Angularity
Modelled ballast	0.12889	0.2476	0.3854
	0.12889	0.2476	0
	0.12889	0.2476	0.0322
	0.12889	0.2476	0.0992
Platy Particle	0.4	0	0
	0.4	0	0.0323
	0.4	0	0.099
Elongated Particle	0	0.2	0
	0	0.2	0.0323
	0	0.2	0.099

Table 4.4: Table containing the form and angularity for shapes containing both angularity and form

4.2 Particle Size Distribution

To help constrain the models and ensure compatibility of results, the total volume of solids (v_s) contained within each model is kept as close to $0.2m^3$ as possible This is consistent with the approach used in physical tests. By keeping v_s at a constant for a range of different shapes, all with different volumes, the number of particles within a model has to vary.

To avoid issues with mono-disperse models, such as locking, a particle size distribution (PSD) was used.

The PSD for each model is determined by the British standards, which specifies a band for an acceptable ballast particle. Figure 4.10 shows the PSD for ballast. Using these bands a mean sieve size was calculated which the models conform to.

The PSD from the British standards provides a continuous range of acceptable ballast sizes. To simplify the models, a discrete PSD was used, consisting of five equal sized bins spaced at 10, 30, 50, 70, and 90% of passed mass. The corresponding sieve size is then measured using figure 4.10. Table 4.5 shows the sieve size and the proportion of the mass for that bin.

Passing by Mass (%)	10	30	50	70	90
Sieve Size (mm)	28.5	36.5	40.5	46	52

Table 4.5: Bins and their equivalent mass

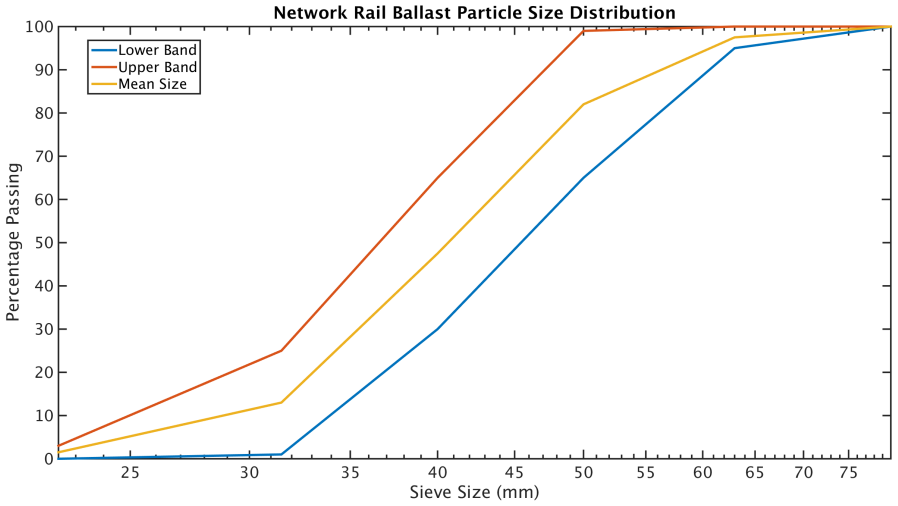

Figure 4.10: The Particle Size distributions from BS EN (2013)

Once the total amount of volume for each bin is known, the number of particles needed is given by Equation (4.3).

$$Number\ Particles = \frac{Vol_{Bin}}{Vol_{Particle}} \tag{4.3}$$

For the mathematically described shapes such as the ellipsoids, platonic solids, and superellipsoids the volume is straightforward to calculate. However, for unique ballast shapes the volume is harder to measure. Using a point cloud representation of a particle, the volume is estimated by summing all the individual voxel's volumes. As this is an estimation the total volume will depend on the of the size of the voxels, with the results converging with smaller and smaller voxels.

4.3 DEM Model

4.3.1 Potential Particles

This study uses potential particles to model different shaped particles. For simple shapes, such as spheres and ellipsoids, the representation of the particles surface can be defined precisely as a single continuous function. The smooth continuous function that describes a particles shape is called a "potential function" with the surface being defined when this function is equal to zero. Whilst simple shapes have a single function defining it's surface more complicated shapes can be described by multiple functions, for example intersecting planes (Figure 4.11). However using these planes to describe a particle directly would cause there to be a discontinuity between the surfaces so a small radius

of curvature is added (Figure 4.12). This ensures that the particle is modelled by a continuous function without a break from a corner or edge (Figure 4.13).

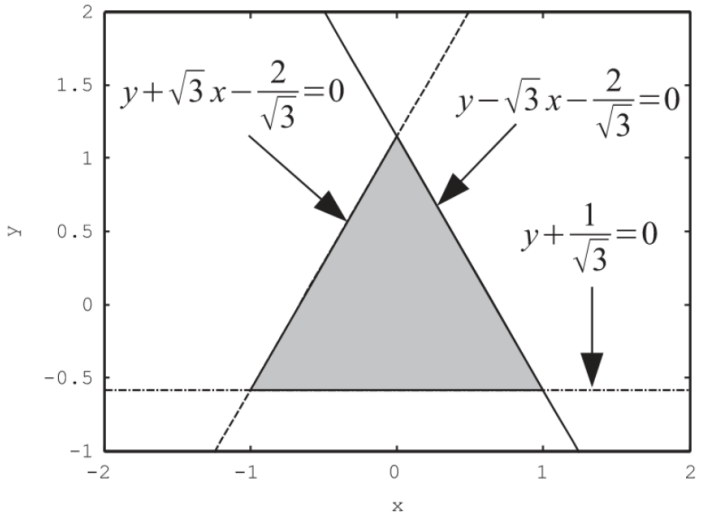

Figure 4.11: An equilateral triangle constructed using planes, (Harkness, 2009)

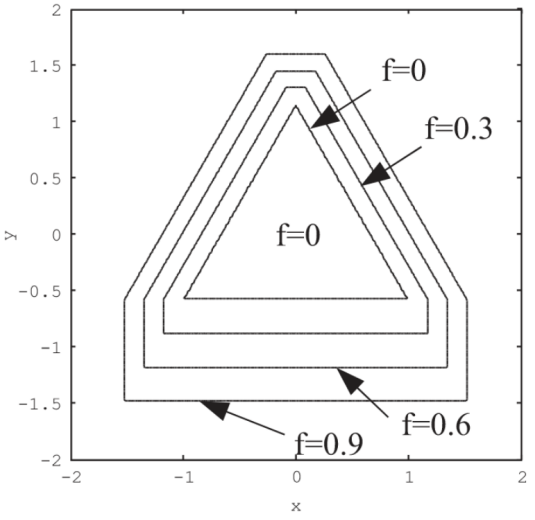

Figure 4.12: An equilateral triangle with discontinuitys, (Harkness, 2009)

Contacts between two particles are defined when the two different potential particles are equal for a given contact point X, Figure 4.14. When two particles are overlapping the contact can not be described by a single contact point instead the contact is described based upon the maximum overlap distance between the two particles, Equation (4.4).

$$f_1(\mathbf{x}) = f_2(X - \delta\mathbf{nx}) \tag{4.4}$$

$\mathbf{x}$ the contact point for particle 1

δ is the overlap between the particles

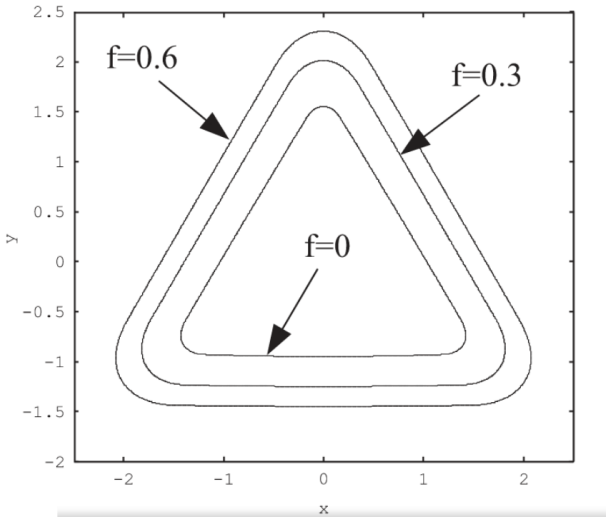

Figure 4.13: An equilateral triangle with a radius of curvature, (Harkness, 2009)

n is the unit vector normal to f_1

Equation (4.4) is solved using a NewtonRaphson method to find the point of contact (X) and the overlap distance (Delta).

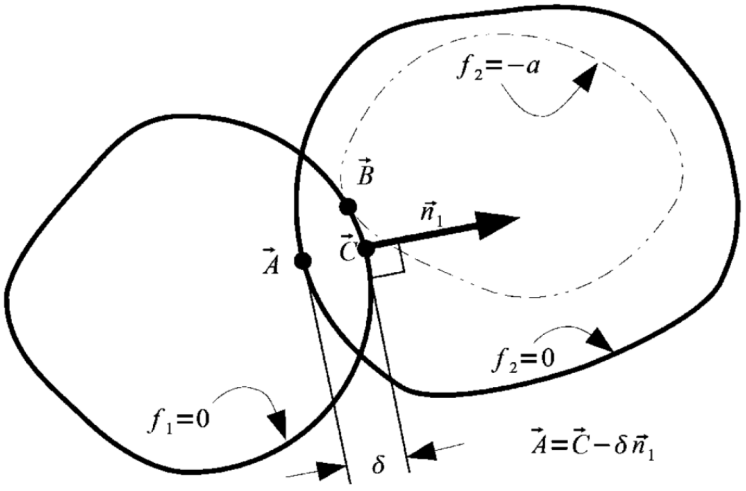

Figure 4.14: Overlap between two potential particles, (Harkness, 2009)

To calculate the reaction forces between these particles using a spring dashpot model the overlap distance is needed as well as a contact stiffness. The contact stiffness is calculated using a Hertzian contact model with the spring stiffness being derived from the relative curvature of the surface at the point of contact.

Properties	Value
Density ρ	$2700Kg/m^3$
Surface Friction Angle	30°
Bulk Modulus (K)	$50GPa$
Poisons Ratio ν	0.3

Table 4.6: Model parameters

4.3.2 Particle Parameters

Ballast particles are typically composed of crushed granite. To ensure the particles are comparable to a physical model, the particle's mechanical properties are equal to granite. Table 4.6 shows the mechanical properties used in the simulations. The value for roughness for granite is highly dependant on the surfaces it is in contact with and whether or not there is any liquid at the contact. Previous studies have shown that increasing an interparticle friction angle past 30° has insignificant change in the mobilised angle of friction at critical state. Therefore interparticle friction of 30° is used.

4.3.3 Model Creation

The DEM models use a rectangular cell rather than a cylindrical boundary used in physical triaxial tests. The boundary condition applied to the cell are periodic, allowing for the models to deform whilst keeping a rectangular cell. Using this type of boundary condition removes boundary effects as the simulation is effectively infinite in all directions. This however has the disadvantage of not allowing gravity within the model as any acceleration due to gravity would grow exponentially as the particles entered a freefall.

The initial size of the cell was 4m high, 2m wide and deep; this was to ensure there is enough free space for the particles are able to be distributed randomly within the space without coming into contact with each other. Whilst the particles are spatially distributed randomly they were also given a random orientation. This random position and orientation is there to reduce any initial bias from the model's set-up. Any artefacts of structure created at this stage could persist through out the whole model run. A scenario where all the particles are aligned would not be representative of a granular material.

Once the particles have been distributed within the cell, the cell is then compressed down to a target void ratio of 2.0, Figure 4.15 shows a spherical model at a void ratio of 2.0.

The cell was then further compressed down to a void ratio of 0.65 using constant velocity applied to all boundaries inwards (Figure 4.16).

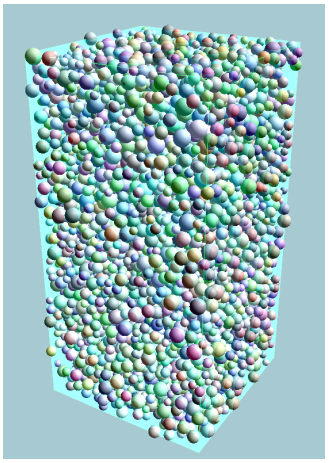

Figure 4.15: Model creation at a void ratio of 2

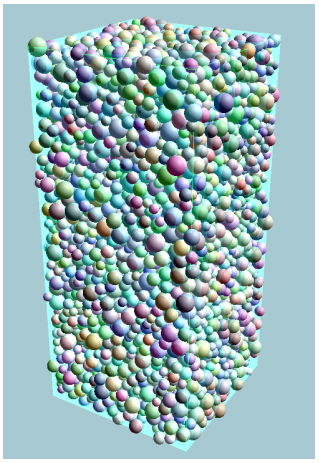

Figure 4.16: Model creation at a void ratio of 0.65

Once the void ratio has been achieved, the boundaries were set to be stress controlled with a target confining pressure of 100kPa. 100kPa was used as an arbitrary value however this has no effect on the mobilised angle of friction at critical state. Figure 4.17 shows a model once it has reached equilibrium and is in an isotropic state of 100kPa.

After the model has reached an isotropic state, triaxial compression stress conditions were applied. The lateral boundary stress was kept at 100kPa whilst a vertical velocity downwards was applied to the top boundary. The models are strained until a vertical strain of 60% is reached. Figure 4.18 shows a model at 60% strain.

4.4 Model Sensitivity

To test the sensitivity of the models to their initial configurations, identical spherical models are used with the only difference being their initial starting configuration of particle and void ratio.

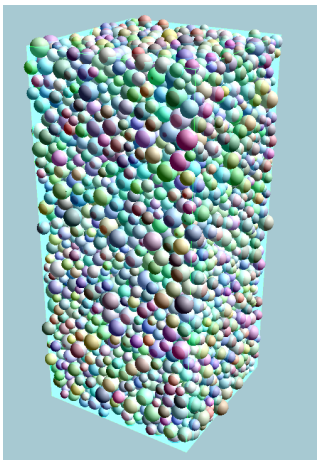

Figure 4.17: Model creation at under isotropic stress conditions

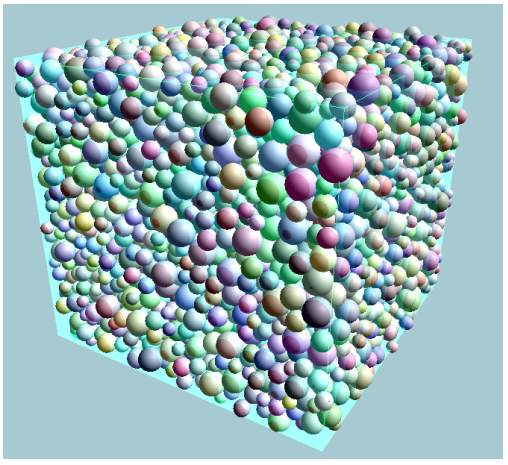

Figure 4.18: Model whilst being strained

Figure 4.19 shows the mobilised angle of friction against the vertical strain. All these models initially have different responses to the loading with the densest model having the stiffest response and the loosest having a less stiff. However they all exhibit the characteristics of a dense soil by initially reaching a peak strength and reducing. Despite their initial configurations all models eventually reach a steady state with their mobilised angle of friction levelling out and remaining relatively constant.

4.5 Model Performance

The model's simulation time is dependant on two main factors, how complicated the potential particle is and the number of particles. The main computational cost is related to the contact detection algorithm which first has to determine if two particles are in contact. Once a contact has been detected a further algorithm is applied to calculate the overlap between the particles. Due to the serial nature of the contact detection algorithm every particle has to be checked against the surrounding particles to check if

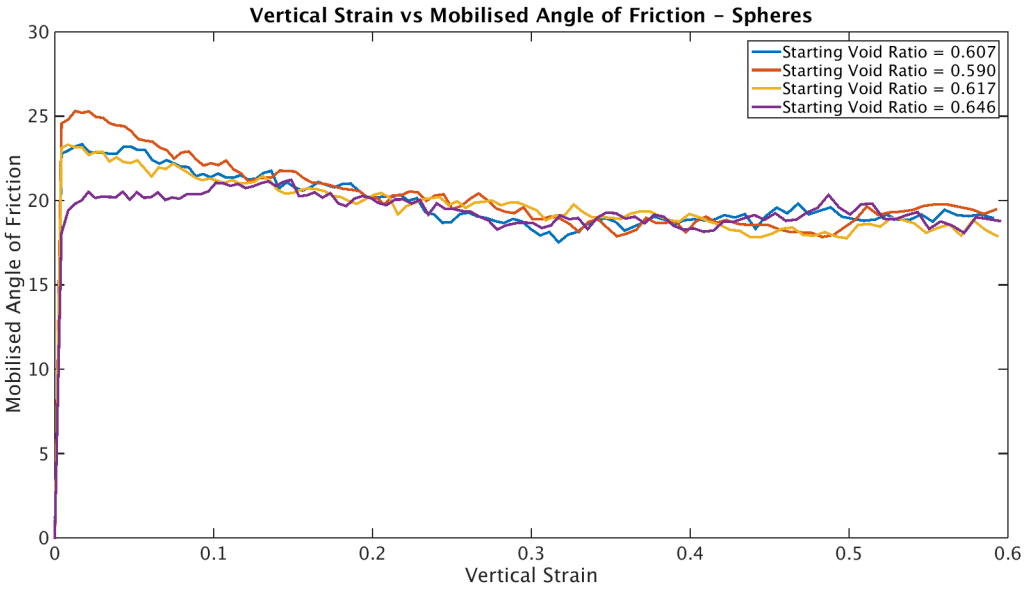

Figure 4.19: Mobilised angle of friction against vertical strain - Spherical models

they are in contact. Therefore increasing the number of particles in the simulation leads to a significant increase in simulation time. For every contact that has been detected a numerical solver is applied to calculate the overlap and contact point which increases in cost as the particle's shape becomes increasingly complex.

Table 4.7 shows the different simulation times for a range of different models. The spherical model had the least amount of simulation time, this was due to it's simple shape. The increased simulation time between the platy and spherical models is mainly due to the significantly increased number of particles within the platy model. Comparing models with roughly equal number of particles such as the platy and tetrahedron model, and the super sphere and ballast particle models, it can be seen that as the particle shape increases in complexity the simulation time also increases.

4.6 Validation

The potential particles method has been used in a previous study, Harkness et al. (2016), in which the author studied the effect of different cell pressures on simulated triaxial tests. These simulated tests were then compared against representative scaled ballast laboratory triaxial tests, comparing their mobilised angle of friction and volumetric strain. The model used a membrane as the boundary conditions and a Hertzian contact model. The shapes of the simulated ballast particles where approximated using real ballast particles as a reference. Two different cell pressures were modelled, the first using 15kPa and the second using 200kPa.

Shape Set	Platyness	Elongation	Angularity	Number of Particles	Simulation Time (Hours)
Spherical	0	0	0	6518	1
Platy	0.500	0	0	16300	25
Elongated	0	0.300	0	2832	5.5
Super-sphere	0	0	0.102	4209	10
Tetrahedron	0	0	0.481	15991	48
Ballast Particle	0.129	0.247	0.385	4193	29.5

Table 4.7: Simulation time for a range of different particle shapes and number of particles

Figure 4.20 shows the mobilised angle of friction and volumetric strain against vertical strain for the simulated and physical model with a cell pressure of 15kPa. The results show a good correlation between both the mobilised angle of friction and the volumetric strain.

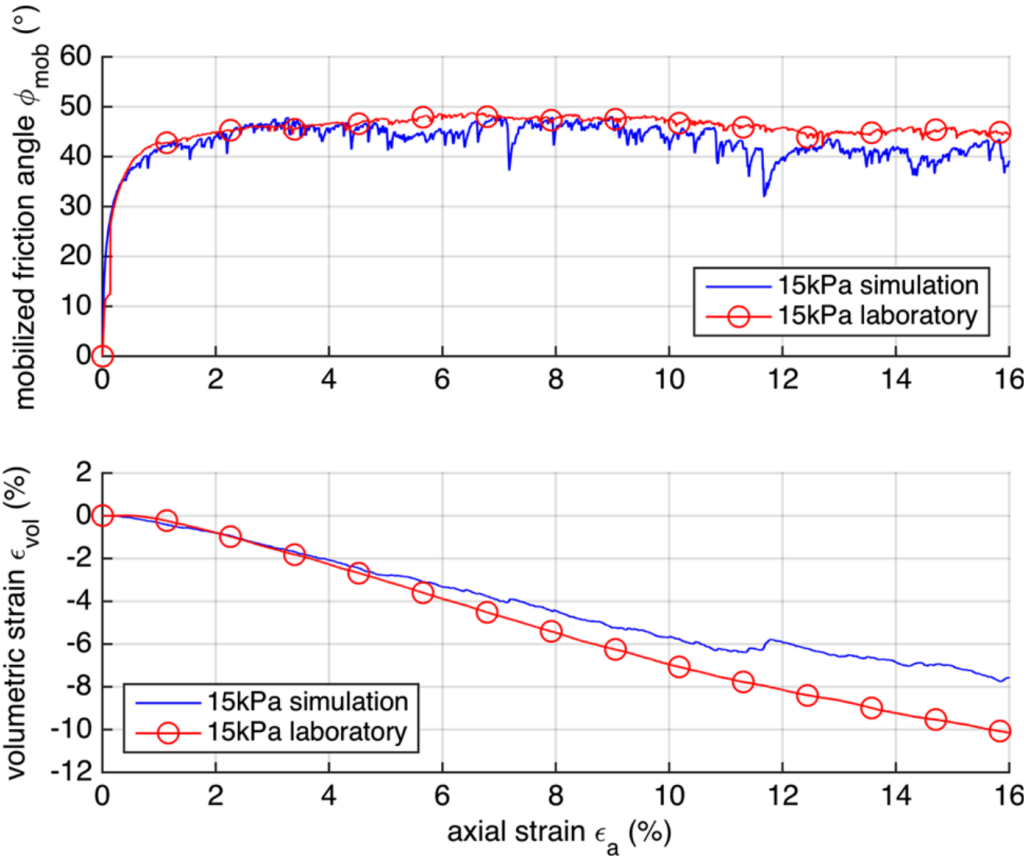

Figure 4.20: Mobilised angle of friction and volumetric strain for a physical and simulated triaxial test at 15kPa (Harkness et al., 2016)

Figure 4.20 shows the mobilised angle of friction and volumetric strain against vertical strain for the simulated and physical model with a cell pressure of 200kPa. The results show less alignment between the physical and the simulated tests. The differences between the mobilised angle of friction show that the modelled ballast has a stiffer initial response when compared to the lab sample as well as having a higher peak angle of friction. At critical state the differences appear to be less pronounced, eventually reaching a similar critical state mobilised angle of friction.

Figure 4.22 shows the results from a further model in which the author modified the inter-particle friction angle so that the simulated tests showed comparable results. In this test the inter-particle friction angle for the 15kPa model was set to 30 degrees and for the 200kPa model it was set to 40 degrees. This shows an improved correlation between the laboratory and simulated test for both sets of cell pressures.

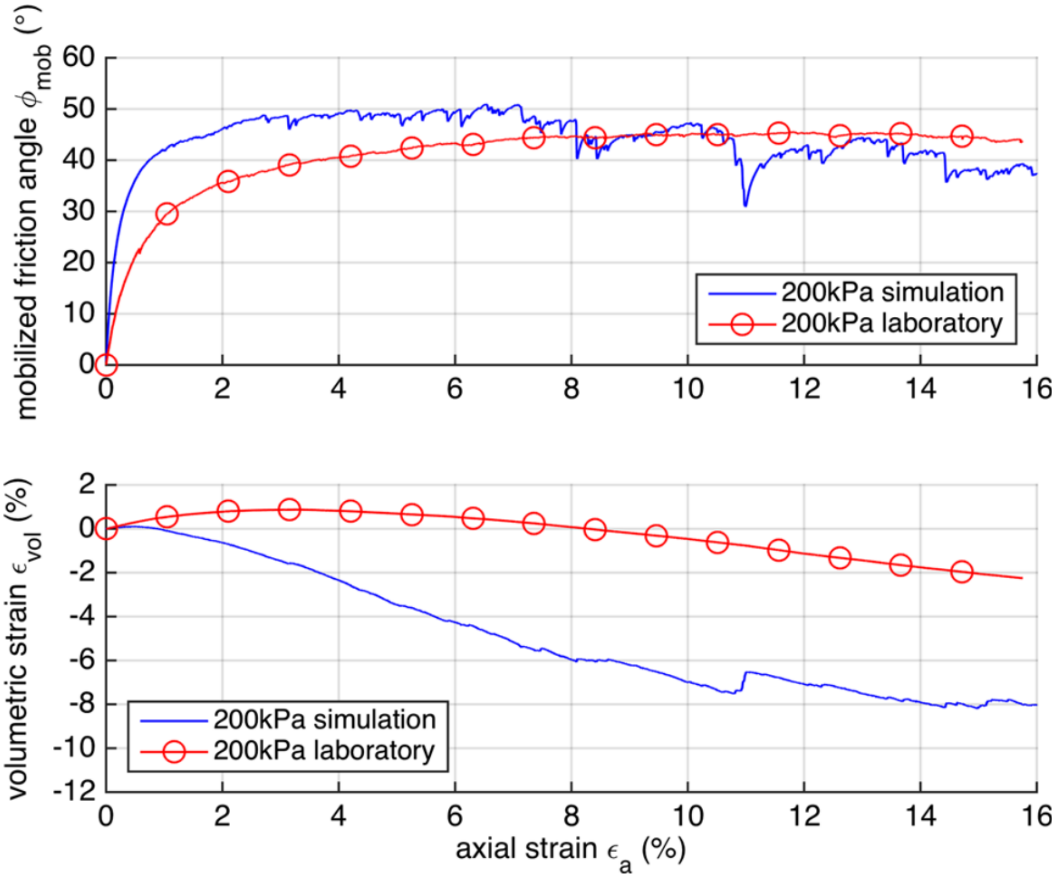

Figure 4.21: Mobilised angle of friction and volumetric strain for a physical and simulated triaxial test at 200kPa (Harkness et al., 2016)

This study shows that at lower cell pressure, the results from both the simulated and laboratory triaxial tests are comparable. However, at the higher cell pressure whilst keeping the material parameters identical, the results show less comparability. Due to limitations with the Hertzian contact model, in order to achieve comparable results throughout the whole test, the material parameters need to be calibrated against a physical test. Notwithstanding this, the models still showed reasonable agreement at critical state between the physical and simulated tests with both models having comparable critical state mobilised angle of frictions.

4.7 Summary

In this chapter, a method was presented to investigate the effect of particle shape on the critical state strength of ballast particles.

To study the effect of particle shape in a systematic way, a wide range of different shapes were used. These shapes were initially subdivided into distinct groups so that different effects of form and angularity could be better explored in isolation and combined.

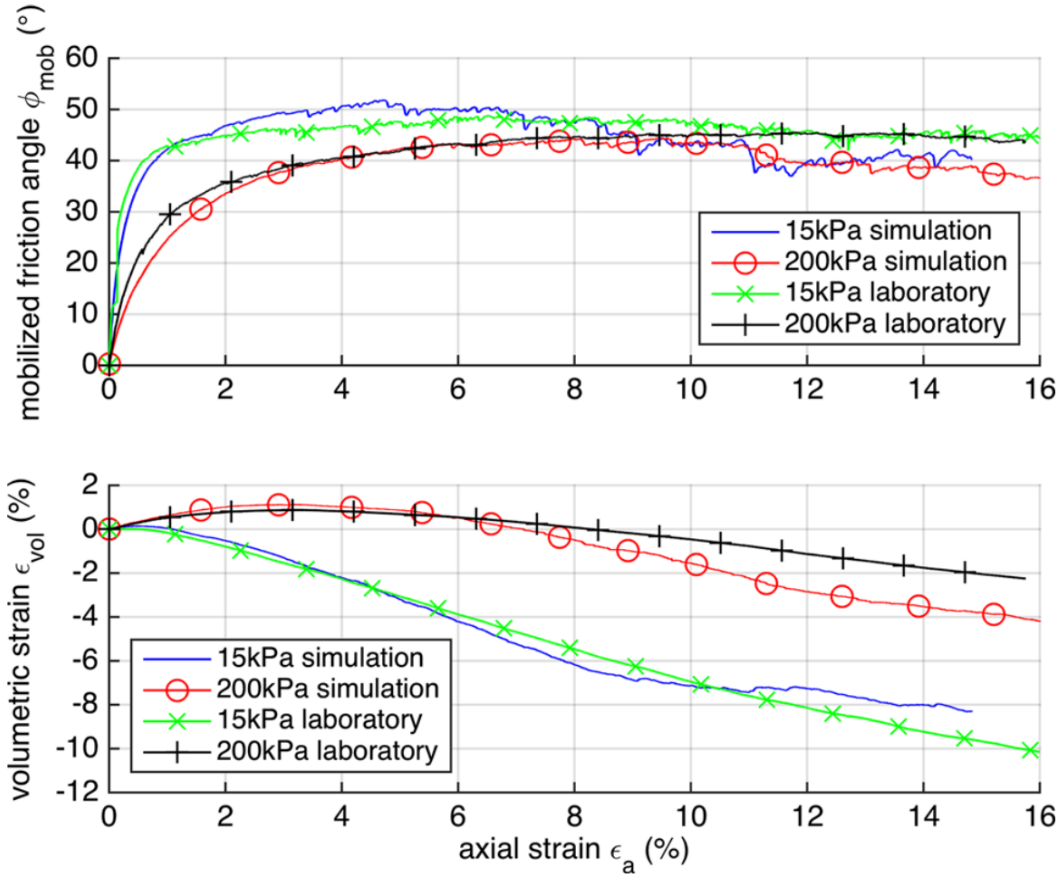

Figure 4.22: Mobilised angle of friction and volumetric strain for a physical and simulated triaxial test at 15kPa and 200kPa with different inter-particle friction (Harkness et al., 2016)

To simulate the effects of different particle shapes the potential particle methods were used, in which particles are represented by smooth continuous functions. The potential particles were then distributed within a periodic cell, compressed to form a cohesive sample, and placed under triaxial compression conditions. The models tried to stay as close to real lab conditions with the PSD of Network Rail ballast as well as consistent model set-up, it was impossible to fully replicate owing to the nature of the numerical simulations.

The sensitivity of the initial starting conditions was also tested using three identical spherical models with random starting position. The result from the triaxial stress conditions showed that the differences in initial void ratio lead to differences in initial stiffness which is consistent with the literature and that after the peak had been passed all models reached an equivalent steady state.

The potential particles method has been used in a previous study, Harkness et al. (2016), in which the author studied the effect of different cell pressures on simulated triaxial tests. These simulated tests were then compared against representative laboratory tests.

The shapes of the simulated ballast particles where approximated using real ballast particles as a reference.

The study shows that at lower cell pressures, the results from both the simulated and laboratory triaxial tests are comparable. However, at higher cell pressures the results indicate less comparability with the simulated model initially acting stiffer than the physical test. As the model approached critical state, the physical and simulated tests converged with both models having comparable critical state mobilised angle of frictions. In order to achieve comparable results throughout the whole test, the material parameters need to be calibrated against a physical test.

Chapter 5

Particle Form

This chapter studies the results from the particles with just form, i.e. the ellipsoidal particles. The results are split into three different categories, they are the Platy (Oblate), Elongated (Prolate) and Mixed particles (Scalene).

5.1 Effect of Platyness (Oblate Ellipsoid)

In this section only the results of the platy particles, forms with no elongation (beginning with a sphere and becoming more oblate) shall be presented and discussed. The results being looked at are:

- Mobilised Angle of Friction
- Critical State Strength
- Particle Orientation
- Particle Rate of Rotation
- Contact Analysis

The range of platyness tested ranges from 0 (Figure 5.1) to 0.6 (Figure 5.2).

5.1.1 Shear Strength

Mobilisation of shear strength of a granular material can be described by the mobilised angle of friction ϕ_{mob}, given by Equation (2.5).

Figure 5.3 plots the mobilised angle of friction against vertical strain for each model. Whilst peak friction angles differ widely, these are not directly comparable because they

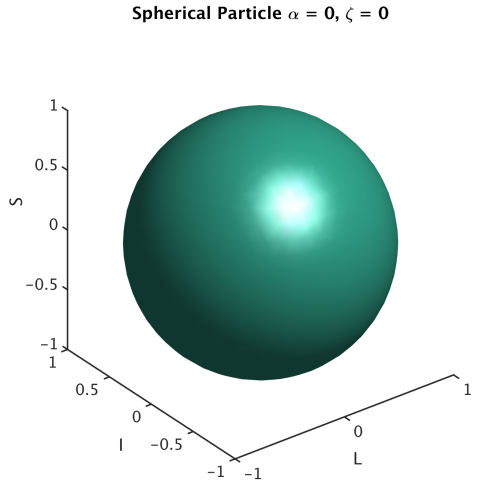

Figure 5.1: Form - Sphere

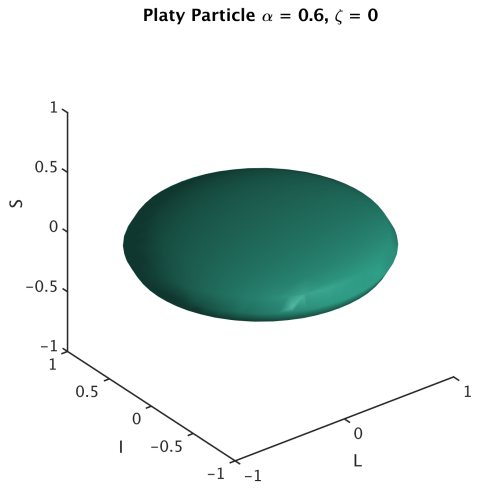

Figure 5.2: Form - Platy particle

may correspond to different initial relative densities of the granular materials modelled. Due to the presumed difference in relative density among models, some reach a very dense packing that results to an almost immediate mobilisation of a very high angle of friction. Other models exhibit a delayed mobilisation of a rather lower peak.

On the other hand, the friction angle at critical state ϕ'_{crit} is independent of the initial void ratio, allowing valid comparisons. Figure 5.4 shows that as the shape of the particles becomes more platy, critical state strength approximately increases linearly.

5.1.2 Particle Orientation Fabric

At the start of the test, particles have a random orientation. However, as shearing takes place, particles will generally reorient themselves and may do so along a preferred

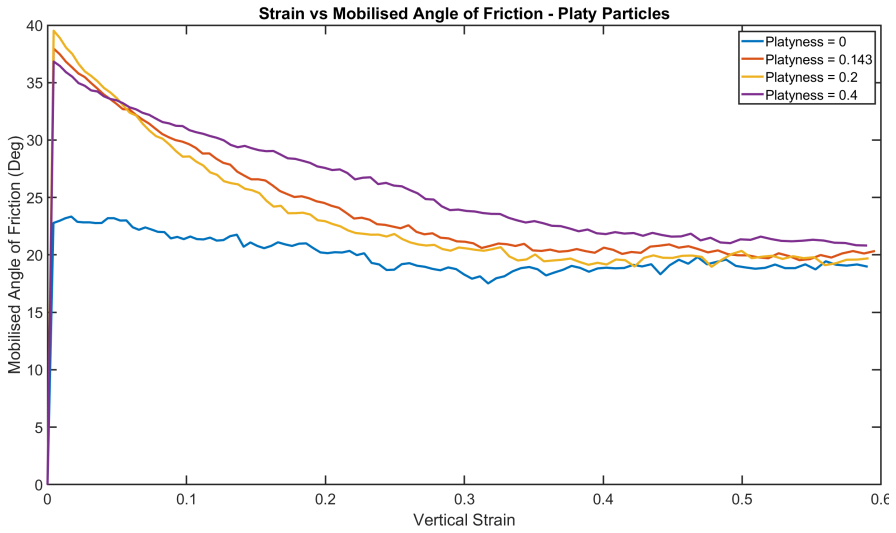

Figure 5.3: Mobilised angle of Friction against Vertical strain - Platy particle

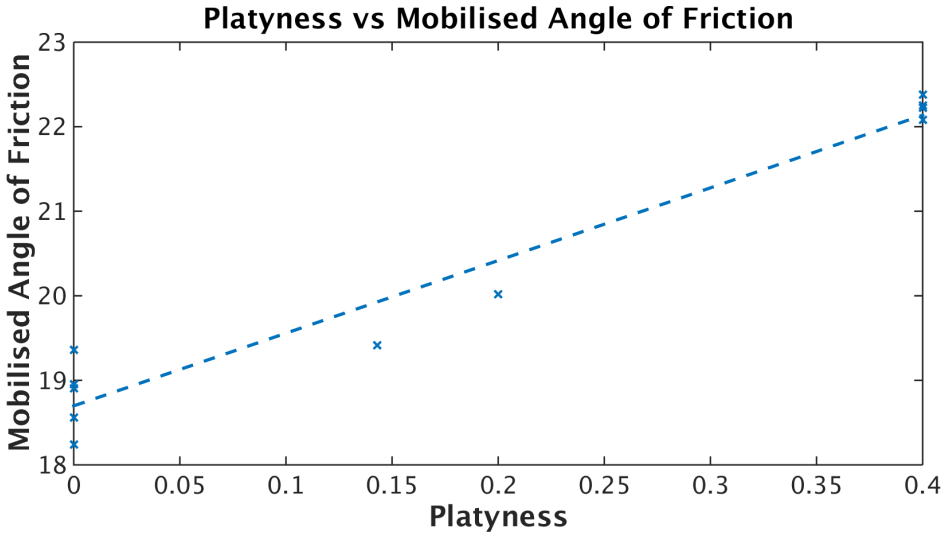

Figure 5.4: Friction angle at critical state against Platyness - Platy particle

direction. The orientation of each (ellipsoidal) particle can be described by a local system of orthogonal vectors in the directions of its three radii (L, I and S.) The average particle orientation with respect to the global model axes can be quantified by a fabric tensor such as that given by Equation (5.1) (Oda, 1972).

$$G_{ij} = \frac{1}{n} \sum_{k=1}^{n} V_i^k V_j^k \tag{5.1}$$

As there is no single vector that describes the orientation of an ellipsoid, this fabric tensor can be calculated for the direction of each one of the three radii. Figure 5.5 shows how the G_{33} component of the fabric tensor corresponding to the S-direction of each particle varies with vertical strain. G_{33} essentially quantifies the prevalence of

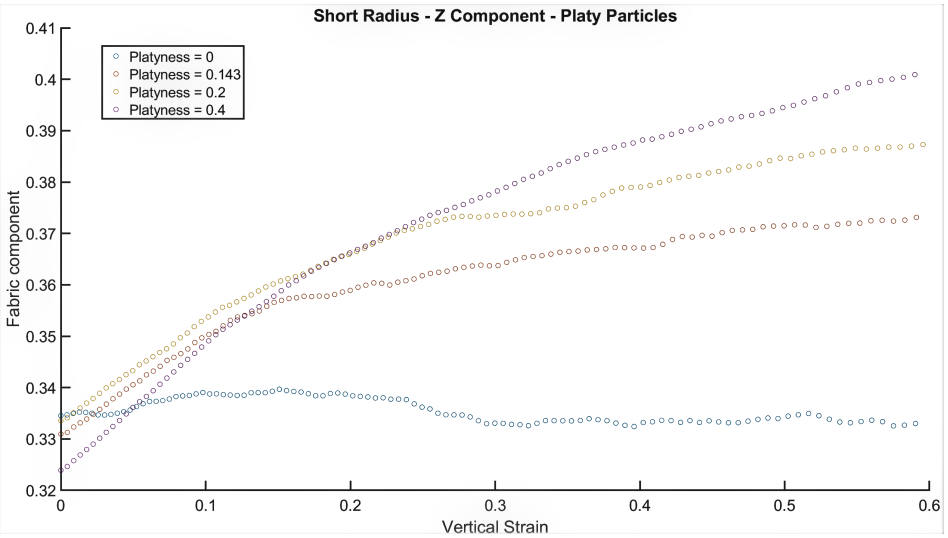

Figure 5.5: Vertical fabric orientation for the particle's S radius against Vertical Strain - Platy particle

particles choosing to reorient their S-axis parallel to the global z-axis, i.e. with their flatter face normal to the maximum principal stress.

All tests started off with random particle orientation, shown by a value of $G_{33} \approx 0.33$ in Figure 5.5. As shear strains increased, however, so did G_{33}, showing that on average particles re-oriented their flatter face normal to the maximum principal stress in the course of shearing. Also, the rate of reorientation progressively decreases as the model approaches critical state, presumably because a configuration that can accommodate further shearing is reached. This general behaviour is observed even for relatively small values of platyness. In contrast, spherical particles do not show any tendency to re-orient and $G_{33} \approx const.$ throughout.

5.1.3 Particle Rotation and Sliding

As a specimen is strained, the particles will displace and rotate to accommodate this by rearranging the structure of the granular skeleton. It is expected that, during this process, particles of different forms will need to translate and rotate in different ways or proportions. Previous numerical studies of 2D assemblies have shown a link between particle rotations and sliding contacts; inhibiting rotation led to larger amounts of sliding and a higher mobilised angle of friction by increasing the amount of energy necessary to distort the skeleton (Bardet, 1994).

Quantifying rotations and rotation increments in 3D in a meaningful way is more challenging, but can be simplified using the algebra of quaternions. Rotation can be considered a quaternion whose real part quantifies the amount of rotation and its three imaginary parts the direction of the axis about which that rotation takes place. The

differences of the real part between relatively closely spaced time-steps, so that the axis of rotation can be considered unchanged. The magnitude of the real component is normalised by the corresponding true vertical strain increment to produce a rate of rotation with strain given by Equation (5.2).

$$\theta = \frac{d\theta_{quat}}{d\epsilon_z} \tag{5.2}$$

Figure 5.6 shows the change in rate of rotation against vertical strain. As straining takes place all models see an intimidate increase in the rate of rotation, the "acceleration" is greatest in the spherical particles with a decreasing initial "acceleration" as the particles become platyier.

These results follow conventional wisdom that spherical particles are the easiest form to rotate and as platyness increases so does rotational resistance.

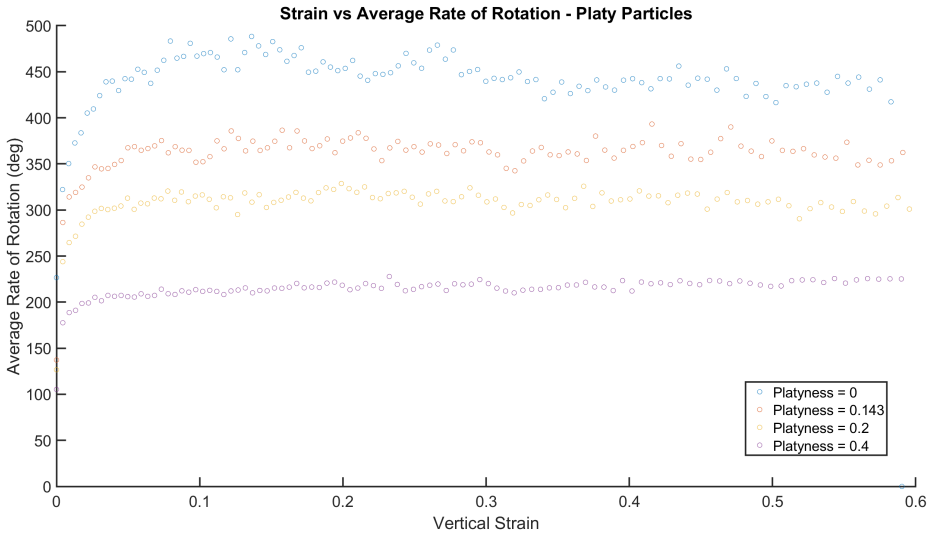

Figure 5.6: Mean rate of rotation against vertical strain - Platy particle

Figure 5.7 shows the distribution of rate of rotation within the model at the initial time step. The yellow patches indicate areas of high rotation and the purple areas of low rotation. This is because of single particles rotating a larger amount. This figure shows that there is no uniformity with the amount of rotation which might indicate a shear band forming within the model.

Figure 5.8 shows the same model with spheres at a later time point near the end of shearing. The model is significantly deformed compared to the initial configuration and there are still patches of high rotation showing that only small number of particles are rotating a large amount.

Figure 5.9 shows the rate of rotation within a model for a platy particle. Compared to the model for spheres there is a greater amount of rotation within the model however this

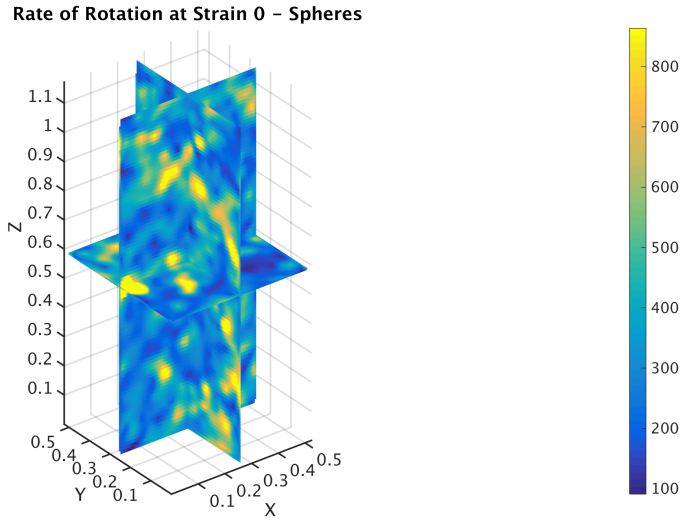

Figure 5.7: A heat map showing the distribution of rotation within a model at the start of straining - Spherical particle

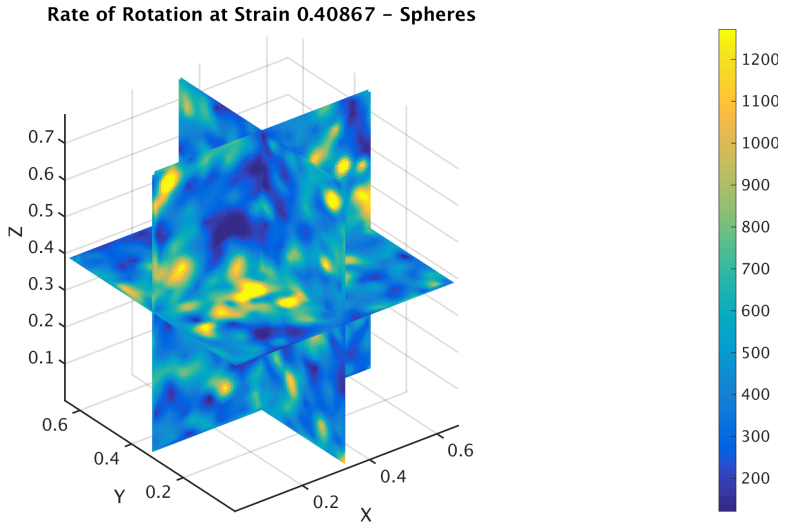

Figure 5.8: A heat map showing the distribution of rotation within a model at 40% strain- Spherical particle

is because of the smaller sized particles meaning that the individual effects of rotation would be smaller and so more particles rotate.

Figure 5.10 shows the platy particles in a strained configuration with no real consistent distribution of rotation seen. Once again indicating that there is no shear band formed. One property of a shear band is that once it has formed it is persistent. Indicating an area of increased movement and rotation.

A particle's contact is considered sliding under Morh's Collumb dry friction when the shear force at the contact reaches a limit, described by Equation (5.3). At this point the contact has developed its maximum shear resistance and the contact slips.

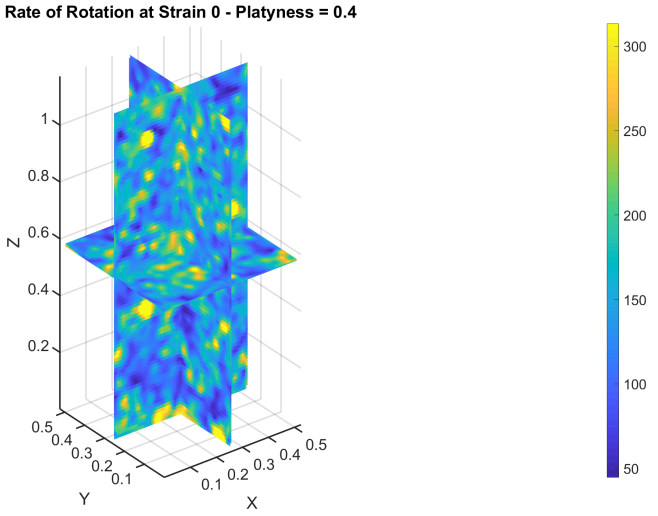

Figure 5.9: A heat map showing the distribution of rotation within a model at the start of straining - Platy particle

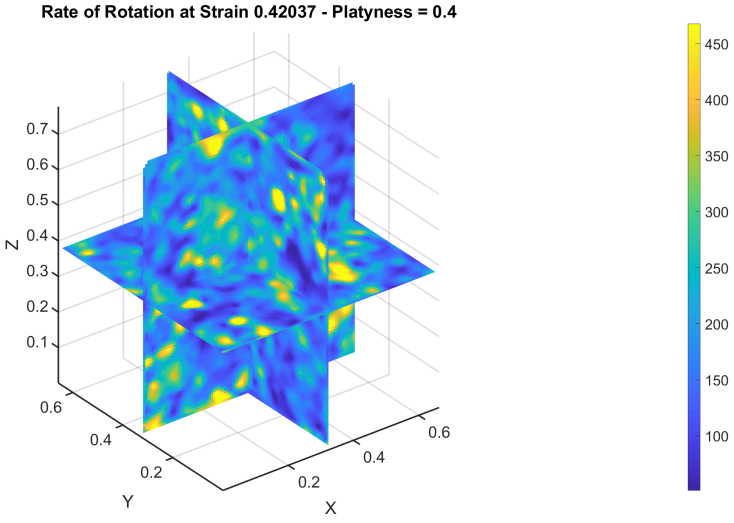

Figure 5.10: A heat map showing the distribution of rotation within a model at 42% strain - Platy particle

$$F_{shear} = F_{norm} \times \mu \tag{5.3}$$

Figure 5.11 shows the change in proportion of contacts that are sliding against vertical strain. At the start of straining there are no contacts that are sliding as the model is stable under isotropic stress conditions. As soon as straining commences the contacts are no longer in equilibrium and greater shear forces are developed and reach a peak. At the peak, the least amount of sliding takes place in the spherical model (25% of the contacts sliding) and an increasing amount of sliding is seen in platyier particles with the platyiest model having a peak (57% of contacts sliding). The ordering of the forms remains thought straining.

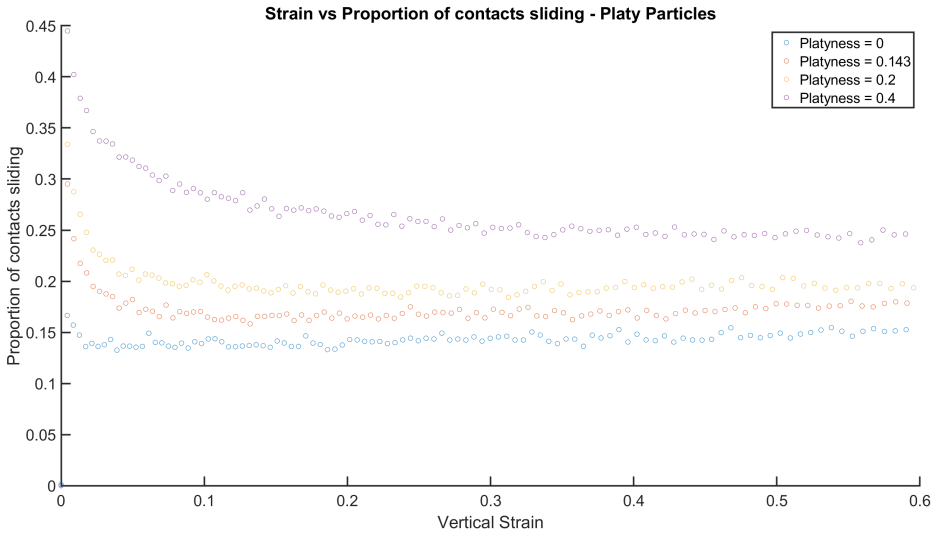

Figure 5.11: Proportion of contacts that are sliding against vertical strain

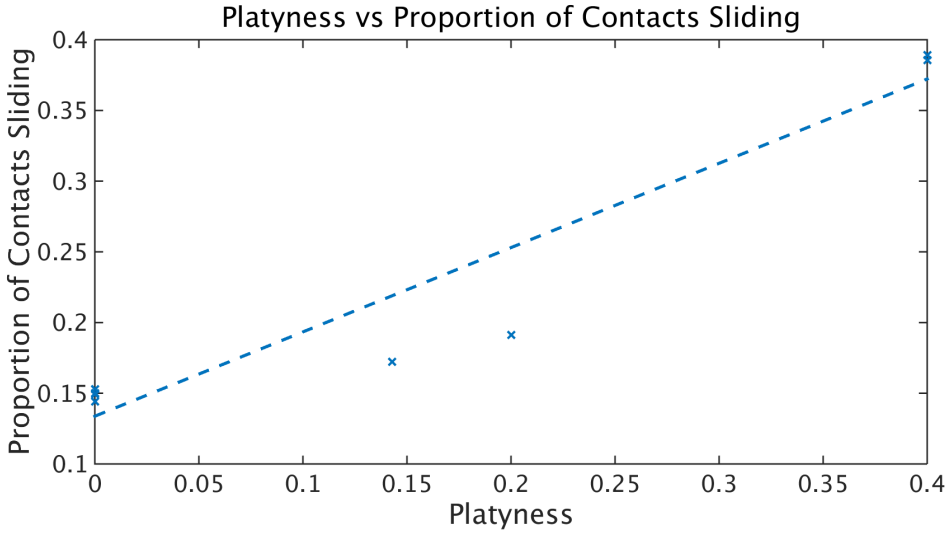

Figure 5.12: Mean proportion of sliding contacts against mean rate of rotation

Spherical particles rotate much more compared to platy particles; the rate of rotation decreases with increased platyness. As platyness increases there is a increase in the proportion of sliding contacts at critical state (Figure 5.12). An inverse relationship is seen between rate of rotation and the proportion of sliding contacts at critical state. Therefore to some extent the higher critical state strength exhibited by platy particles is due to platyness suppressing particle rotation and leading to increased interparticle sliding, a mechanism that in comparison requires more energy to be expended.

5.1.4 Contact Distribution

Contact between two ellipsoids can be any one of six types, depending on which side of one ellipsoid comes into contact with which side of the other. Figure 5.13 shows the

different types of contact. The type of any given contact in a DEM simulation can be determined using the geometry of the contacting particles, the location of the contact point on their surfaces and geometrical arguments. For degenerate cases of ellipsoids, where some of the radii are equal, the independent contact types are fewer: for example only one type of contact is possible between two spheres, where $L = I = S$.

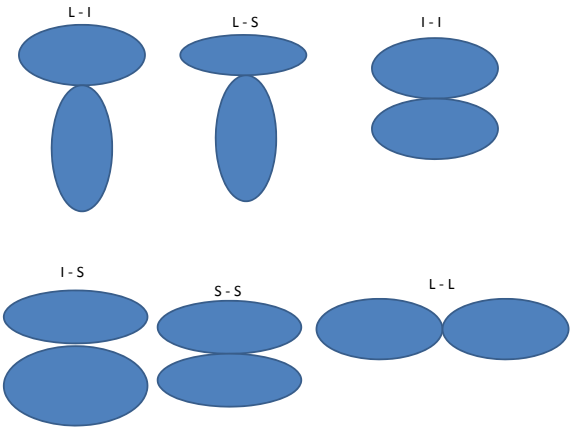

Figure 5.13: Different contact types for ellipsoidal particles

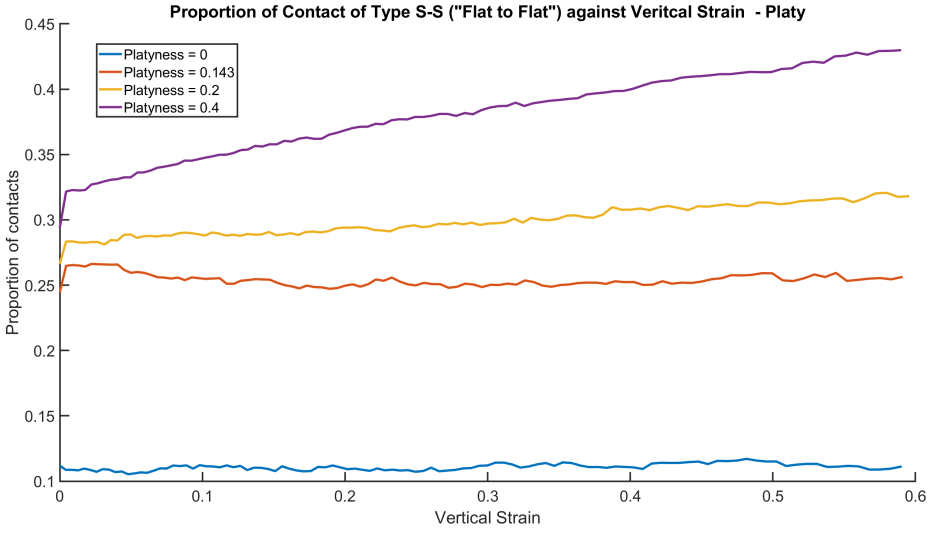

Figure 5.14: Distribution of contact type S-S against Vertical Strain

Figure 5.14 shows how the number of S-S ("flat-to-flat") as a percentage of the total number of contacts develops over time for each model. For spherical particles the difference between L, I and S is simply operational and the data merely confirm that all "types" of contacts occur with the same probability as expected. As the particle shape becomes platyier the proportion of S-S type contacts increases, to some extent reflecting the increasing area of "flat" particle surfaces available for contact. The proportion of S-S contacts in near-spherical particles remains relatively constant (i.e. oscillating around

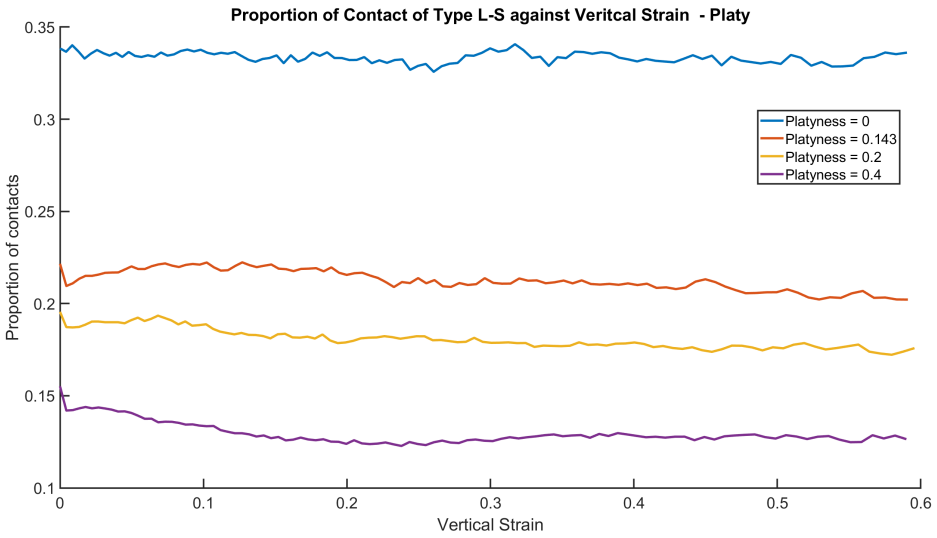

Figure 5.15: Distribution of contact type L-S against Vertical Strain

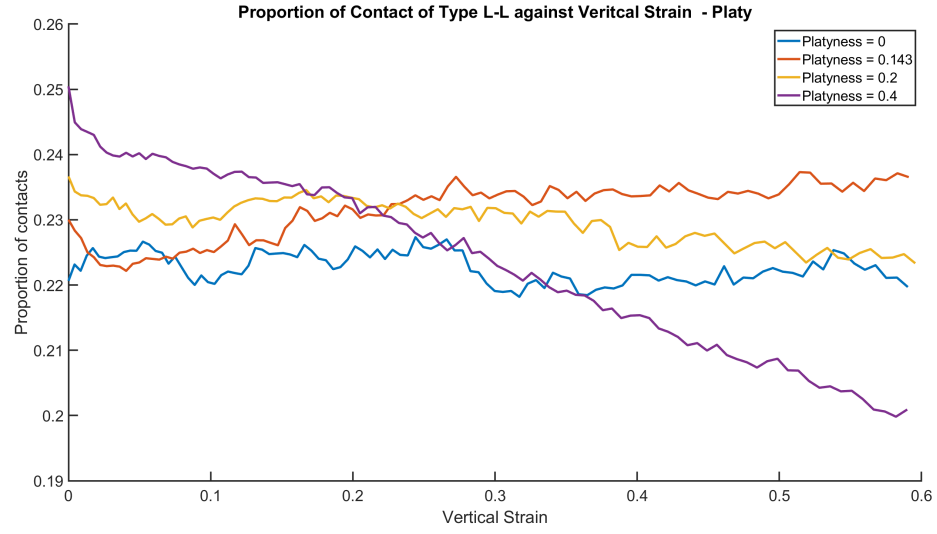

Figure 5.16: Distribution of contact type L-L against Vertical Strain

the same value between 10% and 50% strain). The platyier shapes contacts however become even more prevalent as the specimen is strained. This continuing formation of such contacts coincides with a pronounced reorientation of particle flats normal to the maximum principal stress (Figure 5.5).

Figure 5.15 shows the proportion of L-S ("side-to-flat") contacts over time for all models. Similarly to S-S, it remains relatively constant for near-spherical particles. In contrast to S-S, however, the proportion of L-S contacts for the platyier particles reduces with straining. The proportion of L-L ("side-to-side") type contacts, on the other hand, remains relatively constant throughout for all models (Figure 5.16).

The data suggest that, as the model is strained, platyier particles promote a conversion of less stable L-S to inherently more robust S-S contacts that are less likely to subsequently

break. There appears to be a threshold value $0.2 \leq \alpha_{cr} \leq 0.3$ of platyness, where a transition takes place to this type of "platy" behaviour for $\alpha \geq \alpha_{cr}$, from "near-spherical" behaviour for $\alpha \leq \alpha_{cr}$.

5.1.5 Conclusions

In this section, the results from forms that only contain platyness where presented and discussed. It was seen that spherical particles have the lowest strength with critical state angle of friction increasing linearly with platyness. This increase in strength is a result of a change in deformation mechanism between a rolling regime.

As particles increase platyness, there is an increase in the critical state strength of the granular material. This increase in strength from changing platyness acts complimentary to the increase in strength that comes with increasing particle elongation. The origin of this increase in strength comes from the deformation mechanisms and the efficiency of the dissipation of energy within the system. This indicates that there are two complimentary mechanisms taking place.

The first of these mechanism is particle rotation, which at critical state was to decrease as particle platyness increases. With this decrease in rotation the model still has to deform this means another mechanism must be taking over the deformation of the material. The other mechanism is particle translation, i.e. particles translating relative to each other. This can be described by the proportion of the contacts that are sliding. Whilst the proportion of contacts sliding will contain an amount of particles that are rotationally frustrated (i.e. are rotating at differential rates). However it is assumed that the majority of the sliding is caused by differential translation and not rotation.

As the models become deformed there is also an increase in proportion of S-S contacts (Flat to Flat). The initial proportion of these contacts could be described by the increased surface area associated with the flat face of play particle. As the modelled is strained this proportion of contacts increases indicating that S-S contacts are stabler than any other type of contact.

It is thought that these mechanisms are due to the preferred deformed state. As a model is strained, the particles tend to lay with their shorted axis mostly vertical with this effect become more pronounced as the particle shape becomes increasingly platy. As majority of the particles adopted this orientation allowing for a stacking effect of the particle structure similar to how other flat circular objects stack such as coins. This stacking structure would result in a reduced rotation as individual particles would become "pinned" by the surrounding particles forcing the deformation to occur as sliding instead. It is unknown how the model would react if the particles where placed in this deformed state initially however it is possible that this would lead for a model to reach a critical state faster.

5.2 Effect of Elongation (Prolate Ellipsoid)

In this section only the results of the elongated particles, forms with zero platyness starting from a sphere and becoming more prolate (Figure 5.17), shall be presented and discussed. The results being looked at are:

- Mobilised Angle of Friction
- Critical State Strength
- Particle Orientation
- Particle Rate of Rotation
- Contact Analysis

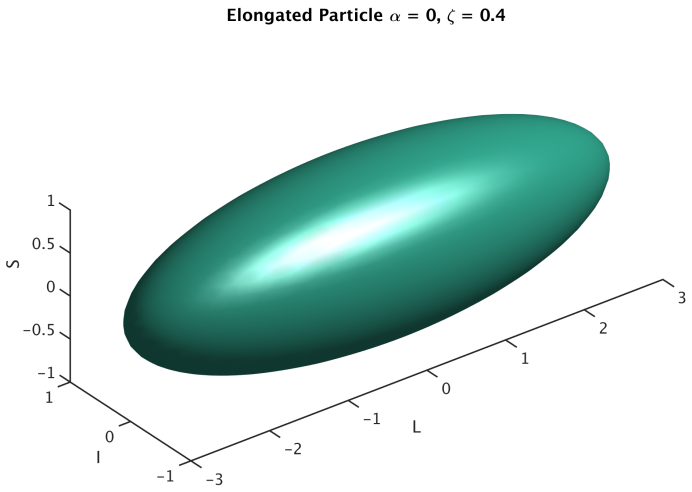

Figure 5.17: Form - Elongated particle

5.2.1 Shear Strength

Shear strength of a granular material can be described by the mobilised angle of friction ϕ_{mob}, given by Equation (2.5).

Figure 5.18 plots the mobilised angle of friction against vertical strain for each model. As with platy forms peak friction angles differ widely, these are not directly comparable because they may correspond to different initial relative densities. Due to the presumed difference in relative density among models, some reach a very dense packing, that results to an almost immediate mobilisation of a very high angle of friction. Other models exhibit a delayed mobilisation of a rather lower peak.

Figure 5.19 shows that as the shape of the particles becomes more elongated, critical state strength increases roughly linearly with elongation.

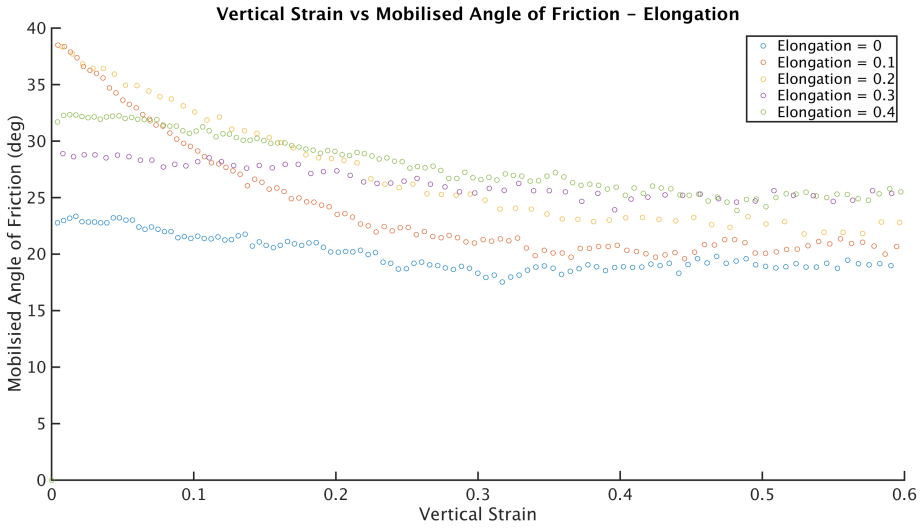

Figure 5.18: Mobilised angle of Friction against Vertical strain

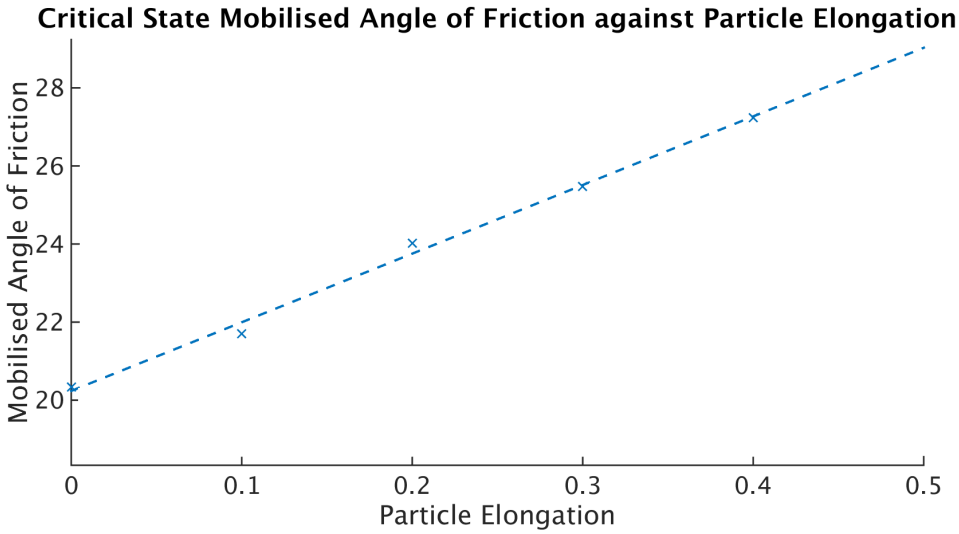

Figure 5.19: Friction angle at critical state against Platyness

5.2.2 Particle Orientation Fabric

At the start of the test, particles have a random orientation. However, as shearing takes place, particles will generally reorient themselves and may do so along a preferred direction. The orientation of a scalene (ellipsoidal) particle can be described by a local system of orthogonal vectors in the directions of its three radii (L, I and S).

For elongated forms (prolate ellipsoids) only the L axis is needed to describe the orientation of the particle due to the symmetry around the L axis. Figure 5.20 shows how the G_{33} component of the fabric tensor corresponding to the L-direction of each particle varies with vertical strain. G_{33} essentially quantifies the prevalence of particles choosing to reorient their L-axis parallel to the global z-axis

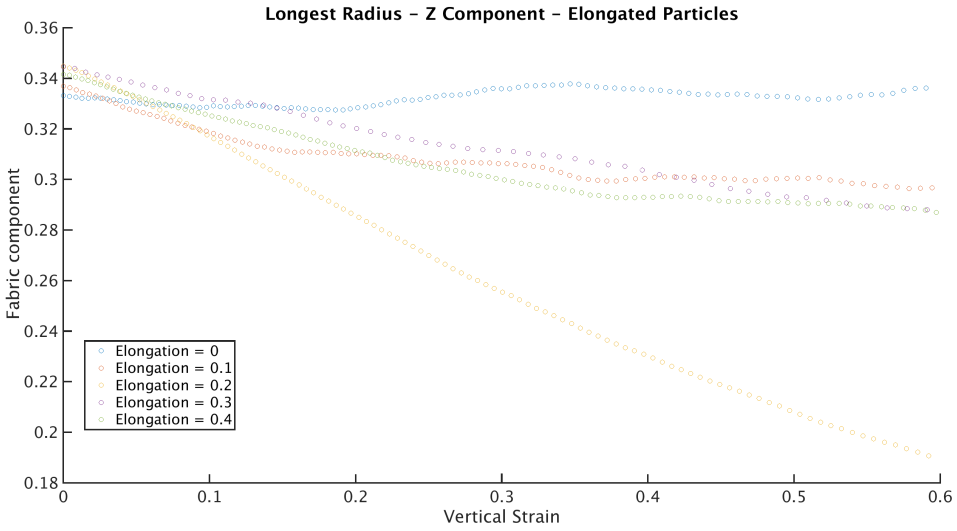

Figure 5.20: Vertical fabric orientation for the particle's L radius against Vertical Strain

All tests started with random particle orientation, shown by a value of $G_{33} \approx 0.33$ in Figure 5.20. As vertical strains increased G_{33} decreased, showing that on average particles re-oriented their longest axis to lay flat, orthogonal to the maximum principal stress in the course of shearing. Also, the rate of reorientation progressively decreases as the model approaches critical state, presumably because a configuration that can accommodate further shearing is reached. This general behaviour is observed even for relatively small values of elongation. In contrast, spherical particles do not show any tendency to re-orient and $G_{33} \approx const.$ throughout.

5.2.3 Particle Rotation and Sliding

As a specimen is strained, the particles will displace and rotate to accommodate this by rearranging the structure of the granular skeleton. Rotations quantified by Equation (5.2).

Figure 5.21 shows the change in rate of rotation against vertical strain. As straining takes place all models see an intimidate increase in the rate of rotation, the "acceleration" is greatest in the form S1 (spherical particles) with a decreasing initial "acceleration" as the particles become elongated. These results follow convential wisdom that spherical particles are the easiest form to rotate and as elongation increases so does rotational resistance. However this gives no indication as to which axis the particles prefer to rotate about.

Figure 5.22 shows the distribution of rotation within the elongated model at the initial time step. There are patches of high rotation within the model which correspond to single particles with high rotation. These areas of rotation are also surrounded with

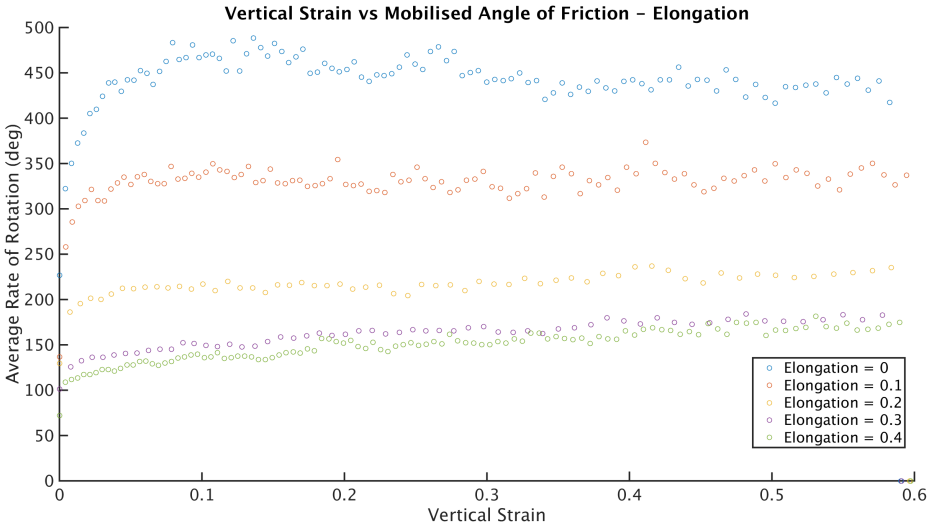

Figure 5.21: Mean rate of rotation against vertical strain

areas of higher rotation, indicating that the rotation is being distributed to the rest of the particles. As with the platy particles there is no evidence of a shear band at a later time point (Figure 5.23).

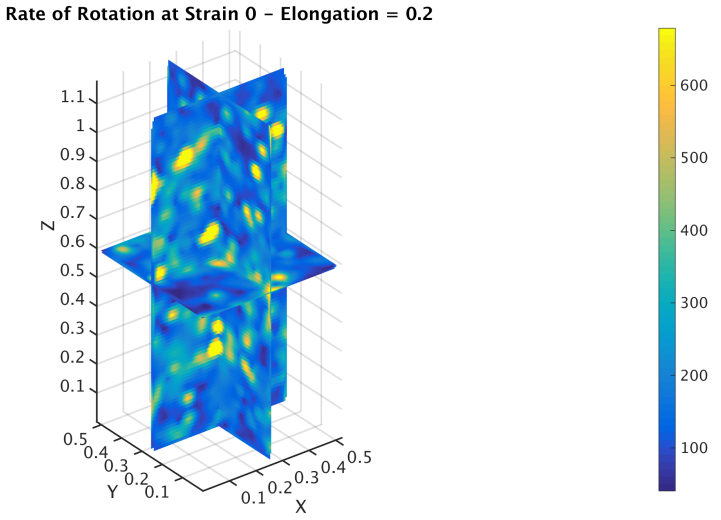

Figure 5.22: A heat map showing the distribution of rotation within a model at the start of straining - Elongated particle

Figure 5.25 shows the change in proportion of contacts that are sliding against vertical strain. At the start of straining there are no contacts that are sliding as the model is stable under isotropic stress conditions. As soon as straining commences the contacts are no longer in equilibrium and greater shear forces are developed and reach a peak. At the peak, the least amount of sliding takes place in spherical model at 25% of the contacts sliding and an increasing amount of sliding is seen in elongated particles with the elongated model having a peak of 60% of contacts sliding. The ordering of the forms remains through out straining.

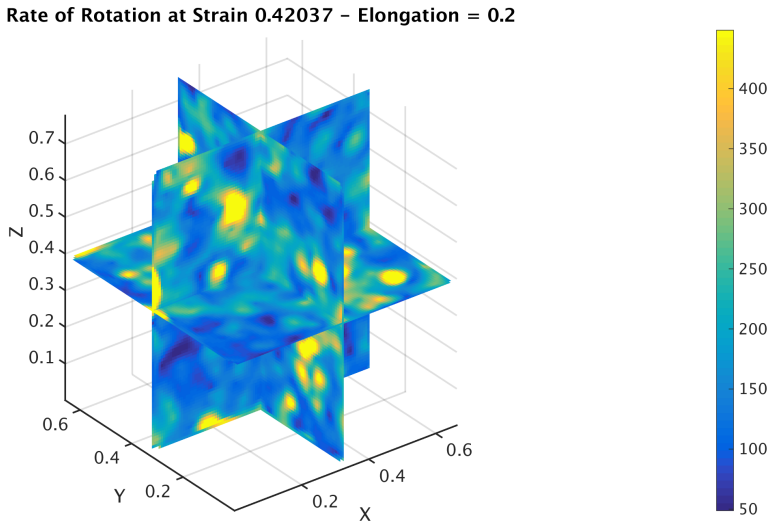

Figure 5.23: A heat map showing the distribution of rotation within a model at 42% strain - Elongated particle

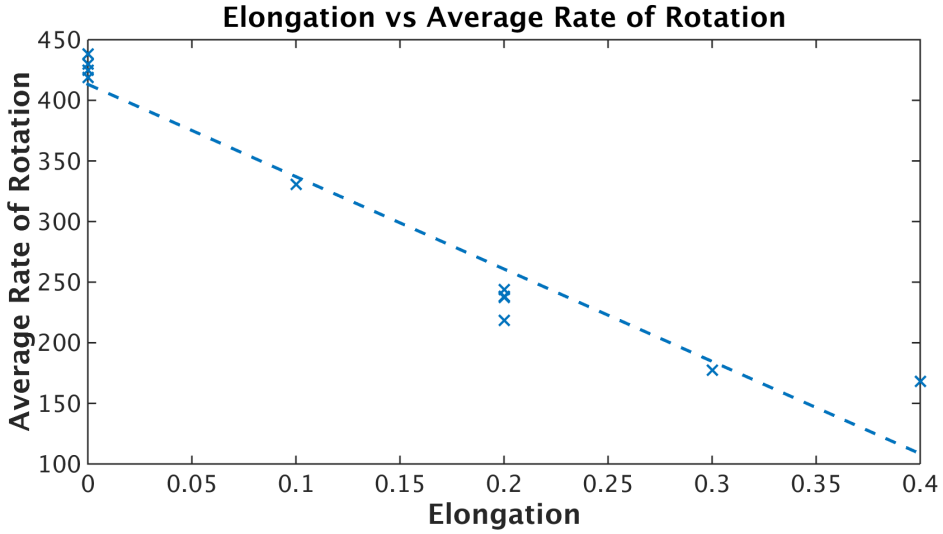

Figure 5.24: Mean rate of rotation at critical state against particle elongation

Spherical particles rotate much more compared to elongated particles; the rate of rotation decreases with increased elongation (Figure 5.24). As elongation increases there is a reduction in the proportion of sliding contacts at critical state (Figure 5.26). An inverse relationship is seen between rate of rotation and the proportion of sliding contacts at critical state. Therefore to some extent the higher critical state strength exhibited by elongated particles is due to elongation suppressing particle rotation and leading to increased interparticle sliding, a mechanism that in comparison requires more energy to be expended.

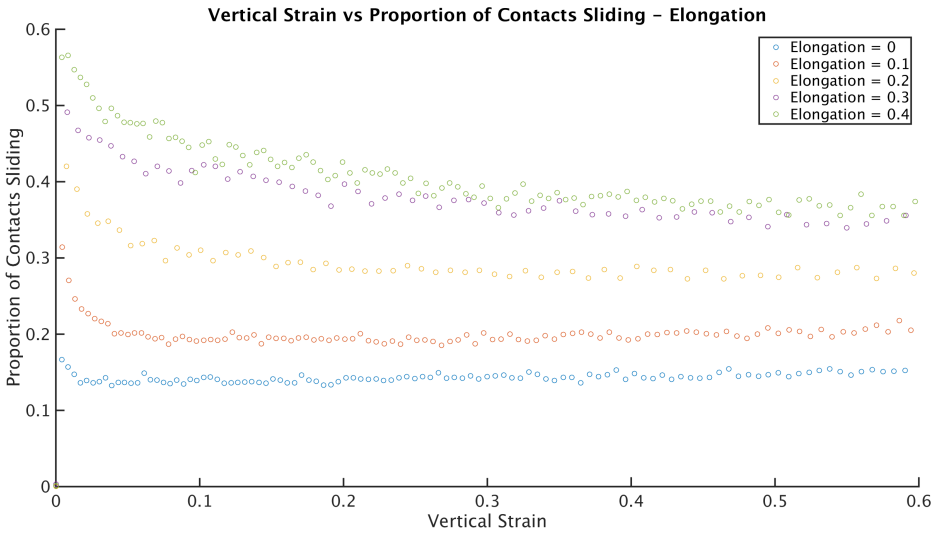

Figure 5.25: Proportion of contacts that are sliding against vertical strain

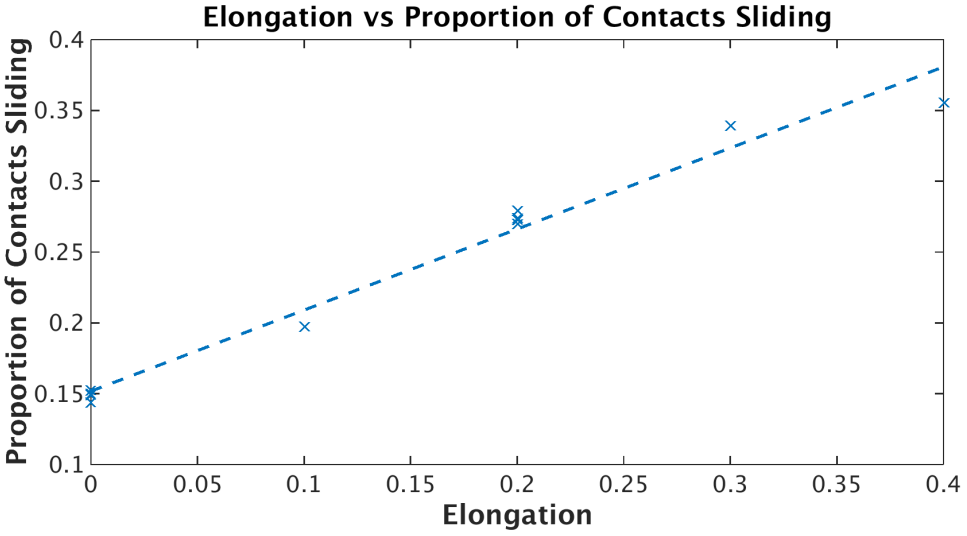

Figure 5.26: Proportion of contacts that are sliding against particle elongation

5.2.4 Contact Distribution

As with platy particles the types of contacts are sorted based upon the location of the contact point. Figure 5.27 shows how the number of *S*-*S* ("flat-to-flat") as a percentage of the total number of contacts develops over time for each model. (For spherical particles the difference between *L*, *I* and *S* is simply operational and the data merely confirm that all "types" of contacts occur with the same probability as expected.) As particle form becomes more elongated there is an increase in the proportion of *S*-*S* type contacts. As particles become increasingly elongated the relative proportion of the contact area for the s axis will increase. Unlike platy particles there is no significant change in the proportion of contact types over time.

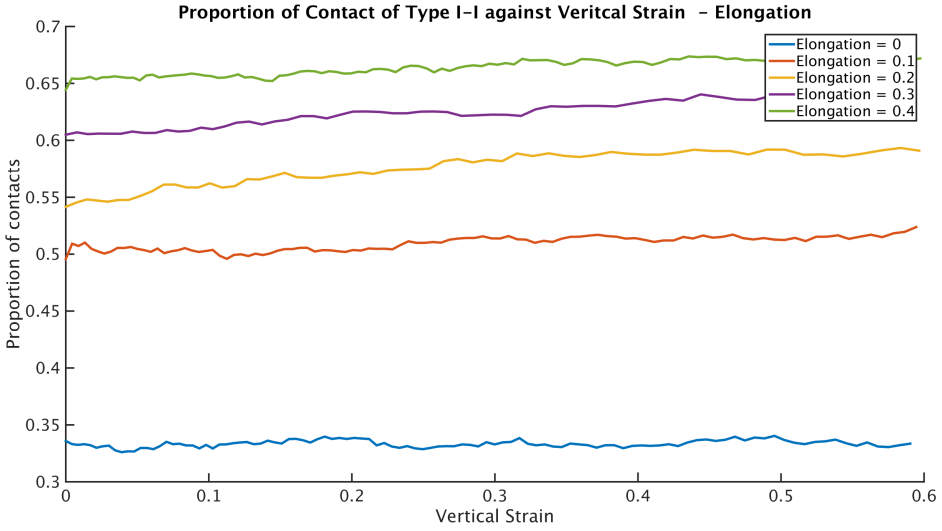

Figure 5.27: Distribution of contact type I-I against Vertical Strain - Elongation

Figures 5.28 and 5.29 show the distribution of L-S ("side-to-flat") and L-L ("side-to-side") type contacts over vertical strain. Similarly to S-S type contacts these both see a reduction in the proportion of contacts in line with the change in proportion of surface area.

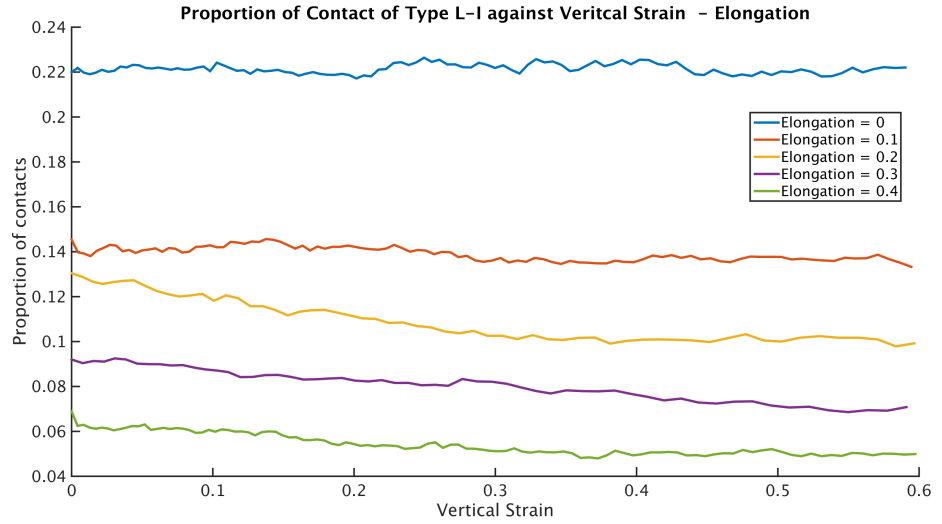

Figure 5.28: Distribution of contact type L-I against Vertical Strain - Elongation

5.2.5 Conclusions

In this section, the results of forms that only contain elongation where presented and discussed. It was seen that spherical particles have the lowest strength with critical state angle of friction increasing with elongation. As with particle platyness the different deformation mechanisms of particle rotation and particle sliding where considered.

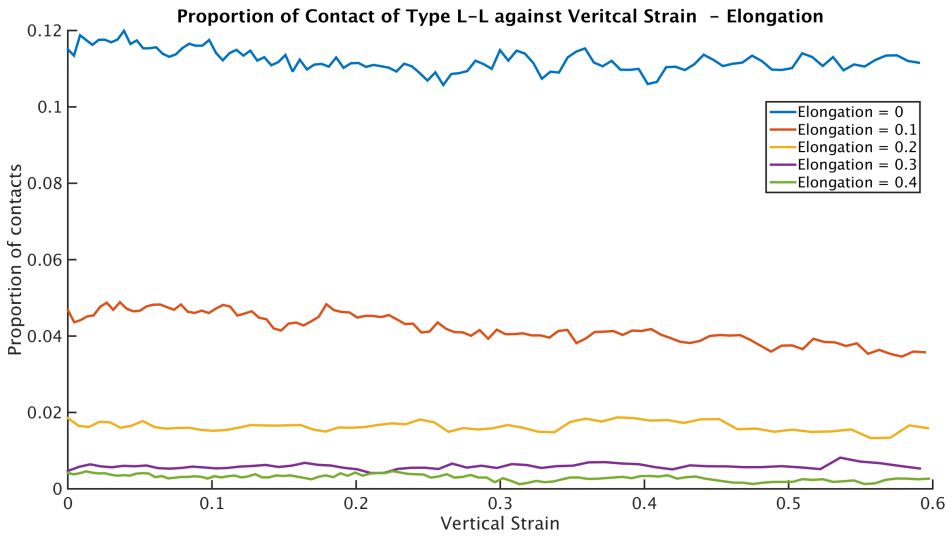

Figure 5.29: Distribution of contact type *L*-*L* against Vertical Strain - Elongation

As the particles become increasingly elongated the average amount of rotation within the system decreased. Similarly the proportion of sliding contacts increased, this indicates that as the particles became elongated the primary deformation mechanic changed from being purely rotation to being a combination of rotation and sliding. This change in deformation regime also lead to an increased critical state strength with in the model.

This change in mechanism can be related to the deformed state of the models as critical state, with the elongated particles tending to having the longest axis horizontal. For an individual elongated particle on a flat surface, this orientation is stable compared to a similar particle orientated vertically when subjected to a vertical compressing force. However with a purely elongated particle this increased stability does not stop any rolling in the equal axis as it still has a cross section of a sphere in the I-S plane.

The majority of the types of contacts consisted how I-I (side to side). As the models increased in elongated the initial proportion of side to side type contacts increases in proportion to the relative surface area associated with a side. It is argued that the I-I contact provides a stabilising force to a particle due to the support provided from having multiple contacts spread along it's base.

Whilst a single elongated particle may not be the most stable of particles due to the ability to roll in a single direction this can be compensated with a collection of particles. Due to the random orientation of the initial system of particles there was no preferred direction on the global X-Y plane orthogonal to the compressing force. As the model becomes strained there is no evidence of a preferred orientation appearing this shows that the particles maintain their scattered structure. This scattered structure is essential to the models strength as there is a potential for the system to align in the horizontal plane. If the particles aligned in this direction the system would no longer be

considered elongated particles as if a 2d section was cut through the sample it would appear as circles. Which has been shown in the literature to be significantly weaker. This highlights that whilst particle elongation is an important factor in the development of microstructures within a granular material, it is still dependant on the initial conditions to allow for these microstructures to form.

The strength of a collection of elongated particles relies on a random orientation or particles in the horizontal plane. This random orientation helps provide each particle with increased stability due to multiple particles supporting their bases, reducing the amount of rotation in the horizontal direction. This reduced rotation means forces the particles to slide and translate to accommodate the strain, leading to an increase strength within the model. This forms a lattice type structure similar to a bird's nest made out of sticks.

5.3 Effect of Particle Form (Scalene Ellipsoid)

In this section the results for all scalene ellipsoids will be presented, including the results from the previous sections (Prolate and Oblate ellipsoids). The particles cover a range of different forms over distributed over the form diagram, figure 4.2. Using the results and conclusions from the sections on platy and elongated ellipsoids the individual failure mechanisms will be explored on how they interact.

5.3.1 Critical State Strength

Figure 5.30 shows a heat map of the critical state values taken from the ellipsoidal models, including the results from platy and elongated particles. This shows that spherical particles have the lowest strength, as seen before but also that the effect elongation has is more significant than the effect of platyness. The highest strength is seen in particles that have both elongation and platyness.

5.3.2 Particle Rotation and Sliding

The effect of platyness and elongation can be thought of as separate mechanisms with their effects being cumulative. Varying particle elongation appears to have a greater impact on causing contacts to slide (Figure 5.31) whereas platyness causes the particles to rotate less (Figure 5.32). Elongation has a significant impact on strength it could be argued that an increased sliding could lead to an increase in strength.

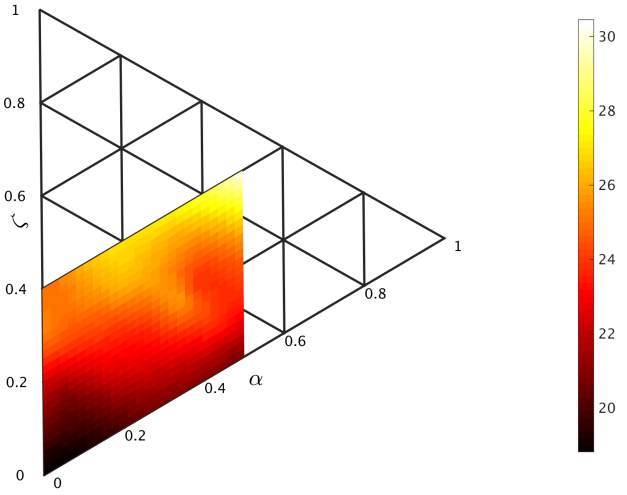

Figure 5.30: Friction angle at critical state against particle form

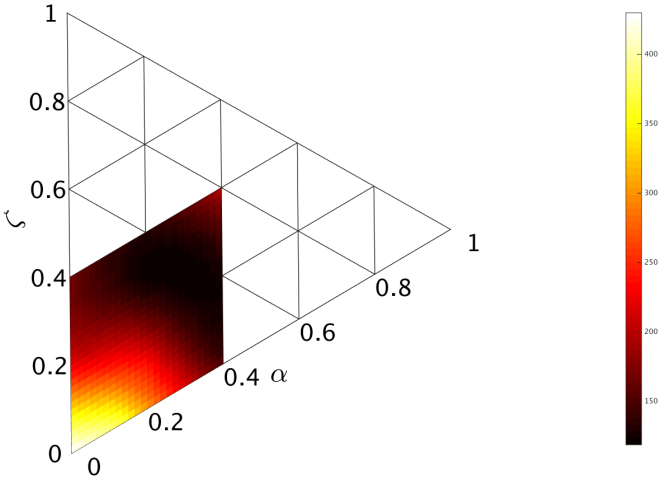

Figure 5.31: Mean rate of rotation at critical state against particle form

5.3.3 Micromechanics

Figure 5.33 compares the orientation of the longest axis of a scalene ellipsoid with equal elongation and platyness against the same results for a sphere. This shows that the same effect as seen with elongation of the particle orientating its longest axis perpendicular to the principal stress is occurring.

Similarly figure 5.34 compares the shortest axis fabric tensor against the vertical component of a sphere and as with platy particles the S axis is orientating itself to be in line with the principal stress. This shows that both effects from particle platyness and particle elongation are present and are complementary to each other.

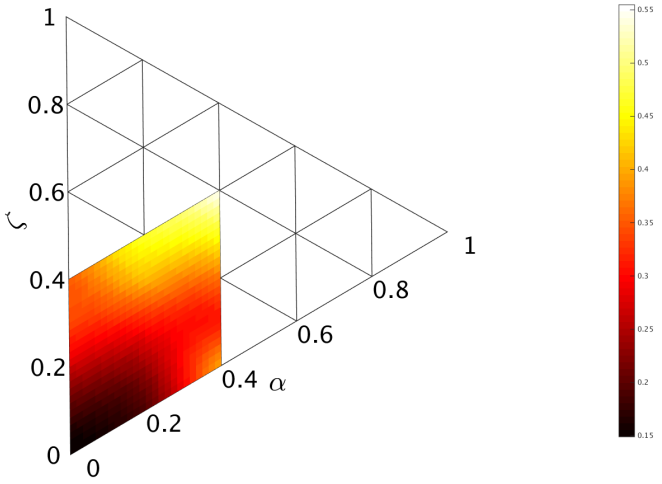

Figure 5.32: Proportion of contacts sliding at critical state against particle form

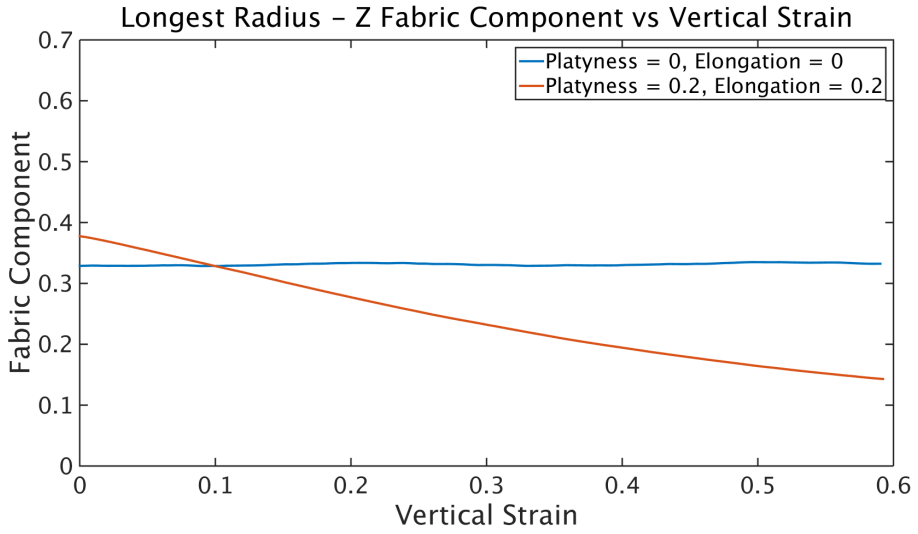

Figure 5.33: Vertical fabric component for the L radius against vertical strain - Scalene Particle

5.3.4 Conclusions

In this section the results from models containing pure form (ellipsoidal particles) where discussed. A systematic approach was used to understand the complete effects of particle form with a range of ellipsoids with no form (spheres), platy particles (disks), elongated particles (needles), and a mixture of forms in-between.

As a particle deviates from a sphere there was a resulting increase in critical state strength. The effect of particle elongation is seen to be more critical factor in increasing particle strength compared to platyness alone however the highest strength is measured in particles with both platyness and elongation.

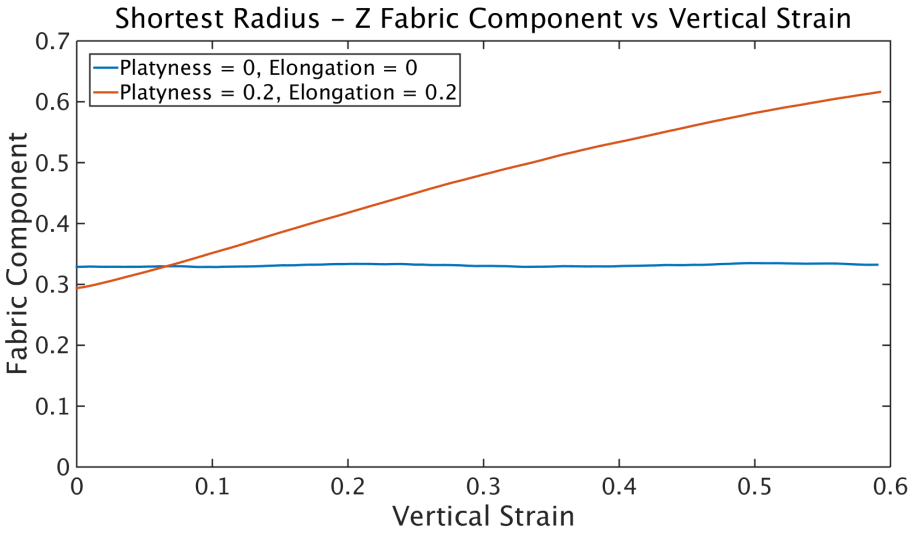

Figure 5.34: Vertical fabric component for the S radius against vertical strain - Scalene Particle

For each model two main deformation mechanisms where considered; rotational and sliding. Typically as a model became stronger there was a higher proportion of sliding contacts and a decreased amount of rotation within the sample compared to a spherical particle models.

These two different microstructures complemented each other with particles that had a mixture of platyness an elongation showing the characteristics of these microstructures. For a particle that had a mixture of form there is an increase in proportion of flat-flat type contacts as well as a preference to orientating the flatter face normal to the major principal stress which is evidence of the similar stacking structure seen in purely platy particles. The particle's longest axis was also orientated orthogonal to the principle stress, in the plane orthogonal plane there is still a random orientation with no preferential direction indicating that a similar nest like structure has formed. As a particle's form increased in both platyness and elongation these microstructures became increasingly pronounced.

5.4 Conclusions

In this chapter DEM was used to investigate the effect of particle form on critical state strength. This was done by subjecting a sample to triaxial compression conditions with a periodic boundary. The results of particle form where initially split into elongation and platyness so that their effects may be studied separately. After this the full results from particle form this included particles with both elongation and platyness.

The results from the platy particles showed spherical particles had the lowest critical state strength and that increasing particle platyness lead to an increase in strength.

This increase in strength was accompanied by a transition from a rolling deformation mechanic to a sliding mechanic. This change in mechanism was caused by microstructures forming with in the model. As a platy model is strained, the particles tend to lay with their shorted axis mostly vertical. Accompanying this change in particle orientation there is was an increase in the proportion of flat-flat contacts, flat-flat contacts are considered stronger than other type of contacts. This leads to a stacking effect of the particle structure similar to how other flat circular objects stack such as coins.

The results of the elongated particles, it was seen that spherical particles have the lowest strength with critical state angle of friction increasing with elongation. As the particles became increasingly elongated the average amount of rotation within the system decreased, as well as this there was an increase in proportion of sliding contacts. This change in mechanism indicates that as the particles became elongated the primary deformation mechanic changed from being purely rotation to being a combination of rotation and sliding. This change in deformation regime also lead to an increased critical state strength with in the model.

This change in mechanism can be related to the deformed state of the models as critical state, with the elongated particles tending to having the longest axis horizontal. The majority of the types of contacts consisted how I-I (side to side). It is argued that the I-I contact provides a stabilising force to a particle due to the support provided from having multiple contacts spread along it's base.

The strength of a collection of elongated particles relies on a random orientation or particles in the horizontal plane. This random orientation helps provide each particle with increased stability due to multiple particles supporting their bases, reducing the amount of rotation in the horizontal direction. This reduced rotation means forces the particles to slide and translate to accommodate the strain, leading to an increase strength within the model. This is might form a lattice type structure similar to a bird's nest made out of sticks.

The results from the complete range of different shaped ellipsoids particles it was found that as a particle deviates from a sphere there was a resulting increase in critical state strength. This result is consistent with the literature where by in 2D simulations studying the effects of particle form circular particles had a lower critical state strength than other forms. The measure of particle elongation is seen to be more critical factor in increasing particle strength compared to platyness alone however the highest strength is measured in particles with both platyness and elongation.

As with the previous results, as a model became stronger there was a higher proportion of sliding contacts and a decreased amount of rotation within the sample compared to a spherical particle models.

These two different microstructures seen in platy and elongated models complemented each other with particles that had a mixture of platyness an elongation showing the characteristics of both microstructures. As a particle's form increased in both platyness and elongation the characteristic of these microstructures became increasingly pronounced.

These results show that particle form helps for these microstructures to develop within the model. These microstructures help reduce the overall amount of rotation with in a model and thus force granular particles to displace by sliding over each other increasing the critical state strength. Whilst these results show that these microstructures develop whilst the model is strained it is unknown what the impact of a designed initial fabric might be.

Chapter 6

Particle Angularity

In this chapter the results for angular particles, particles with no form, will be discussed. The results will be split into two main parts; the superellipsoids and the platonic solids. Both sets of shapes are considered to have zero form due to the best geometrically fitting ellipsoid being that of a sphere. The key difference between these two sets of shapes is how their angularity is displayed; superellipsoids have a smooth continuous function describing the surface, whereas the platonic solids are defined by multiple planes describing the faces. This distinction in angularity is key as other measures of angularity (or roundness) within the literature make the distinction between a sharp edge or corner and a curve over a surface. The results being looked at are:

- Mobilised Angle of Friction
- Critical State Strength
- Particle Rate of Rotation

To constrain a superellipsoid to the form of a sphere the radius is kept at a constant, this simplifies the equation for a superellipsoid to (6.1). By varying the values of n between 1 (sphere: Figure 6.1) and 0.3 (blocky sphere: Figure 6.2) a range of different angular shapes are created. In this chapter the values of n for the shapes tested are given in Table 6.1.

$$|x|^{\frac{2}{n}} + |y|^{\frac{2}{n}} + |z|^{\frac{2}{n}} = 1 \tag{6.1}$$

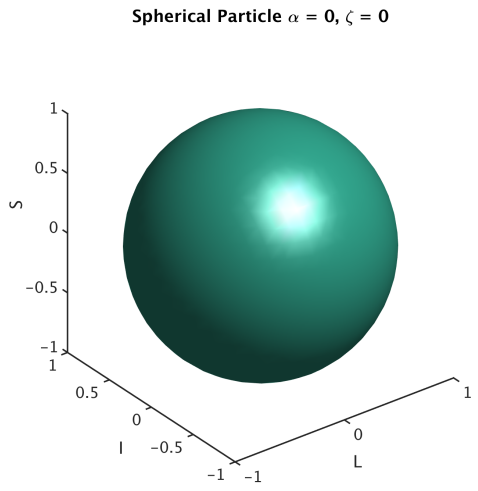

Figure 6.1: superellipsoid - n = 1 sphere

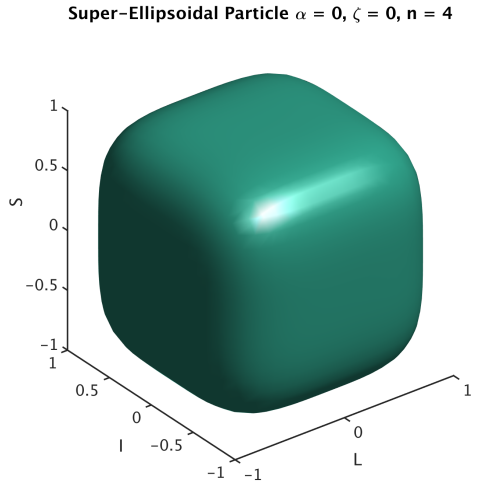

Figure 6.2: superellipsoid - n = 0.5 "blocky" sphere

Type	Measure	Angularity
Superellipsoid	1	0
	0.7	0.0325
	0.5	0.1019
	0.3	0.1799
Platonic solid	Tetrahedron	0.4808
	Cube	0.2087
	Octahedron	0.1844
	Dodecahedron	0.0496
	Icosahedron	0.0429

Table 6.1: Shapes tested and angularity

6.1 Shear Strength

Figure 6.3 shows the mobilised angle of friction against the vertical strain for the superellipsoids. All the models here follow the shape of a densely packed model, with an initial peak eventually reaching a critical state.

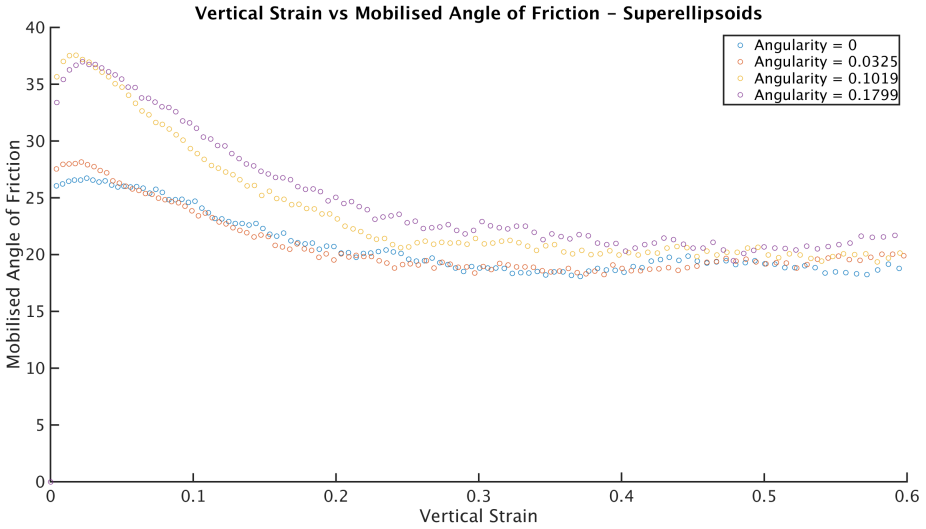

Figure 6.3: Mobilised angle of Friction against Vertical strain - Superspheres

At the critical state there is only a small difference between the strength of near spherical superellipsoids. The angularity of 0.0325 and the angularity of 0 are almost identical in value. The biggest difference is seen at the higher angularity but even this effect is relatively minor.

Figure 6.4 shows the mobilised angle of friction against the vertical strain for the platonic solids. All the models here follow the shape of a densely packed model, with an initial peak eventually reaching a critical state.

Looking at the critical state values of the platonic solids a similar trend is seen. The near zero angularity models have a relatively similar strength but as the angularity increase so does the strength. The highest strength is seen in the tetrahedron shaped particles, with an angularity of 0.4808 and a critical state of 26.6, compared to the lowest dodecahedron with a critical state of 19 degrees.

Figure 6.5 compares these critical state values against the particles angularity for both the superellipsoids and the platonic solids

There is a general linear relationship between the measured angularity of a particle and the mobilised angle of friction at critical state. However, each individual model is open to variation. This matches to similar findings found in the literature where angular particles where generated with flat planes defining their faces and sharp edges. In this study the author compared the effect of angularity on the stress ratio at critical state

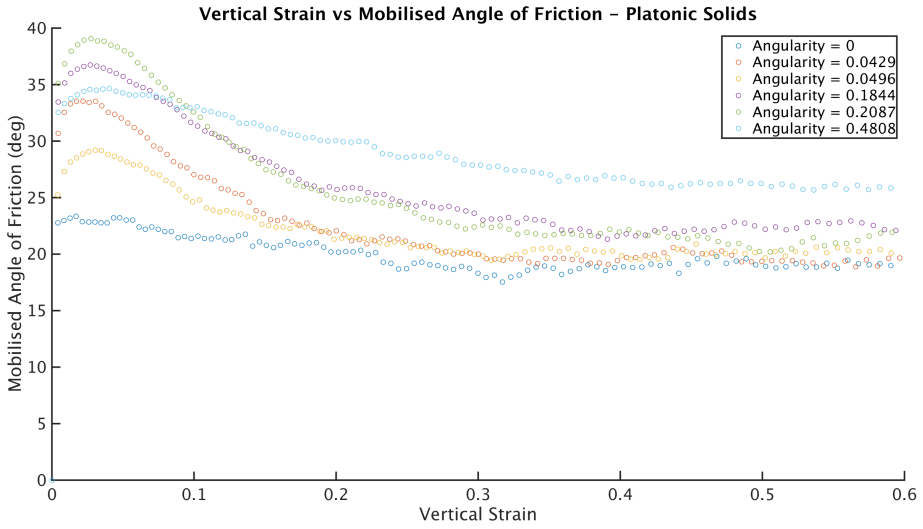

Figure 6.4: Mobilised angle of Friction against Vertical strain - Platonic Solids

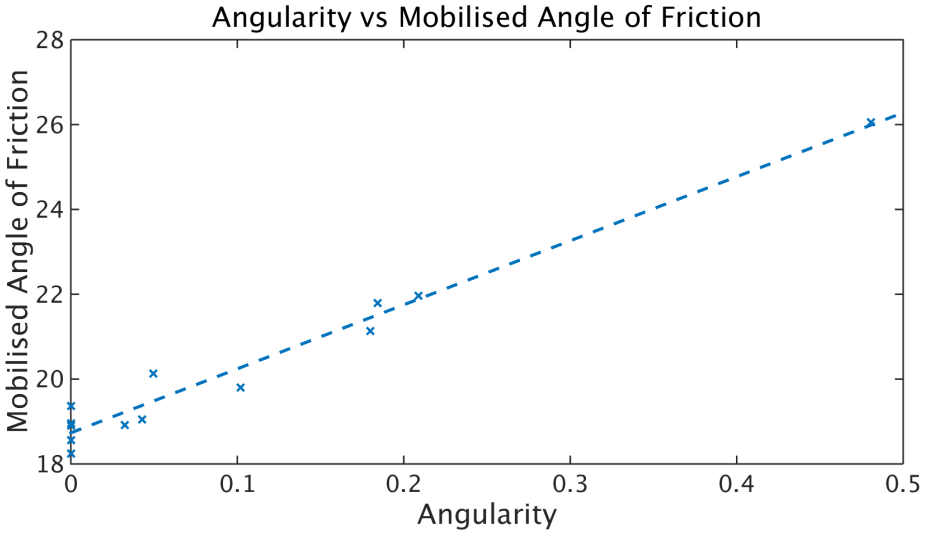

Figure 6.5: Friction angle at critical state against angularity

and found that as the measured angularity increased so did the critical state strength, (Radjaï et al., 2013).

Despite both the platonic solids and the superellipsoid's having no direct connection between their shapes, they both appear to follow the same linear relationship. This is significant as it indicates that the particle's strength at critical state here is independent of how the angularity is created.

6.2 Particle Rotation

As in the previous chapter, the average rate of rotation is calculated using equation (5.2).

Figure 6.6 shows the average rate of rotation for the model against the vertical strain for the superellipsoid particles. The spherical model has the highest amount of rotation and the lowest amount of rotation is in the model with the highest angularity. As the particles become increasingly angular there is a reduction in the overall rate of rotation within the models.

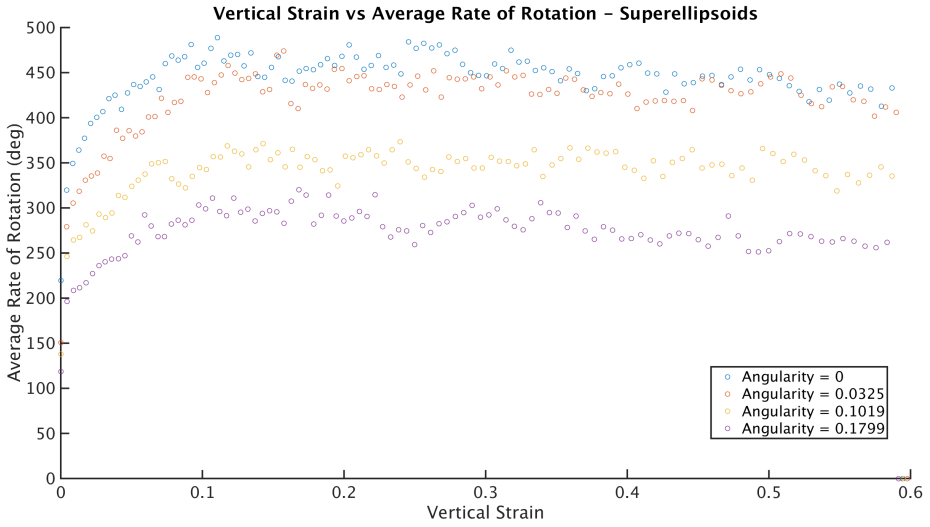

Figure 6.6: Average rate of particle rotation against vertical strain - Superspheres

Figure 6.7 shows the average rate of rotation for the model against the vertical strain for the platonic solids. The true sphere has the highest amount of rotation and the lowest amount of rotation for the tetrahedron shaped particle. As the particles become increasingly angular there is a reduction in the overall rate of rotation within the models.

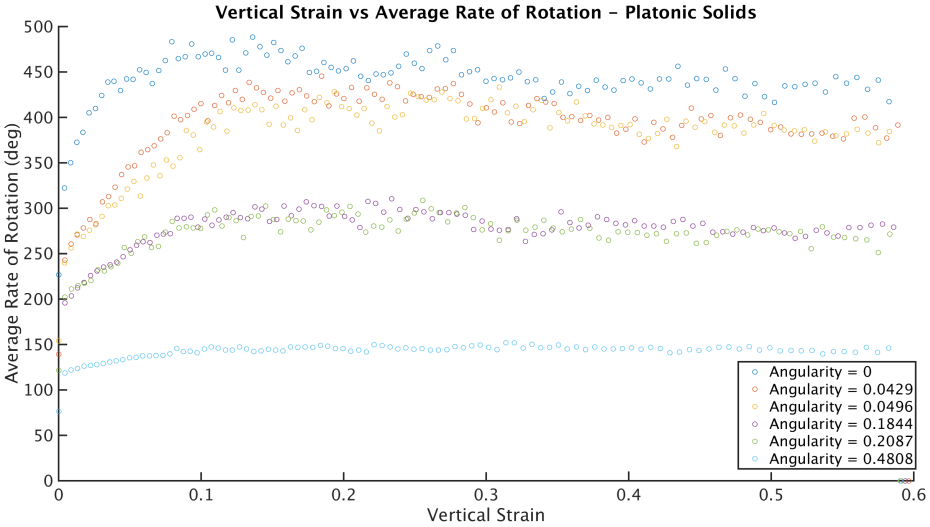

Figure 6.7: Average rate of particle rotation against vertical strain - Platonic Solids

Figure 6.8 shows the average rate of rotation for the model at critical state against the particle angularity. There is a linear relationship between the amount of rotation at critical state and the particle's measured angularity. This follows the same trend as with the critical state angle of friction.

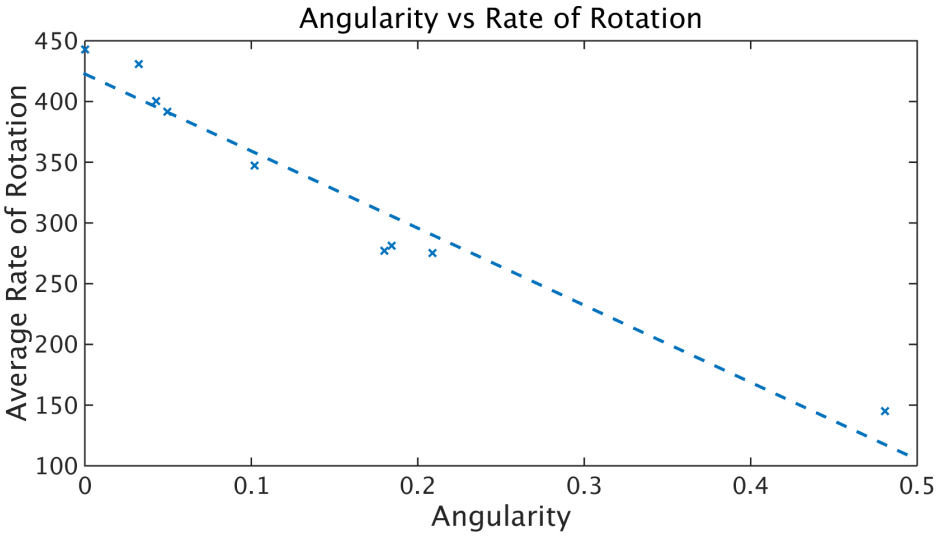

Figure 6.8: Average rate of particle rotation at critical state against angularity

6.3 Particle Sliding

Figure 6.9 shows the proportion of contacts that are sliding against vertical strain for superellipsoid particles. The spherical model has the lowest amount of sliding and as the angularity increases so does the amount of sliding.

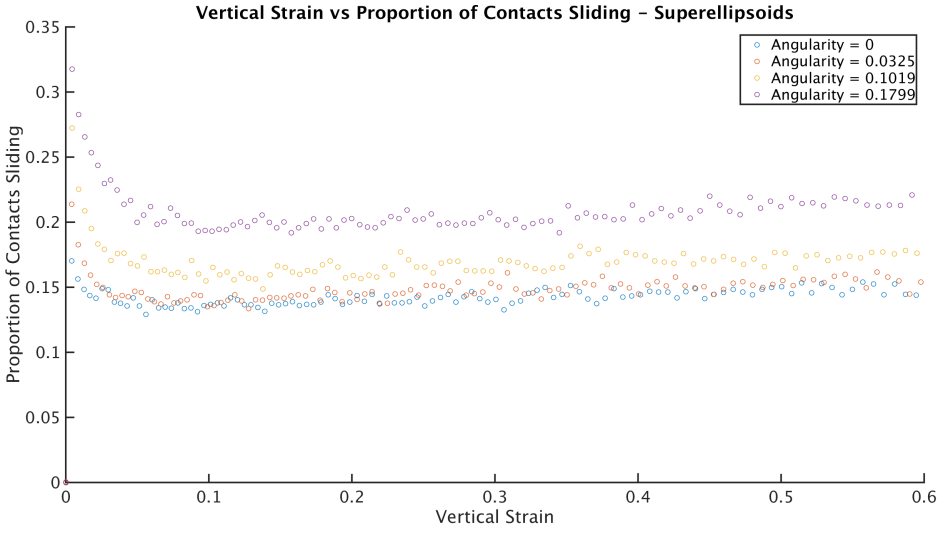

Figure 6.9: Proportion of sliding contacts against vertical strain - Superspheres

Figure 6.10 shows the proportion of contacts that are sliding against vertical strain for plantonic solids. The icosahedron model, having the greatest amount of faces and lowest angularity, has the least amount of sliding. The tetrahedron model has the greatest.

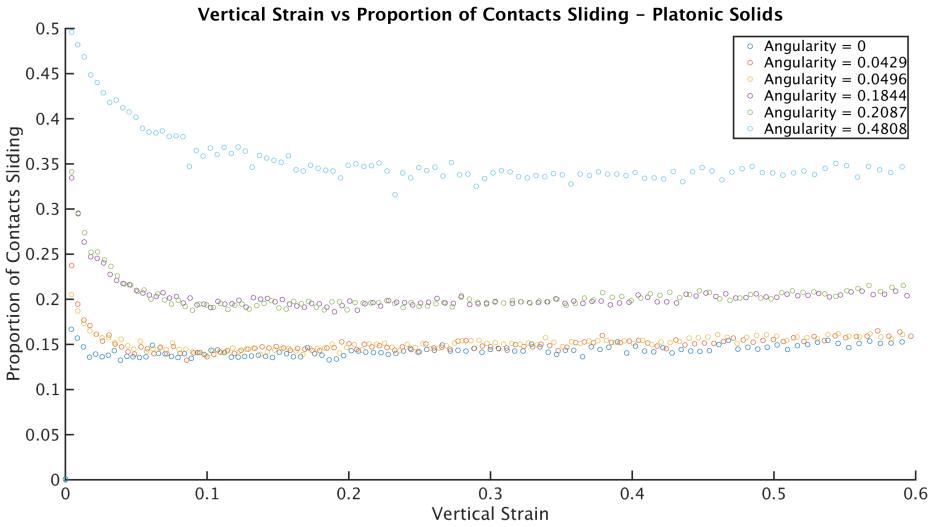

Figure 6.10: Proportion of sliding contacts against vertical strain - Platonic Solids

Figure 6.11 shows the proportion of contacts sliding for the model at critical state against the particle angularity. There is a linear relationship between the proportion of contacts sliding at critical state and the particle's measured angularity.

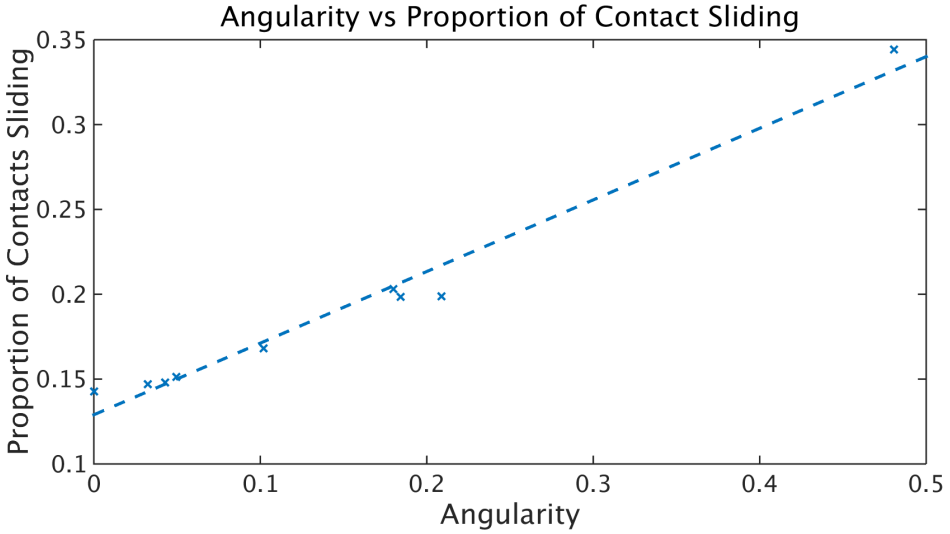

Figure 6.11: Proportion of sliding contacts at critical state against angularity

6.4 Micromechanics

As with particle form, this increased strength is accompanied by a decreased amount of rotation and an increase amount of proportion of contacts sliding. This lead to an

increases in the amount of energy loss within a system and leading to a stable structure. However unlike particle form, it is impossible to distinguish between the different types of contacts as these particles are symmetrical and all faces as considered equal.

A previous study modelling platonic solids showed that as a particle becomes increasingly angular stacking microstructures formed, for example cubes tended to align with their faces touching, which caused an interlocking behaviour reducing the amount of rotation, (Höhner et al., 2014). It is thought that similar microstructures are developing within the model as it is strained and the particles rotate and translate. For cubes this may resemble blocks stack upon each other helping to transfer the compressive load through the flat faces. Whereas tetrahedrons could form a crystalline structure by the particles surrounding a single particle being offset by 60 degrees. Figure 6.12 shows a 2D example with equilateral triangles. Due to their regular nature it is possible to construct a structure with all the angular particles by connecting the flat faces. These microstructures would provide an interlocking behaviour causing the transition from the rotating to sliding mechanism.

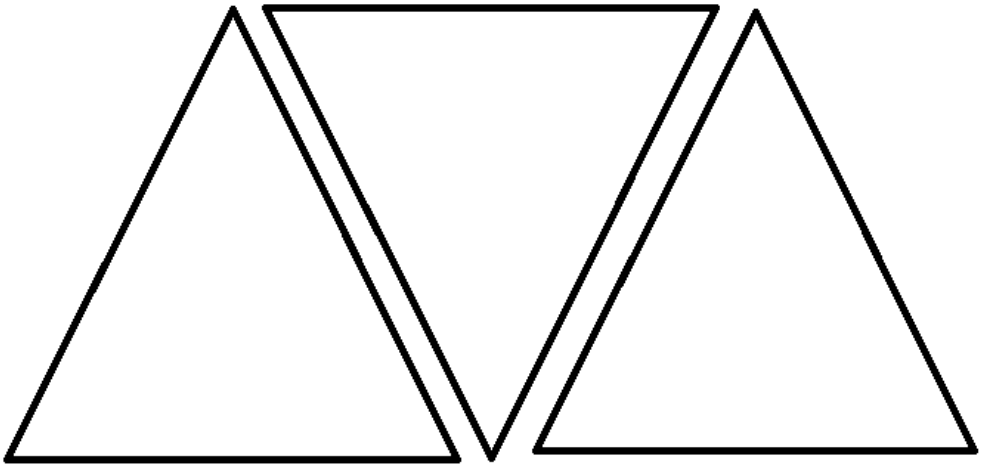

Figure 6.12: Example crystalline structure for equilateral triangles

6.5 Conclusions

In this chapter, the results are considered from models containing only angular particles with zero form. This was done by subjecting a sample to triaxial compression conditions with a periodic boundary. These shapes consisted of two distinct sets, superellipsoids (with equal axis) and platonic solids. Both sets of shapes are considered to have zero form due to the best geometrically fitting ellipsoid being that of a sphere. The key difference between these two sets of shapes is how their angularity is displayed; superellipsoids have a smooth continuous function describing the surface, whereas the platonic solids are defined by multiple planes describing the faces. This distinction in angularity is key

as other measures of angularity (or roundness) within the literature make the distinction between a sharp edge or corner and a curve over a surface.

The results from both sets of particles follow a linear relationship between the critical state angle of friction and the measured angularity, suggesting that there is not a difference between either sets of particles. This follows similar results to a previous study in which angular particles where constructed and modelled using flat planes showing that as particles became increasingly angular the critical state strength also increased.

At critical state the average amount of rotation within a model decreases linearly as the angularity increases. The proportion of sliding contacts shows the inverse relationship with the amount of sliding increasing linearly with particle angularity. There is also no visible difference between the platonic solids or superellipsoids with both following the same relationships.

As with particle form, this increased strength is accompanied by a decreased amount of rotation and an increase amount of proportion of contacts sliding. This lead to an increases in the amount of energy loss within a system and leading to a stable structure. However unlike particle form, it is impossible to distinguish between the different types of contacts as these particles are symmetrical and all faces as considered equal.

A previous study modelling platonic solids showed that as a particle becomes increasingly angular stacking microstructures formed, for example cubes tended to align with their faces touching, which caused an interlocking behaviour reducing the amount of rotation, (Höhner et al., 2014). It is thought that similar stacking microstructures are forming in this model with the interlocking behaviour causing the transition from the rotating to sliding mechanism.

Chapter 7

Particle Shape

In this chapter the results of particles that contain both angularity and form will be analysed. Using different base forms for the superellipsoids, a range of different forms and angularities are explored.

Three base forms are used; a platy form (platyness = 0.4 and elongation = 0), a elongated form (platyness = 0 and elongation = 0.2), and the equivalent scalene ellipsoid of a modelled ballast particle (platyness = 0.12889 and elongation = 0.2476).

The platy and elongated forms are, as in the previous chapter, with these forms acting as a base and the angularity is achieved by using high order superellipsoids, Figure 7.2 and 7.3. For the modelled ballast the equivalent scalene ellipsoid will be the case for zero angularity with the modelled ballast (Figure 7.1) having the highest angularity.

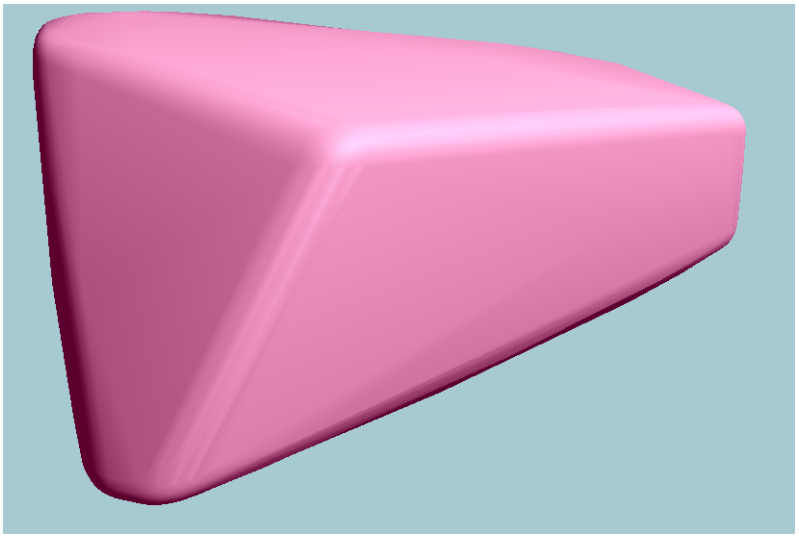

Figure 7.1: Ballast particle

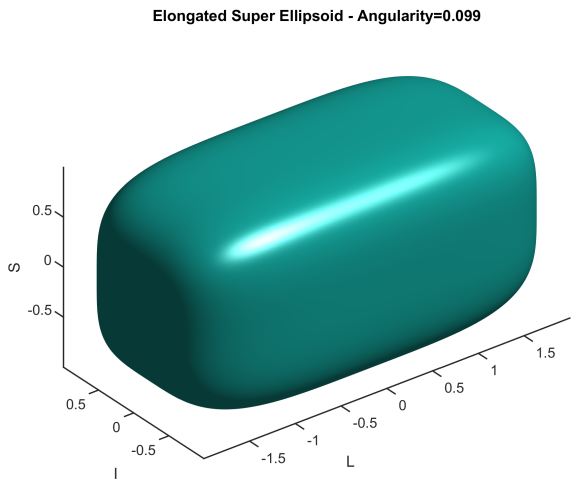

Figure 7.2: Elongated Superellipsoid

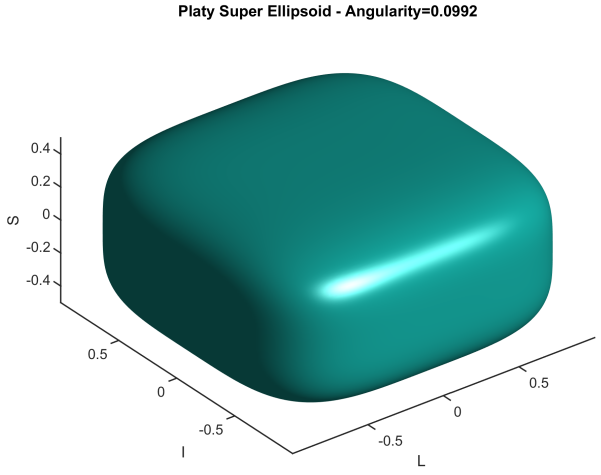

Figure 7.3: Platy Superellipsoid

7.1 Shear Strength

Figure 7.4 shows the mobilised angle of friction for the superellipsoids with a form of platyness = 0.4 and elongation = 0 with increasing angularity. All the models act as a dense soil with an initial stiff response and a sharp initial peak slowly reducing down to a critical state value. The model with the highest value of angularity has the highest critical state angle of friction. The other two models having a lower angularity also having the a lower value of critical state angle of friction, it is harder to distinguish between the two models due to the fluctuations. This is not unexpected as both models are similar in shape. The model with zero angularity has the lowest critical state angle of friction.

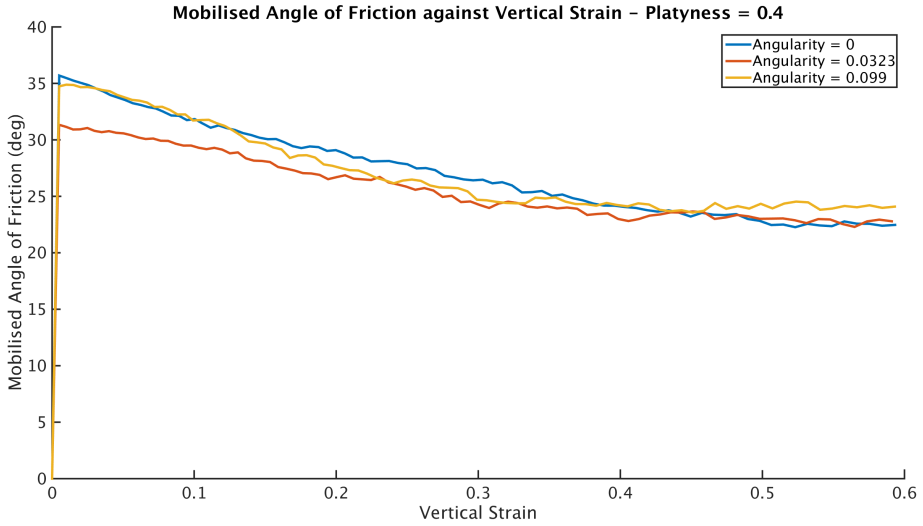

Figure 7.4: Mobilised angle of friction against vertical strain - Platy form

Figure 7.5 shows the mobilised angle of friction for the base form of platyness = 0 and elongation = 0.2. All models act as a dense soil with an initial stiff response and a sharp peak value of mobilised angle of friction to eventually reduce down to a critical state. As the particles become increasingly angular the critical state angle of friction increases as well.

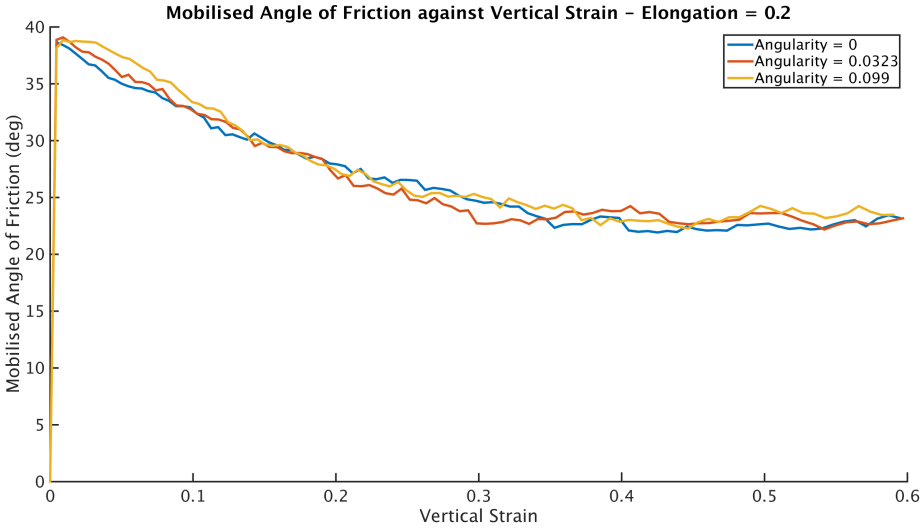

Figure 7.5: Mobilised angle of friction against vertical strain - Elongated form

Figure 7.6 shows the mobilised angle of friction for a modelled ballast particle as well as superellipsoids of the same form with lower angularity. The superellipsoid models act similar to previous models, with a stiff response and a sharp peak to a slowly reduce to a critical state. The modelled ballast particle, with the highest angularity, has an initial stiff response but instead of reaching a sharp peak it slowly reaches a peak value and reduces down to a critical state.

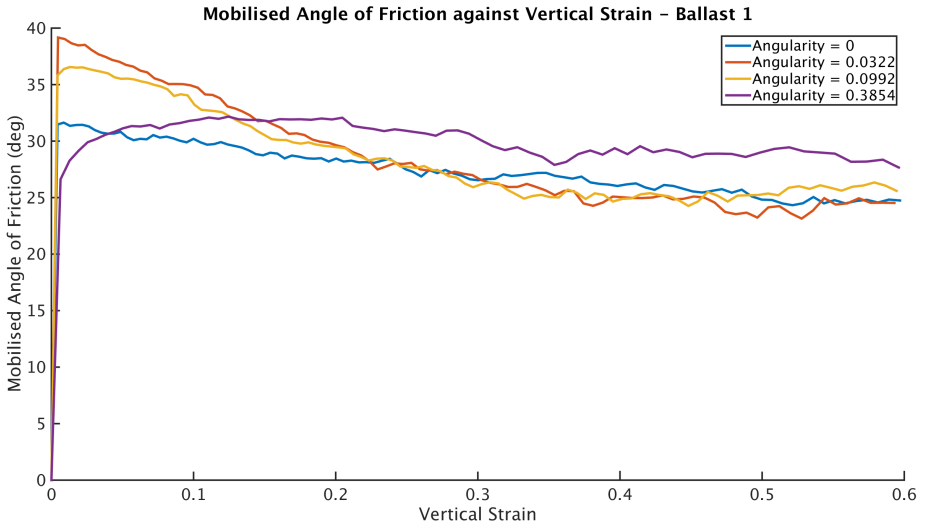

Figure 7.6: Mobilised angle of friction against vertical strain - Modelled ballast form

Figure 7.7 shows the critical state angle of friction against the model's measured angularity. These are grouped by their base form. There appears to be a linear relationship, as the angularity of the model increases so does the measured angle of friction. The gradient of the line varies depending on particle form. Angularity has a greater effect on spherical and platy particles than the elongated particles. The effect of shape on particle strength is a combination of its form and angularity. These are dependant upon each other, as shown here by the gradient variations.

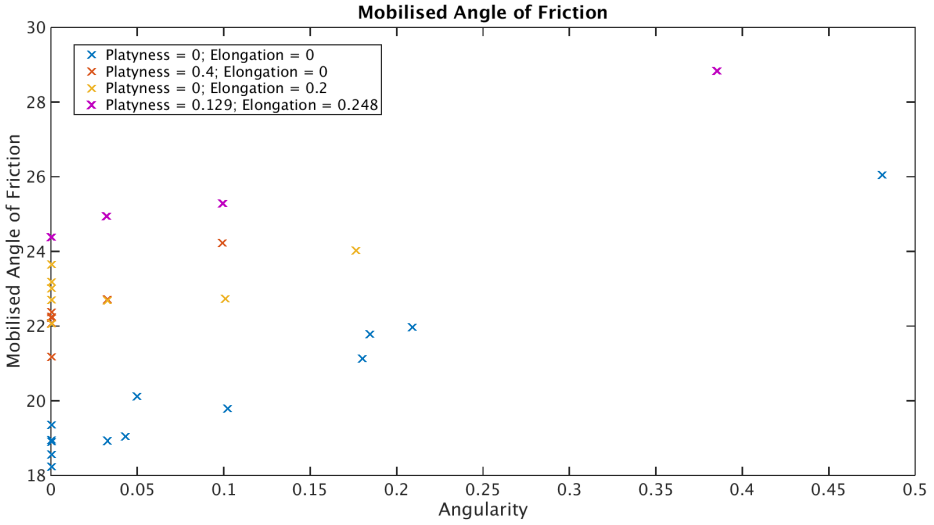

Figure 7.7: Critical state angle of friction against particle angularity for different forms

7.2 Particle Rotation

Figure 7.8 shows the average rate of rotation for the models of platy form. As the particles become increasingly angular the amount of rotation also increases. This is contrary to what has been shown in previous chapters whereby increasing the particle angularity increased the matrix strength but decreased the amount of rotation.

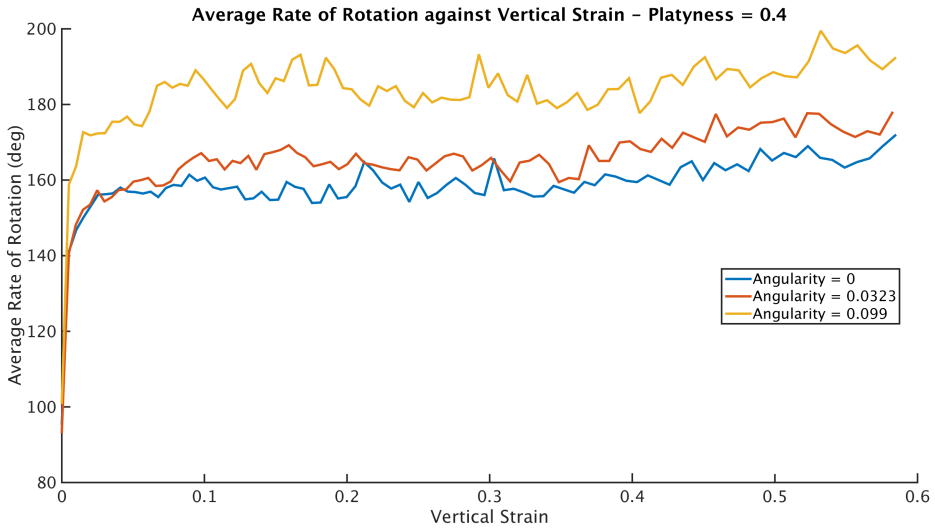

Figure 7.8: Average rate of particle rotation against vertical strain - Platy form

Figure 7.9 shows the average rate of rotation for the models of the elongated form. All the models rotate roughly the same amount regardless of how angular each shape is, this indicates that the increase in strength is not coming from the reduction in the amount of rotation.

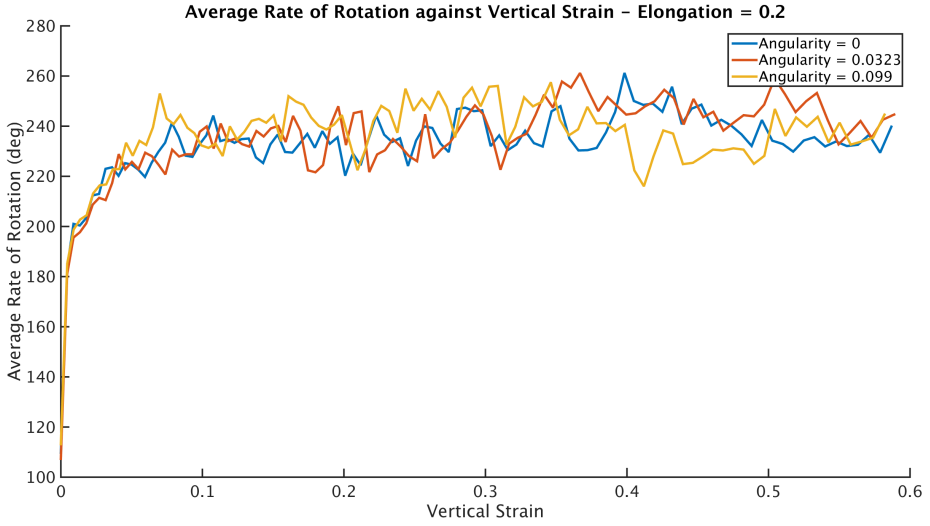

Figure 7.9: Average rate of particle rotation against vertical strain - Elongated form

Figure 7.10 shows the average rate of rotation for the models for the ballast particles and superellipsoids of equivalent form. Here both the superellipsoid with zero angularity (normal ellipsoid) and the modelled ballast particle behave similar to other models in the previous chapter. Whereby the increased angularity leads to a decreased amount of rotation within the model. However the two superellipsoids both have an increased amount of rotation similar to the figures 7.8 and 7.9. This could indicate that the superellipsoids are not consistent with previous results or that the simulation has a limitation with modelling superellipsoids.

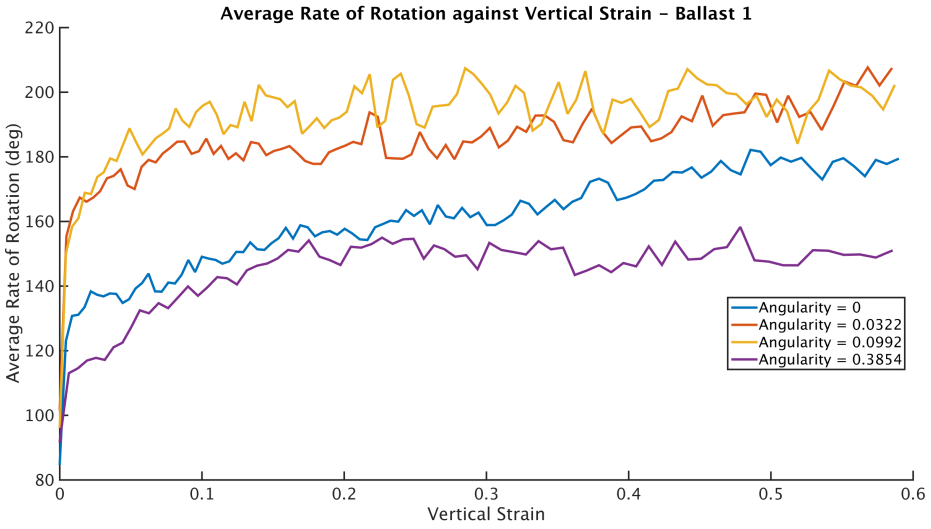

Figure 7.10: Average rate of particle rotation against vertical strain - Modelled ballast form

7.3 Particle Sliding

Figure 7.11 shows the proportion of contacts sliding for the models for platy form. The models start with an initially high amount of sliding and slowly reduces until the a steady state value is reached. This steady state value is very similar for all the models, with the most angular model having a slightly lower amount of sliding taking place compared to the other two models. This is also inconsistent with the previous chapter whereby models with increased angularity experienced a higher amount of sliding as well as a higher critical state angle of friction.

Figure 7.12 shows the proportion of contacts sliding for the model for the elongated form. The models start with an initially high amount of sliding and slowly reduces until the a steady state value is reached. As with particle rotation, figure 7.9, all models act very similarly with very little difference between them at different angularity.

Figure 7.13 shows the proportion of contacts sliding for the models for the modelled ballast particles and superellipsoids of equivalent form. The models start with an initially

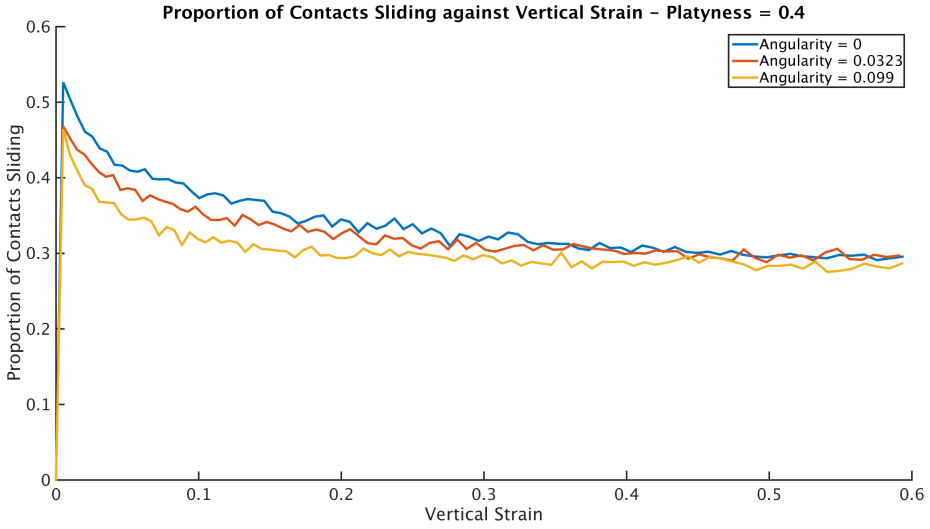

Figure 7.11: Proportion of sliding contacts against vertical strain - Platy form

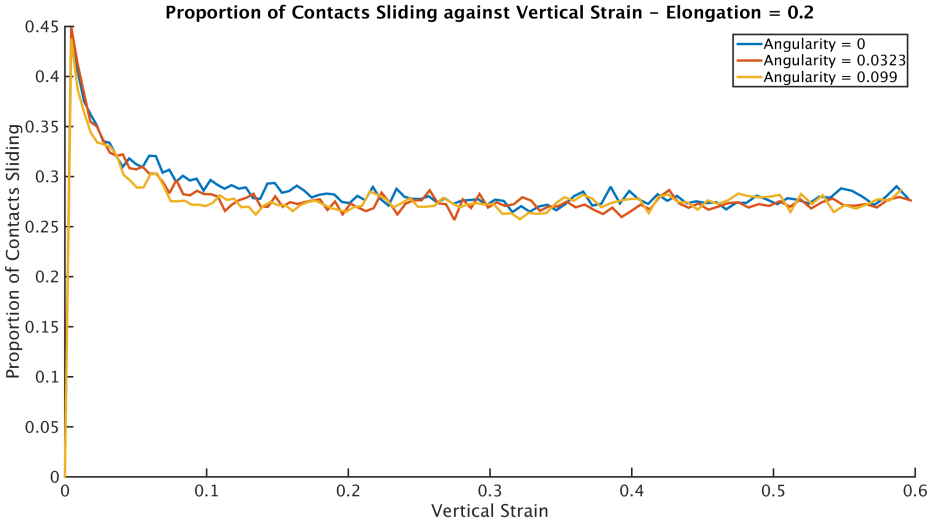

Figure 7.12: Proportion of sliding contacts against vertical strain - Elongated form

high amount of sliding and slowly reduces until the a steady state value is reached. Both the model with zero angularity (ellipsoid) and the highest angularity (modelled ballast) behave consistently with previous models The higher strength being associated with a increase in the proportion of contacts sliding at critical state.

7.4 Micromechanics

In this section different microstructures are explored by studying the different contact types and particle fabric for the superellipsoidal particles.

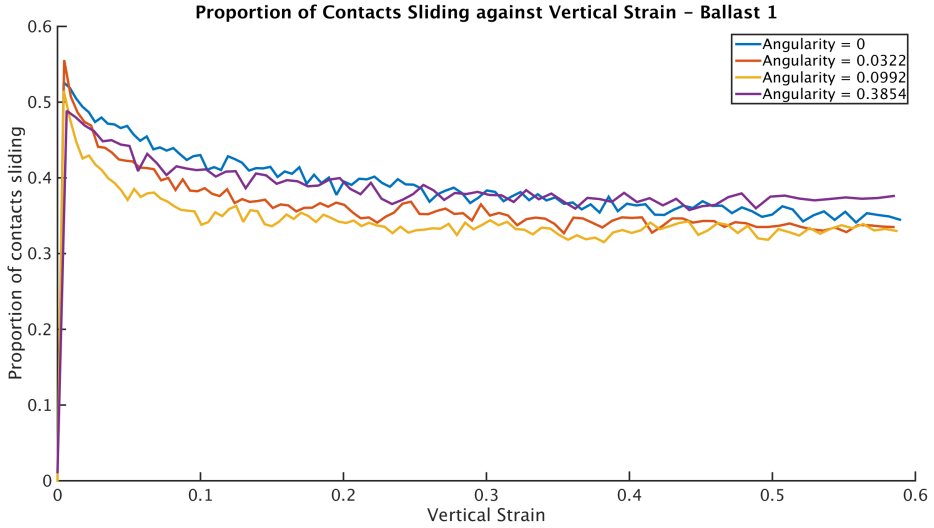

Figure 7.13: Proportion of sliding contacts against vertical strain - Modelled ballast form

Figure 7.14 shows the proportion of S-S type contacts against vertical strain for the platy superellipsoid with an angularity of 0.0992. As the modelled is strained the proportion of contacts with flat-flat contacts increases, indicating that these are stronger contacts.

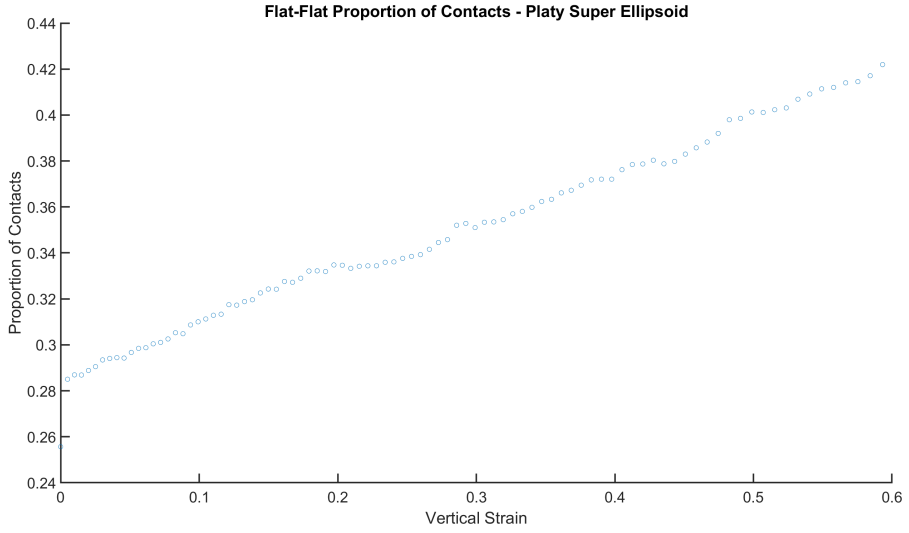

Figure 7.14: The proportion of S-S type contacts against vertical strain for a platy superellipsoid

Figure 7.15 shows the Z component of the fabric tensor for the L, I and S of the particles. As the model is strained the S axis (the flatter face) changes from an initial random orientation to a vertical orientation. The Z component for the L and I axis initially starts off with a random orientation and slowly inverse to the S axis, meaning that the L and I axis are increasingly orientated horizontally.

This shows that the angular platy particles tend to orientate flat face vertically, as well as having a preference for flat to flat type contacts. These results show the same

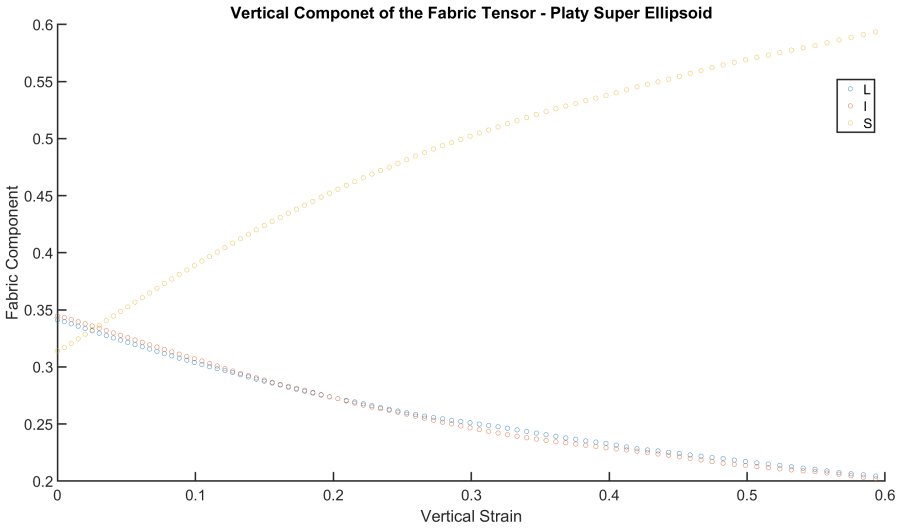

Figure 7.15: The Z component of the fabric tensor for a platy superellipsoid

characteristics as the microstructure seen in the purely platy particles.

Figure 7.16 shows the Z component of the fabric tensor for the L, I and S for the elongated superellipsoid with an angularity of 0.099. As the model is strained the Z component of the L axis decreases from an initial random orientation to preferring to orientate horizontally. The Z component for the I and S axis initial starts off with a random orientation and slowly increase inversely to the S axis, meaning that the I and S axis are increasingly orientated vertically. Due to the symmetry of the I and S axis there is no preference between their orientations. These results are similar to the nest like microstructure formed in the purely elongated particles.

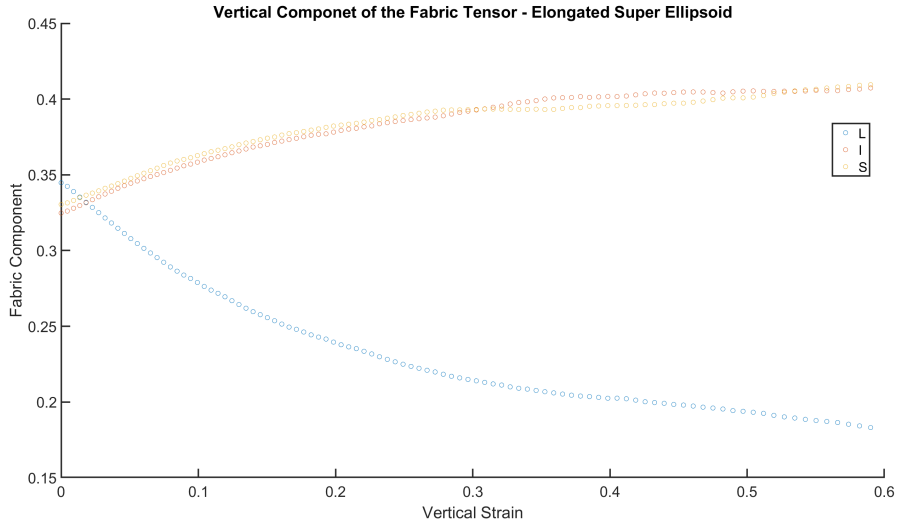

Figure 7.16: The Z component of the fabric tensor for an elongated superellipsoid

These results show that particles with both angularity and form show the characteristics of the underlying form's microstructure. And as a particle becomes increasingly angular

there is an increase in particle strength however this relationship between angularity and change in strength is not uniform for different forms. This suggests that both the effect particle angularity is dependent on the particle's form. Angularity amplifying the effect of particle form by strengthening the underlying microstructure with interlocking.

7.5 Conclusions

In this chapter DEM was used to investigate the effect of particle shape on critical state strength. This was done by subjecting a sample to triaxial compression conditions with a periodic boundary. To study the combined effect of form and angularity the particles were subdivided into three groups based upon the particles measured form. This was done so that the effect of platyness, elongation, and form with a mixture of elongation and platyness could be analysis independently. Each group of particles had the same measured form whilst varying measured angularity.

The results from critical state strength shows that as particles become increasingly angular there is a subsequent increase in critical state strength. The spherically formed particles had the lowest critical state strength whereas the mixed formed particles had the highest critical state strength. This result is consistent with the results from the previous chapter whereby zero angularity spheres had the lowest strength and mixed particles had the highest. However, unlike the previous chapter, the results from the different sets did not follow the same relationship with each set increasing at different rates. This suggests that the effect of particle angularity is not independent of the particle form as was originally thought.

The angular platy model had a higher proportion of flat-flat contacts which increased as the model was strained. They particles had a preference to orientate with the flatter face vertically. The same microstructure as the purely platy particles whereby platy particles showed a stacking effect.

The angular elongated model had a preference to orientate with the longest axis horizontal. The intermediate and shortest axis, being equivalent due to symmetry, tended to orientate vertically. These are the same characteristics as the microstructure seen previously in the purely elongated particles, whereby the elongated particles formed a nest-like structure

Investigating the combination of particle form and angularity together, it was found that both measures act cooperatively in regards to increasing the angle of friction at critical state. It is also seen that these two effects are not independent of each other, as the effectiveness of particle angularity is dependent on the underlying form of the shape. Particles with both angularity and form show the characteristics of the underlying microstructure. The effect of angularity is to amplify the effect of particle form allowing

for the microstructure that develops to be strengthened by the interlocking effect of particle angularity and thus increasing the critical state strength.

Chapter 8

Conclusions

This thesis investigated the effect of particle shape on the critical state strength of granular materials, specifically railway ballast.

The particles were modelled using DEM and set up in a periodic cell under triaxial stress conditions (stress controlled lateral boundaries and a constant velocity applied to the top boundary).

Each model consisted of a single shape, with a PSD equivalent to network rail ballast, thus any changes to the granular properties could be attributed solely to the shape of the particle. By investigating what happens when a model reaches the critical state allows for a comparison between different particle shapes.

A review of the different measures and definitions of particle shape showed that shape can be split into the categories: form, angularity and surface roughness.

The general shape of a particle's form is normally measured in the following using the longest (L), intermediate (I) and shortest (S) dimensions. Particle angularity describes the general curvature of a particle surface, whilst surface roughness describes the microscopic undulation on a particle surface and is usually defined based upon the inter-particle angle of friction.

As discussed in Chapter 3, the previous measures of particle form were found to be lacking. Therefore, this study proposed a new method to define a particle's form being an equivalent scalene ellipsoid. To define the form of the equivalent scalene ellipsoid, the particle's L, I and S was considered and two terms were defined, platyness (describing the flatness of the particle), and elongation (describing the particle length). Using a combination of these two terms, every scalene ellipsoid can be defined.

To study the effect of form, particles were used that had form but no angularity i.e. ellipsoidal particles. These ellipsoidal particles were further subdivided into three categories: platy particles, elongated particles, and particles that contain both elongation and platyness.

To study the effect of particle platyness, which ranges from a sphere to a 2D disk, a selection of particles were chosen and modelled. It was found that as the platyness of the models increased there was a linear increase in the critical state strength. Strength is controlled by the micro-mechanics within the model, causing microstructures to form. The increased critical state strength was linked to a decrease in the average rate of rotation within the model and an increase in the proportion of sliding contacts; this led to additional energy being expended. This was due to the platyier particles preferring to align their flatter faces normal to the major principal stress. These particles also preferred to form "flat-to-flat" contacts, thus causing the particles to stack and form a strong microstructure.

By looking at the effect of particle elongation, which ranges from a sphere to a 1D line, a selection of particles were chosen and modelled. As with particle platyness, by increasing particle elongation, starting from that of a sphere, there is a linear increase in critical state strength. The models showed that elongated particles have a preference to orientate so that their longest axis is orthogonal to the principle stress. This led to a nest-like structure forming, helping to support and distribute the load efficiently. Therefore, each particle was supported by multiple contacts allowing the load to be distributed and increasing the strength of the model.

To understand the combined effect of elongation and platyness a distribution of scalene ellipsoids was tested. The models showed that spheres had the lowest critical state strength and any increase in elongation or platyness led to an increase in strength. The measure of elongation had a greater effect on increasing the strength when compared to that of platyness. The highest critical state strength was shown in particles that had both elongation and platyness. This increase in strength was also accompanied by a decrease in the average rate of rotation within the model and an increase in the proportion of sliding contacts. The particles with both elongation and platyness showed a combination of the elongated and platy microstructures. The model showed that the longest axis preferred to orientate itself horizontally and its shortest axis vertically, as well as having an increased proportion of S-S type contacts.

As discussed in Chapter 3, the existing measures of particle angularity are limited to only using 2D projections of a particle's outline. Thus all previous measures of particle angularity do not take into account the full shape of the particle, leading to a loss of information. This study introduces a new measure of particle angularity using the complete particle shape. This new measure for angularity is defined as the difference

between a particle's shape and its form. Angularity is categorised by measuring the volumetric difference between the shape and the form.

To understand the effect of angularity, particles with zero form and a range of measured angularities were studied, these consisted of two sets of particles: the platonic solids and superellipsoids with equal radii. Within the model the platonic solids were described by a series of planes intersecting a sphere and the superellipsoids by a smooth continuous function. Regardless of the methods used to describe angularity both sets of particles followed the same linear trends. The models showed that shapes with zero angularity had the lowest critical state strength; as angularity increased so did the critical state strength. The increased critical state strength was also accompanied by a decrease in the average rate of rotation and an increase in the proportion of sliding contacts, which led to more energy being expended. This was due to particle angularity causing an interlocking effect between the particles improving the stability of the contacts.

To look at the effects of angularity and form together, the full effect of shape, a selection of base forms was used. For the base forms different angularities were achieved by using superellipsoids and a modelled ballast particle. The modelled showed that both measures of angularity and form interacted cooperatively to increase critical state strength, with the lowest strength being that of a sphere (no form or angularity). All the angular superellipsoids showed the same microstructures as the platy and elongated particles. It was shown that the effectiveness of angularity is dependent on the particle's form, whereby angularity increased the effectiveness of the microstructures. This means that the measures of angularity and form presented here are not independent measures as was previously thought.

To extend these investigations further a greater number of different shapes would be required. These shapes could consist of randomly created particles with similar forms but different angularities. This would allow for a greater understand of the effect form and angularity have on each other. Another approach would be to calibrate the existing models by using physical tests, such as using manufactured particles of certain shapes, for example ellipsoids or platonic solids. These physical tests could then be used to calibrate the DEM method so that the models better reflect the initial response under loading allowing for an investigation into stiffness.

References

Abbireddy, C. O. R. and Clayton, C. R. I. (2010). Varying initial void ratios for DEM simulations. *Géotechnique*, 60(6):497–502.

Ahmed, S., Harkness, J., Le Pen, L., Powrie, W., and Zervos, A. (2015). Numerical modelling of railway ballast at the particle scale. *International Journal for Numerical and Analytical Methods in Geomechanics*, 40(5):713–737.

Aschenbrenner, B. (1956). A new method of expressing particle sphericity. *Journal of Sedimentary Petrology*, 26(1):15–31.

Azéma, É. and Radjaï, F. (2010). Stress-strain behavior and geometrical properties of packings of elongated particles. *Physical Review E*, 81(5):1–17.

Azéma, É., Radjaï, F., Saint-Cyr, B., Delenne, J.-Y., and Sornay, P. (2013). Rheology of three-dimensional packings of aggregates: Microstructure and effects of nonconvexity. *Physical Review E*, 87(5):052205.

Azéma, É., Radjaï, F., and We, D. (2012). Force chains and contact network topology in sheared packings of elongated particles. *Physical Review E*, 85(3):031303.

Bardet, J. P. (1994). Observations on the effects of particle rotations on the failure of idealized granular materials. *Mechanics of Materials*, 18:159–182.

Barret, P. J. (1980). The shape of rock particle, a critical review. *Sedimentology*, 27:291–303.

Benn, D. I. and Ballantyne, C. K. (1993). The description and representation of particle shape. *Earth Surface Processes and Landforms*, 18(7):665–672.

Blott, S. J. and Pye, K. (2008). Particle shape: a review and new methods of characterization and classification. *Sedimentology*, 55(55):31–63.

Boton, M., Azéma, É., Estrada, N., Radjaï, F., and Lizcano, A. (2013). Quasistatic rheology and microstructural description of sheared granular materials composed of platy particles. *Physical Review E*, 87(3):032206.

BS EN (2013). *BSI Standards Publication Aggregates for railway ballast BS EN 13450:2013 BSI.* BSI Standards Limited 2013.

Cambou, B., Jean, M., and Radjaï, F. (2008). *Micromechanics of granular materials*, volume 77. John Wiley & Sons.

Cho, G.-C., Dodds, J., and Santamarina, J. C. (2006). Particle Shape Effects on Packing Density , Stiffness and Strength Natural and Crushed Sands. *Journal of Geotechnical and Geoenvironmental Engineering*, 132:591–602.

Clayton, C. R. I., Abbireddy, C. O. R., and Schiebel, R. (2009). A method of estimating the form of coarse particulates. *Géotechnique*, 59(6):493–501.

Corey, A. (1949). *Influence of shape on the fall velocity of sand grains*. PhD thesis.

Cox, E. (1927). A method of assigning numerical and percentage values to the degree of roundness of sand grains. *Journal of Paleontology*, 1(3):179–183.

Delaney, G. W. and Cleary, P. W. (2010). The packing properties of superellipsoids. *EPL (Europhysics Letters)*, 89(3):34002.

Delaney, G. W., Hilton, J. E., and Cleary, P. W. (2011). Defining random loose packing for nonspherical grains. *Physical Review E*, 83(051305).

Dobkins, J. F. and Folk, R. L. (1970). Shape development on Tahiti-Nui. *Journal of Sedimentary Petrology*, 40(4):1167–1203.

Donev, A., Stillinger, F. H., Chaikin, P. M., and Torquato, S. (2004). Unusually Dense Crystal Packings of Ellipsoids. *Physical Review Letters*, 92(25):255506.

Estrada, N., Radjaï, F., Taboada, A., and Azéma, É. (2011). Identification of rolling resistance as a shape parameter in sheared granular media. *Physical Review E*, 84(011306):1–5.

Estrada, N., Taboada, A., Radjaï, F., Nakagawa, M., and Luding, S. (2009). Shear strength and fabric properties in granular media with interlocked particles. *AIP Conference Proceedings*, 1145(2009):373–376.

Folk, R. L. (1955). Student Operator Error in Determination of Roundness, Sphericity, and Grain size. *Journal of Sedimentary Research*, 25(4).

Harkness, J. (2009). Potential particles for the modelling of interlocking media in three dimensions. *International Journal for Numerical Methods in Engineering*, 80:157315(June):1573–1594.

Harkness, J., Zervos, A., Le Pen, L., Aingaran, S., and Powrie, W. (2016). Discrete element simulation of railway ballast: modelling cell pressure effects in triaxial tests. *Granular Matter*, 18(3):65.

Heitkam, S., Drenckhan, W., and Fröhlich, J. (2012). Packing Spheres Tightly: Influence of Mechanical Stability on Close-Packed Sphere Structures. *Physical Review Letters*, 108(14):148302.

Höhner, D., Wirtz, S., and Scherer, V. (2014). A study on the influence of particle shape and shape approximation on particle mechanics in a rotating drum using the discrete element method. *Powder Technology*, 253:256–265.

ISO (2009). Soil Quality Determination of Particle Size Distribution in Mineral Soil Material Method by Sieving and Sedimentation. *International standard*, 2002:30.

Iwashita, K. and Oda, M. (1999). *Mechanics of Granular Materials: An Introduction*. CRC Press.

Janke, N. (1966). Effect of shape upon the settling velocity of regular convex geometric particles. *Journal of Sedimentary Research*.

Janoo, V. (1998). Quantification of shape, angularity, and surface texture of base course materials. Technical report.

Jensen, R. and Bosscher, P. (1999). DEM simulation of granular mediastructure interface: effects of surface roughness and particle shape. *International Journal for Numerical and Analytical Methods in Geomechanics*, 23:531–547.

Ken-Ichi, K. (1984). Distribution of directional data and fabric tensors. *International Journal of Engineering Science*, 22(2):149–164.

Krumbein, W. C. (1941). Measurement and Geological Significance of Shape and Roundness of Sedimentary Particles. *Journal of Sedimentary Research*, Vol. 11(2):64–72.

Kuenen, P. (1956). Experimental abrasion of pebbles: 2. Rolling by current. *The Journal of Geology*, 64(4):336–368.

Le Pen, L. (2008). *Track behaviour: the importance of the sleeper to ballast interface*. Doctoral thesis, University of Southampton.

Le Pen, L., Powrie, W., Zervos, A., Ahmed, S., and Aingaran, S. (2013). Dependence of shape on particle size for a crushed rock railway ballast. *Granular Matter*, 15:849–861.

Lees, G. (1964). A new method for determining the angularity of particles. *Sedimentology*, 3(5):2–21.

Li, X.-S. and Dafalias, Y. F. (2012). Anisotropic Critical State Theory: Role of Fabric. *Journal of Engineering Mechanics*, 138(3):263–275.

Mollanouri Shamsi, M. and Mirghasemi, A. A. (2012). Numerical simulation of 3D semi-real-shaped granular particle assembly. *Powder Technology*, 221:431–446.

Nguyen, D.-H., Azéma, É., Sornay, P., and Radjaï, F. (2015). Effects of shape and size polydispersity on strength properties of granular materials. *Physical Review E*, 91(3):032203.

Oda, M. (1972). Initial fabrics and their relations to mechanical properties of granular material. *Soils and Foundations*, 12(1):17–36.

Oda, M. and Kazama, H. (1998). Microstructure of shear bands and its relation to the mechanisms of dilatancy and failure of dense granular soils. *Géotechnique*, 48(4):465–481.

O'Sullivan, C., Bray, J. D., and Riemer, M. F. (2002). Influence of Particle Shape and Surface Friction Variability on Response of Rod-Shaped Particulate Media. *Journal of Engineering Mechanics*, 128(11):1182–1192.

Pentland, A. (1927). A method of measuring the angularity of sands. In *Proceedings and transcription of the Royal Society of Canada*, volume 21.

Potticary, M., Harkness, J., and Zervos, A. (2015). An investigation in the effect of particle platyness on the strength of granular materials using the discrete element method. In Oñate, E., M., Bischoff, Owen, D., Wriggers, P., , , and Zohdi, T., editors, *Particle-based Methods IVFundamentals and Applications*, pages 767–778, Barcelona. International Center for N umerical Methods in Engineering.

Potticary, M., Zervos, A., and Harkness, J. (2014). A numerical investigation into the effect of particle form on the strength of granular materials. In *Proceedings of the 22nd UK Conference of the Association for Computational Mechanics in Engineering*.

Potticary, M., Zervos, A., and Harkness, J. (2016). The effect of particle elongation on the strength of granular materials. In *24th Conference on Computational Mechanics*, pages 239–242.

Powrie, W. (2004). *Soil Mechanics: Concepts and Applications*. Spon Press.

Radjaï, F. and Azéma, É. (2009). Shear strength of granular materials. *European Journal of Environmental and Civil Engineering*, 13(2):203–218.

Radjaï, F., Dubois, F., and Azéma, É. (2013). Packings of irregular polyhedral particles: Strength, structure, and effects of angularity. *Physical Review E*, 87(062203):1–15.

Radjaï, F. and Richefeu, V. (2009). Contact dynamics as a nonsmooth discrete element method. *Mechanics of Materials*, 41:715–728.

Radjaï, F., Roux, S., and Moreau, J. J. (1999). Contact forces in a granular packing. *Chaos: An Interdisciplinary Journal of Nonlinear Science*, 9(3):544–550.

Riley, N. (1941). Projection sphericity. *Journal of Sedimentary Research*, 11(2):94–97.

Rothenburg, L. and Bathurst, R. (1989). Analytical study of induced anisotropy in idealized granular materials. *Géotechnique*, 39(4):601–614.

Rousé, P. C., Fannin, R. J., and Shuttle, D. A. (2008). Influence of roundness on the void ratio and strength of uniform sand. *Géotechnique*, 58(3):227–231.

Santamarina, J. C. and Cho, G.-C. (2004). Soil behaviour: The role of particle shape. In *Advances in geotechnical engineering: The skempton conference*, volume 1, pages 1–14.

Sneed, E. and Folk, R. L. (1958). Pebbles in the lower Colorado River, Texas a study in particle morphogenesis. *The Journal of Geology*, 66(2):114–150.

Sukumaran, B. and Ashmawy, A. K. (2001). Quantitative characterisation of the geometry of discret particles. *Géotechnique*, 51(7):619–627.

Tickell, F. and Hiatt, W. (1938). Effect of angularity of grain on porosity and permeability of unconsolidated sands: Geological Notes. *AAPG Bulletin*, 22(9):1272 – 1274.

Wadell, H. (1932). Volume, Shape, and Roundness of Rock Particles. *The Journal of Geology*, 40(5):443–451.

Wadell, H. (1933). Sphericity and roundness of rock particles. *The Journal of Geology*, 41(3):310–331.

Wadell, H. (1935). Volume, Shape, and Roundness of Quartz Particles. *The Journal of Geology*, 43(3):250–280.

Wentworth, C. (1919). A laboratory and field study of cobble abrasion. *The Journal of Geology*, 27(7):507–521.

Wentworth, C. (1922). The shape of beach pebbles. Technical report.

Williams, E. (1965). A Method of Indicating Pebble Shape with One Parameter: NOTES. *Journal of Sedimentary Research*, 35(4):993–996.

Youd, T. (1973). Factors controlling maximum and minimum densities of sands. *Evaluation of Relative Denisty and Its Role in Geotechnical Projects Involving Cohesionless Soils*, pages 98–112.

Zingg, T. (1935). *Beitrag zur Schotteranalyse*. PhD thesis, Min. Petrog.